Stress fields for the interaction of in-plane and out-of-plane forces in reinforced concrete shell elements

PAR

Marie-Rose BACKES

EPFL

ÉCOLE POLYTECHNIQUE
FÉDÉRALE DE LAUSANNE

Suisse
2017

Foreword

The thesis of Marie-Rose Backes investigates on the application of the stress field method for analysis and design of concrete planar members subjected to in-plane and out-of-plane actions. This topic is very relevant for practice as many structural elements carrying large in-plane shear forces (such as the webs of box-girder bridges) are also subjected to non-negligible transverse bending and shear (for instance due to asymmetric loading cases in the deck slab). Despite the fact that the presence of the out-of-plane actions may reduce the resistance to carry in-plane actions, this interaction has been scanty investigated in the past and not much detailed design guidelines can be found in codes of practice.

The work of Marie-Rose Backes approaches this issue from the perspective of the stress field method. This technique was shown in the past to be a consistent tool for design of such members, although solutions were mostly developed on the basis of rigid-plastic material behaviour, with the need to assume some level of simplification on the modelling. The present work is a step forward in this field by introducing the considerations of the elastic-plastic stress field method developed at the Structural Concrete Laboratory of EPFL. Such approach allows overcoming most previous difficulties and provides a detailed reading of the state of stresses and strains developed. In addition, it is also shown that under some reasonable assumptions, the procedure can eventually be simplified and used in a practical manner for common design cases.

Lausanne, December 2016.

Prof. Dr Aurelio Muttoni   Dr Miguel Fernández Ruiz

Acknowledgements

tional encouragement and love throughout all these years I have been so far from them. Last but not least, I thank Philippe, the most precious person to me, for his faithful support, endless patience and tremendous love that helped me through all the stages of this PhD. Thank you.

Marie-Rose

Abstract

Plane reinforced concrete (RC) elements are used in a large variety of structures. Their principal function is to carry forces that act in the plane of the element, but external actions and connections to other structural elements generally introduce additional out-of-plane forces. In practice, the design of such elements is often performed in a simplified manner, neglecting the interaction between these different internal forces. However, especially for existing structures the need for more precise and kinematically consistent analysis tools arises. This thesis provides novel tools based on the elastic-plastic stress field (EPSF) method to investigate the interaction between in-plane and out-of-plane forces in plane RC elements in general and the effect of transverse bending on the longitudinal shear resistance of beams in particular.

A general multi-layered (ML) EPSF approach is developed. Applied to a unitary web segment, in-plane shear-transverse bending interaction diagrams are established and compared to existing rigid-plastic (RP) interaction models. In general, it is found that the influence on the shear resistance is less pronounced, especially in case of small transverse moments. The shear transfer actions admitted in RP models that consist in a shift of the compression field to the bending compression side and a rearrangement of the stirrup forces are confirmed. However, it is shown that the stress field is highly non-linear in the transverse directions (stress/strain distribution and inclination) and strongly depends on the intensity of the applied transverse moment. The concrete strength reduction factor η_ε is generally higher and high shear reinforcement ratios or asymmetric layouts allow equilibrating small moments without disturbing the stress field in the concrete. This increases the predicted shear resistance. The longitudinal deformation is shown to have a non-negligible effect on the overall interaction and ultimate resistance.

A simplified verification method for beams in practice is proposed. Based on the EPSF finite element method (FEM), it considers the influence of the transverse moment by means of a reduced web width and an effective shear reinforcement ratio. Validation with tests from the literature gave safe but not overly conservative results and consistent predictions of the failure modes. The method provides enhanced lower-bound solutions.

Plane EPSF analyses of experimental tests suggest that the influence of the transverse bending moment in beams is less pronounced than predicted by interaction models, especially if ductile failure modes occur. However, more experimental data is required to validate this observation.

A non-linear FEM based on the ML-EPSF is developed. It aims to extend the field of application of the EPSF FEM by accounting for in-plane (normal and shear) and out-of-plane (bending and shear) actions in plane RC elements. Concrete is modelled by ML in-plane elements that are combined with out-of-plane shear elements. Reinforcing steel is modelled separately by bar elements. Benchmark tests and validation with experimental data show that the proposed FEM is a promising tool for the design and assessment of plane reinforced concrete elements primarily subjected to combinations of in-plane forces and out-of-plane bending moments.

Keywords

Résumé

Les éléments structuraux plans en béton armé se retrouvent dans une grande variété d'ouvrages. Leur fonction principale est de transférer des efforts agissants dans le plan de l'élément, mais des actions externes et la connexion à d'autres éléments structuraux engendrent aussi des efforts hors du plan. Dans la pratique, le dimensionnement est souvent fait de manière simplifiée, en négligeant toute interaction entre ces différents efforts. Pour les structures existantes, souvent des outils d'analyse plus précis sont requis afin de valider la sécurité structurale dans un contexte de plus en plus exigeant. Cette thèse présente plusieurs outils permettant d'étudier l'interaction entre les efforts en plan et hors du plan. Une attention particulière est portée sur l'influence du moment transversal sur la résistance à l'effort tranchant d'éléments poutres.

Une méthode multicouche générale, basée sur les champs de contraintes élastiques-plastiques (EPSF) est développée. Elle est appliquée aux âmes de poutres pour établir des diagrammes d'interaction effort tranchant – flexion transversale qui sont comparés à des modèles rigides-plastiques existants et dont le principe consistant à excentrer le champ de compression et à réarranger les efforts dans les étriers a pu être validé. Par contre, il est montré que le champ de contraintes est hautement non-linéaire dans la direction transversale (intensité et inclinaison des déformations/contraintes) et fortement dépendant de l'intensité du moment transversal. Les facteurs obtenus pour la résistance du béton η_ε sont généralement plus élevés et la déformation axiale a une influence significative sur l'effet du moment. En cas de taux d'armature d'effort tranchant élevés ou d'étriers asymétriques, un faible moment n'influence guère les contraintes dans le béton. Ces effets contribuent à une interaction moins prononcée et une résistance à l'effort tranchant plus élevée.

Pour la pratique, une méthode de vérification simplifiée pour les poutres avec flexion transversale est proposée. Combinant la méthode aux éléments finis (FEM) pour les EPSF avec des considérations basées uniquement sur l'équilibre des moments, la méthode fournit une borne inférieure améliorée de la résistance. L'effet du moment est pris en compte par une réduction de l'épaisseur de l'âme et un taux d'armature effectif. La méthode est validée par des essais de la littérature, les prédictions sont du côté de la sécurité et les modes ruptures sont correctement représentés.

Des analyses par la EPSF-FEM suggèrent que dans les poutres l'influence du moment transversal est moins importante que prédite par les modèles d'interactions, mais plus de résultats expérimentaux sont nécessaires pour confirmer ceci.

Dans le but d'étendre le champ d'application des EPSF, une méthode aux éléments finis non-linéaire basée sur la nouvelle approche multicouche des EPSF est développée. Elle permet d'étudier le comportement d'éléments plans en béton armé soumis à des charges en plan et hors du plan (moments et forces). Le béton est modélisé par des éléments multi-couches dans le plan, qui sont combinés à des éléments de cisaillement hors du plan. L'armature est modélisée séparément par des éléments barre à excentricité hors du plan. La validation avec des tests de référence et des essais expérimentaux a montré qu'il s'agit d'un outil prometteur pour le dimensionnement et la validation d'éléments soumis primaire-ment à des efforts membranaires et flexionnels.

Mots-clés

Panneaux en béton armés, champs de contraintes élastiques-plastiques, champ de con-traintes multicouche, résistance à l'effort tranchant, interaction entre effort tranchant et flexion transversale, méthode aux éléments finis non-linéaire.

Zusammenfassung

Stahlbetonscheiben stellen einen wesentlichen Bestandteil vieler Bauwerke dar. Ihre Hauptaufgabe ist die Aufnahme von in der Scheibenebene wirkenden Kräften. Äussere Einwirkungen und der Verbund mit dem restlichen Bauwerk erzeugen jedoch zusätzliche Querkräfte. In der Praxis erfolgt die Bemessung meist in vereinfachter Weise oder die Interaktion von Membran- und Querkräften wird ganz vernachlässigt. Der Tragsicherheitsnachweis bestehender Tragwerksteile benötigt jedoch meist präzisere Verfahren. Diesbezüglich beschreibt die vorliegende Arbeit neuartige, auf der Methode der elastisch-plastischen Spannungsfelder (EPSF) beruhende, Verfahren zur Berechnung von scheibenartigen Stahlbetonbauteilen unter kombinierter Membran- und Querkraftbeanspruchung. Insbesondere wird die Auswirkung von Querbiegung auf den Schubkraftwiderstand von Stahlbetonträgern untersucht.

Zur Untersuchung der Interaktion von Längsschub und Querbiegung im Trägersteg wurde ein allgemeines, auf der EPSF Methode beruhendes, Schichtmodell (ML) wurde entwickelt. Die Ergebnisse werden mit starr-plastischen Interaktionsmodellen verglichen, bei welchen die Aufnahme des Querbiegemoments durch eine Verlagerung des Schubdruckfeldes zur Biegungsdruckzone hin und durch ungleiche Kräfte in den Bügelstegen erfolgt. Dieser Ansatz kann als korrekt bestätigt werden. Die neue Methode jedoch zeigt, dass das Spannungsfeld in der Querrichtung eine stark nichtlineare Verteilung aufweist und signifikant von der Intensität des Quermoments abhängt. Des Weiteren, sind die berechneten Betondruckfestigkeitsfaktoren η_ε im Schnitt höher und hohe Schubbewehrungsgrade bzw. asymmetrische Bügelanordnungen ermöglichen den Ausgleich kleiner Momente ohne grössere Beeinträchtigung das Betondruckfelds. Dies führt zu einem höheren rechnerischen Querkraftwiderstand. Ausserdem wird gezeigt, dass die Verformung in Längsrichtung einen signifikanten Einfluss auf die Interaktion und somit auf den allgemeinen Tragwiderstand hat.

Ein vereinfachtes Nachweisverfahren für Träger wird vorgeschlagen. Es basiert auf der Finite-Elemente-Methode (FEM) zur automatischen Erstellung elastisch-plastischer Spannungsfelder und berücksichtigt den Einfluss des Quermomentes anhand einer reduzierten Stegbreite und eines effektiven Schubbewehrungsanteils. Vergleiche mit Testergebnissen, dass die so ermittelte Schubtragfähigkeit einen sicheren und für die Praxis dennoch nicht zu konservativen Wert darstellt. Im Vergleich zu starr-plastischen Interaktionsmodellen führt dieses Verfahren zu einem verbesserten unteren Grenzwert der Traglast.

Nachrechnungen anhand der ebenen EPSF suggerieren, dass der Einfluss des Quermoments in Trägern einen kleineren Einfluss hat als von Interaktionsmodellen vorausgesagt, insbesondere bei duktilem Versagen. Zusätzliche Tests sind jedoch nötig um diese Beobachtung zu bestätigen.

Mit dem Ziel, den Anwendungsbereich der EPSF-FEM zu erweitern, wurde ein nichtlineares FEM-Programm, basierend auf der ML-EPSF Methode, entwickelt, welches sowohl Membran- als auch Querkräfte berücksichtigt. Der Beton wird mit ebenen ML Elementen modelliert, die mit Querelementen zur Aufnahme der Querkraft kombiniert werden. Die Stahlbewehrung wird getrennt hiervon mit Stabelementen modelliert. Die Validierung mit Testergebnissen zeigt, dass die vorgeschlagene FEM ein vielversprechendes Werkzeug zur Bemessung ebener Stahlbetonelemente, die hauptsächlich durch Kombinationen von Membrankräften und Querbiegemomenten belastet sind, ist.

Stichwörter

Stahlbetonscheiben, elastisch-plastische Spannungsfelder, Mehrlagige Spannungsfelder, Querkraftwiderstand, Interaktion von Längsschub und Querbiegung, nichtlineare Finite-Elemente-Methode.

Riassunto

Elementi bidimensionali in calcestruzzo armato sono adottati in una vasta gamma di strutture. La loro funzione principale è trasmettere sforzi che agiscono nel piano medio dell'elemento; tuttavia azioni esterne o connessioni ad altri elementi strutturali possono introdurre sforzi addizionali fuori piano. Nella pratica progettuale, il dimensionamento di tali elementi è spesso svolto in maniera semplificata, trascurando l'interazione tra questi differenti sforzi. Nonostante tali assunzioni, specialmente per strutture esistenti, il bisogno di uno strumento di analisi piu' preciso è necessario. Questa tesi fornisce nuovi strumenti di analisi basati sul metodo dei campi di tensione elasto-plastici (EPSF) al fine di investigare l'interazione tra sforzi nel piano e fuori piano per elementi in calcestruzzo armato bidimensionali e, in particolare, l'effetto del momento trasversale sulla resistenza a taglio longitudinale di travi.

Un approccio ad elementi finiti shell multi-layered secondo il metodo dei campi di tensione elasto-plastici (EPSF) è stato sviluppato. Tale approccio è applicato ad elementi di travi di lunghezza unitaria al fine di stimare i diagrammi di interazione taglio-momento che sono confrontati a modelli rigidi-plastici esistenti. In generale, è stato rilevato che l'influenza sulla resistenza a taglio è meno marcata, specialmente nei casi di bassi valori di momenti trasversali agenti. La trasmissione delle azioni di taglio ammessa nei modelli rigidi infinatamente plastici è confermata sia per quanto riguarda lo spostamento della zona compressa che per quanto riguarda il riordinamento degli sforzi nell'armatura verticale. Tuttavia, è stato mostrato che i campi di tensione sono decisamente nonlineari in direzione trasversale (distribuzione sforzo/deformazione e inclinazione del campo di sforzi) e dipendono dall'intensità del momento trasversale applicato. Il fattore di riduzione della resistenza del calcestruzzo η_ϵ è, generalmente, piu' elevato e alti tassi di armatura a taglio o disposizioni asimmetriche permettono di equilibrare leggeri momenti senza disturbare i campi di tensione. Ciò incrementa la resistenza a taglio predetta. La deformazione longitudinale sembra avere un effetto non trascurabile sull'interazione globale e sulla resistenza ultima.

Un metodo semplificato per la verifica di travi è stato proposto. Tale metodo considera l'influenza del momento trasversale attraverso la riduzione di spessore della sezione e un tasso d'armatura a taglio effettivo. La validazione di tale modello con tests di letteratura fornisce risultati prudenti ma non del tutto conservativi e predizioni coerenti con i modi di rottura.

Un approccio ad elementi finiti multi-layered non lineari basato su un approccio EPSF è stato, successivamente, sviluppato. Tale metodologia mira ad estendere il campo di applicazione dell' approccio FEM, precedentemente proposto, tenendo conto di azioni nel piano e fuori piano (taglio e sforzo normale e momento) cui sono soggetti pannelli in calcestruzzo armato. Il calcestruzzo è modellato con elementi piani multilayered combinati con elementi a taglio fuoripiano. Tests di riferimento e validazioni con risultati sperimentali mostrano che il modello FEM proposto è uno strumento promettente per il dimensionamento e la verifica di pannelli in calcestruzzo armato soggetti a una combinazione di sforzi nel piano e momenti.

Parole chiave

Pannelli in calcestruzzo armato, campi di tensione elasto-plastici, campi di tensione multi-layered, resistenza a taglio, interazione di taglio nel piano e momento trasversale, metodo ad elementi finiti non lineari.

Contents

Notations

<u>Latin upper case:</u>

A_i	FE triangle area measured from node i
A_s	reinforcing bar cross section of the rebar FE
A_{sw}	shear reinforcement cross section area
$A^{(e)}$	area of the triangular finite element
B	reduced area for shear
E_c	modulus of elasticity of concrete
$\bar{E}_{c1_l}, \bar{E}_{c2_l}$	secant modulus of elasticity for concrete in the principal stress direction ($_1$, $_2$) in layer l
E_s	modulus of elasticity of steel
$\bar{E}_s$	secant modulus of elasticity for steel
E_h	hardening modulus of steel
F_c	vertical component of the resultant of the inclined compression field in the concrete due to shear, per unit length
$F_{c,m}$	vertical compressive force due to transverse bending, per unit length
F_s	force in the shear reinforcement, per unit length / nodal force is s direction
$F_{s,c}, F_{s,t}$	force in the shear reinforcement on the bending compression ($_c$) and bending tension side ($_s$) of the web, per unit length
F_{sw}	force in the shear reinforcement
F_x, F_y, F_z	nodal forces in x, y and z direction
G	shear modulus
L	span, distance between supports
L_i	quadratic shape function at i
M	mesh fineness
M_i	quadratic shape function at i

M_s	nodal moment about the s axis (local coordinate system)
M_x, M_y	nodal moment about the x and y axis
N_i	linear shape function at node i
$\bar{N}_i$	quadratic shape function at node i
R	resultant of stirrup forces $F_{s,t}$ and $F_{s,c}$, force per unit length
Q	concentrated load
Q_{EPSF}	failure load according to elastic-plastic stress field calculation
$Q_{EPSF,m}$	failure load according to elastic-plastic stress field calculation with simplified approach for the transverse bending moment
$Q_{ML-EPSF}$	failure load according to multi-layered elastic-plastic stress field calculation
Q_{exp}	experimental failure load
Q_x, Q_y, Q_z	in-plane (x, y) or out-of-plane (z) nodal load acting on the FE model
V	shear force, in-plane shear force
V_{lim}	shear force, limit between predominant shear and predominant transverse bending
V_R, $V_{R,c}$, $V_{R,s}$	shear resistance of the element, of the concrete (c), of the reinforcement (s)
V_{R0}	shear resistance in case of simultaneous concrete and shear reinforcement failure, $V_{R0} = V_{R,s} = V_{R,c}$

Latin lower case:

a	distance between loads / element size
a_i, a_j, a_k	parameter of the linear shape function N_i at node i
a_s	reinforcement cross section area, per unit length
a_{sw}	shear reinforcement cross section area, per unit length
b	width of the OP FE
b_e	minimum web width required to resist the shear force
b_i, b_j, b_k	parameter of the linear shape function N_i at node i
b_m	web width required to resist the transverse bending moment
b_w	web width
$b_{w,eff}$	effective web width, for the simplified verification method
b_0	width between the legs of a stirrup ($b_0 = b_w - 2b'$)

b'	position of shear reinforcement in the width of the web, measured from surface
c_i, c_j, c_k	parameter of the linear shape function N_i at node i
$d\gamma_{xy}$	shear strain increment in the $x - y$ plane
$d\gamma_{xy0}$	shear strain increment in the element mid-plane
$d\varepsilon_x, d\varepsilon_y$	strain increment in x or y direction
$d\varepsilon_{x0}, d\varepsilon_{y0}$	strain increment in x or y direction in the element mid-plane
$d\varepsilon_1, d\varepsilon_2$	increment of first and second principal strain ($d\varepsilon_1 \geq d\varepsilon_2$)
$d\chi_x, d\chi_y, d\chi_{xy}$	curvature increment in x and y direction, torsion curvature increment
e_c	eccentricity of the stress field resultant in the concrete
err_F, err_M	FEM error regarding nodal forces (F) and nodal moments (M)
f_c	average compressive strength of concrete (cylinder)
f_{cd}	design value of the concrete compressive strength
$f_{c,red}$	reduced concrete compressive strength according to Swiss Code SIA162:1989 [SIA89] ($= k_c f_{cp}$ in SIA262:2013)
f_{cp}	equivalent plastic concrete compressive strength
$f_{cp,eff}$	effective concrete compressive strength
f_s	yield stress of reinforcing steel
f_{sd}	design value of the reinforcing steel strength
h	height of the OP FE
i	layer number in ML-EPSF model / node number in the FE model
k	analytical variable / iteration step
k_c	concrete strength reduction factor for transverse tensile strain
l	analytical variable / layer number in the ML-IP FE / length of OP and rebar FE
l_{ij}	length of the element side between nodes i and j
l_x, l_y	panel size in x and y direction
m	transverse moment, out-of-plane moment, per unit length / analytical variable
m_c	transverse bending moment equilibrated by the concrete, per unit length

Notations

m_{cx}, m_{cy}, m_{cxy}	out-of-plane moment carried by concrete in x or y direction, torsional moment
m_{exp}	experimental transverse failure moment
m_{lim}	transverse moment, limit between predominant shear and predominant transverse bending
m_q	applied transverse moment, load per unit length
m_{R0}	plastic out-of-plane, transverse bending resistance
m_s	transverse bending moment equilibrated by the shear reinforcement, moment per unit length
m_{sx}, m_{sy}, m_{sxy}	out-of-plane moment carried by steel in x or y direction, torsional moment
m_x, m_y, m_{xy}	out-of-plane moment in x or y direction, torsion moment, per unit length
$\bar{m}$	limit of the transverse moment according to Thürlimann [Thü77]
n	number of ML-IP elements connected to the OP element
n_c	number of concrete layers
n_{cx}, n_{cy}, n_{cxy}	force (stress resultant) in the concrete in x or y direction, shear force in the $x-y$ plane, force per unit length
n_{gdof}	number of nodal degrees of freedom in the FE model ($n_{gdof} = 5 \cdot n_n$)
n_n	number of nodes in the FE model
n_s	number of steel layers
$n_{s,c}, n_{s,t}$	force in the steel reinforcement on the bending compression ("c") and bending tension side ("t") of the web, per unit length
n_{sx}, n_{sy}, n_{sxy}	force (stress resultant) in the steel in x or y direction, shear force in the $x-y$ plane, force per unit length
n_x, n_y, n_{xy}	stress resultant, in-plane force in x or y direction, shear force in $x-y$ plane, per unit length
$n_{y,c}, n_{y,t}$	yield limit of the reinforcement on the on the compression (c) or tension (t) side, force per unit length
q	distributed load, per unit length
s	stirrup spacing / coordinate in the element plane or element axis
t	element thickness
u	in-plane translational degree of freedom, displacement in x direction
v	in-plane translational degree of freedom, displacement in y direction

w	out-of-plane translational degree of freedom, displacement in z direction / out-of-plane deflection
w_a	analytical value of the out-of-plane deflection
x	coordinate in the plane of the element
y	coordinate in the plane of the element
z	lever arm of internal forces / coordinate along the normal to the element mid-plane
$\bar{z}$	eccentricity of the reinforcing bar in the rebar FE
$\bar{z}_i$	distance to the centre of the i-th layer

<u>Latin letters for matrices and vectors</u>

$\mathbf{B}$, $\mathbf{B}_i$	element and nodal generalized strain matrix
$\mathbf{B}_m$, $\mathbf{B}_b$, $\mathbf{B}_s$	membrane, bending and shear contribution to generalized strain matrix $\mathbf{B}$
$\mathbf{F}$	global force vector (of the entire FE model)
$\mathbf{F}^{(e)}$	element nodal force vector
$\mathbf{F}'^{(e)}$	element nodal force vector in local coordinates
$\mathbf{F}_{ext}$	global load vector (of the entire FE model)
$\mathbf{F}_{ext}^{(i)}$	nodal load vector at node i ($Q_{xi}, Q_{yi}, Q_{zi}, M_{xi}, M_{yi}$)
$\mathbf{F}_i^{(e)}$	nodal force vector at node i ($F_{xi}, F_{yi}, F_{zi}, M_{xi}, M_{yi}$)
$\mathbf{F}_{inc}$	global force vector resulting of the incremented displacement field $\mathbf{a}_{inc}$
$\mathbf{F}_{res}$	global residual force vector, unbalanced forces
$\mathbf{F}_{pi_l}$	vector of in-plane forces in $x - y$ coordinates at node i in layer l
$\mathbf{F}_{1i_l}$	vector of in-plane forces in principal stress directions at node i in layer l
$\mathbf{K}$	stiffness matrix
$\mathbf{K}_{sec}$	global secant stiffness matrix (of the entire FE model)
$\mathbf{N}_i$	shape function matrix for node i
$\mathbf{R}$	global reaction force vector
$\mathbf{S}$	transformation matrix
$\mathbf{T}_1$, $\mathbf{T}_2$	transformation matrices
$\mathbf{a}$	global displacement vector (of the entire FE model)

$\mathbf{a}^{(e)}$	element displacement vector
$\mathbf{a}_i^{(e)}$	displacement vector at node i $(u_i, v_i, w_i, \theta_{xi}, \theta_{yi})$
$\mathbf{a}_{inc}$	incremented global displacement field vector
$d\mathbf{F}$	global force increment vector
$d\mathbf{a}$	vector of displacement increments for next iteration
$\mathbf{k}_j$	vector with coefficients of the secant stiffness matrix at degree of freedom j
$\mathbf{u}$	interpolated displacement field vector $(u, v, w, \theta_x, \theta_y)$
$\mathbf{u}'$	interpolated displacement field in local coordinate system

<u>Greek upper case:</u>

$\Gamma^{(e)}$	perimeter of triangular element
ΔF	variation of the force in the shear reinforcement, per unit length
Δb_w	web width reduction, in the simplified verification method
ΔM	moment variation
Δm	variation of / supplementary transverse bending moment, per unit length

<u>Greek lower case:</u>

α	direction of the first principal strain relative to the x axis in the FE model
β	direction of the reinforcing bar, angle measured from the x-axis
β_{ij}	orientation of the element sided ij with respect to the x axis
γ	shear deformation
γ_{sz}	out-of-plane shear deformation along s-axis or IP finite element border
γ_{xy}	shear strain in the $x - y$ plane
γ_{xz}, γ_{yz}	out-of-plane shear deformation
γ_{xy0}	shear strain in the element mid-plane
γ_1	shear deformation leading to highest shear resistance
δ	displacement increment
ε_{cu}	ultimate deformation of concrete
ε_s	strain in reinforcing steel / strain in reinforcing bar of the rebar FE
ε_{s0}	longitudinal deformation in the reference plane of the rebar FE

ε_{su}	ultimate deformation of reinforcing steel
ε_{sy}	yield strain for reinforcing steel ($\varepsilon_{sy} = f_s/E_s$)
$\varepsilon_x, \varepsilon_y, \varepsilon_z$	strain, deformation in x, y or z direction
$\varepsilon_{x0}, \varepsilon_{y0}$	strain in x or y direction in the element mid-plane
$\varepsilon_1, \varepsilon_2$	first and second principal strain ($\varepsilon_1 \geq \varepsilon_2$)
ζ	percentage of total vertical load carried by the stirrups on the tension side
η_{fc}	concrete strength reduction factor for brittle behaviour of concrete
η_ε	concrete strength reduction factor for transverse strain
θ	inclination of the compression field, of the second principal stress
θ_s	rotation of the normal vector about the s axis
θ_x, θ_y	rotation of the normal vector about the x and y axis
θ_0	inclination of the compression field in case of simultaneous concrete and shear reinforcement failure
λ_c, λ_t	amount of activated shear reinforcement on the bending compression (c), tension (t) side
λ_m	average amount of activated shear reinforcement
ν	Poisson's coefficient
ξ	natural coordinate of a linear element
ξ_i	area coordinates for triangles
ρ	longitudinal reinforcement ratio
ρ_x, ρ_y	reinforcement ratio in x or y direction
ρ_w	shear reinforcement ratio
$\rho_{w,c}, \rho_{w,t}$	shear reinforcement ratio of the bending compression (c), tension (t) side
$\rho_{w,eff}$	effective amount of shear reinforcement, in the simplified verification model
σ_c	concrete stress
σ_{cx}, σ_{cy}	concrete compressive stresses in x or y direction
σ_{c1}, σ_{c2}	first and second principal stress in concrete ($\sigma_{c1} \geq \sigma_{c2}$)
σ_s	stress in the reinforcing steel
σ_{sx}, σ_{sy}	stress in the reinforcing layer in x or y direction

σ_p	prestressing stress
σ_v	vertical component of the inclined compressive stress σ_c
σ_x, σ_y	in-plane stress in x or y direction
σ_1, σ_2	first and second principal stress $(\sigma_1 \geq \sigma_2)$
τ_c	nominal tangential stress in concrete
τ_{cxy}	concrete shear stress in the $x - y$ plane
τ_{sxy}	shear stress in the reinforcing layer in $x - y$ plane
τ_{xy}	in-plane shear stress
ϕ	name of a transcendental function / orientation of the OP and rebar FE axis s with respect to the x axis
ϕ_{ij}	angle of orientation of the element side ij with respect to the x axis
ϕ_x, ϕ_y	rotation about x and y axis: difference between rotation of the normal vector and the slop $(\phi_x = \theta_x - \partial w/\partial x)$
χ_s	curvature in s direction
$\chi_x, \chi_y, \chi_{xy}$	curvature in x and y direction, torsion curvature
ω	mechanical shear reinforcement ratio / analytical variable

Greek letters for matrices and vectors

$\boldsymbol{\delta}_j$	vector of displacement increments for degree of freedom j
$\boldsymbol{\varepsilon}$	strain vector $(\varepsilon_x, \varepsilon_y, \gamma_{xy}, \gamma_{xz}, \gamma_{yz})$
$\hat{\boldsymbol{\varepsilon}}$	generalized strain vector
$\hat{\boldsymbol{\varepsilon}}_b$	generalized strain vector for bending effects, curvatures $(\chi_x, \chi_y, \chi_{xy})$
$\hat{\boldsymbol{\varepsilon}}_m$	generalized membrane strain vector, at the element middle plane $(\varepsilon_{x0}, \varepsilon_{y0}, \gamma_{xy0})$
$\boldsymbol{\varepsilon}_p$	strain vector for in-plane deformations $(\varepsilon_x, \varepsilon_y, \gamma_{xy})$
$\boldsymbol{\varepsilon}_s$	strain vector for out-of-plane shear deformations $(\gamma_{xz}, \gamma_{yz})$
$\hat{\boldsymbol{\varepsilon}}_s$	generalized strain vector for out-of-plane shear deformations $(\gamma_{xz}, \gamma_{yz})$
$\boldsymbol{\varepsilon}_1$	principal strain vector $(\varepsilon_1, \varepsilon_2)$
$\hat{\boldsymbol{\sigma}}_b^{(e)}$	element bending stress resultants (m_x, m_y, m_{xy})
$\hat{\boldsymbol{\sigma}}_m^{(e)}$	element membrane stress resultants (n_x, n_y, n_{xy})

$\boldsymbol{\sigma_p}$ vector of in-plane stresses (σ_x, σ_y, τ_{xy})

$\boldsymbol{\sigma_1}$ principal stress vector (σ_1, σ_2)

Indices

$\cdot_a$	analytical value
$\cdot_c$	on the bending compression side of the web / for concrete
$\cdot_{exp}$	experimental value / expected value
$\cdot_F$	nodal force
$\cdot_i$	number of the layer the ML-EPSF mode / node number in the FE model
$\cdot_j$	node number
$\cdot_k$	node number / at iteration step k
$\cdot_l$	layer number in the FE model
$\cdot_M$	nodal moment
$\cdot_{ML-EPSF}$	according to multi-layered elastic-plastic stress field
$\cdot_{max}$	maximum value
$\cdot_{SIA262:2013}$	according to Swiss Code SIA262:2013 [SIA13]
$\cdot_s$	for steel
$\cdot_t$	on the bending tension side of the web
$\cdot^T$	matrix transpose

Additional symbols and abbreviations

↗	increasing value
↘	decreasing value
→	value tends to
∝	proportional
COV	coefficient of variation
EP	elastic-plastic
EPSF	elastic-plastic stress field
FE	finite element
FEM	finite element method
IP	in-plane

ML	multi-layered
ML-EPSF	multi-layered elastic-plastic stress field
NL	non-linear
OP	out-of-plane
RP	rigid-plastic
RPSF	rigid-plastic stress field
gdof	global degree of freedom
tol	tolerance for acceptable error of the FEM predictions

Chapter 1   Introduction

1.1   Problem statement

Plane reinforced concrete structural elements like flat shells or panels are used in a large variety of structures. Although their principal static function is mostly to carry forces that act in the plane of the element, boundary conditions, external actions and connections to other structural elements can introduce additional out-of-plane actions. Spatial structures composed of multiple flat elements like folded shells or box-girder bridges are typical examples to this.
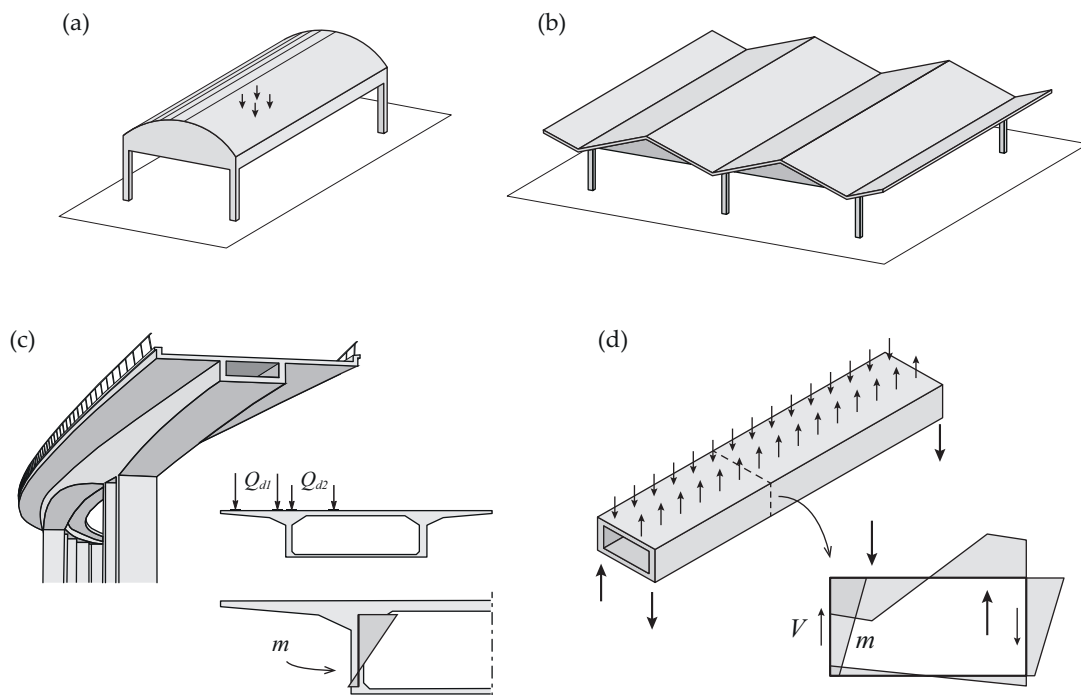
Figure 1.1   Spatial structures composed of plane structural elements: (a) long span barrel vault with edge beam; (b) Folded plat shell structure; (c)-(d) box-girder structures subjected to in-plane shear and transverse bending in the webs.

The design of structural concrete elements subjected to in-plane loads like longitudinal shear and bending has been extensively studied over the past century. Several equilibrium based methods, from strut-and-tie models to stress fields and non-linear finite element analyses, exist and can be consistently used when stirrups are arranged. A topic where less

research effort has been devoted to is the interaction between in-plane (longitudinal) shear and out-of-plane (transverse) bending that is though present in numerous structures and in particular in box-girder bridges.

Girder elements are mainly subjected to membrane actions resulting from longitudinal shear, bending and torsion. However, various out-of-plane actions can lead to additional transverse bending moments in the girder webs. In box-girder elements these moments are typically introduced by the connection of the web with the top and bottom slabs. Depending on the bending stiffness of that connection, loads on the cantilever or in the middle span of the deck slab lead to more or less significant transverse bending moments. In case of none or insufficient transverse stiffeners, introduction of longitudinal torsion additionally increases the out-of-plane moment. In principle, box girder webs are thus always subjected to a combination of in-plane shear and out-of-plane bending moments.

Out-of-plane actions in beam webs and in reinforced concrete elements in general question the applicability and thus the safety of design methods for plane elements that neglect these actions. Indeed, the very few experiments that had been conducted on plates and beam elements with combinations of in-plane and out-of-plane loads, such as by Kirschner [Kir86] and Kaufmann [Kau76], have suggested that the actual in-plane resistance might be more or less significantly affected by the out-of-plane actions.

However, due to a lack of experimental data and knowledge on the actual behaviour under the combined action of in-plane and out-of-plane loads, especially in beam-like elements, the interaction is typically not accounted for as such, or treated in a simplified manner, in practice. A commonly used method for box-girder webs for instance, is to neglect the interaction and to perform independent analyses for longitudinal shear and transverse bending and then summing the required shear reinforcement for both actions. Although mostly conservative, this approach is not consistent with the actual behaviour of the web at failure. Additionally, it potentially leads to excessive amounts of shear reinforcement and to inconsistent and unsafe superposition of concrete compressive stresses.

Furthermore, higher traffic loads, deck slab enlargements, redeployment of traffic lanes and many other modifications that are to be expected in the near future will lead to a significant increase of the proportion of the transverse bending actions in girder elements. The topic on in-plane shear transverse bending interactions will thus considerably rise in importance, especially with regard to the maintenance of existing structures.

A better understanding of the interaction between in-plane and out-of-plane forces and the subsequent influence on the in-plane resistance is therefore needed in order to develop more precise and kinematically consistent design and verification methods.

1.2   Objectives

The objective of this research is to provide tools that help improving the knowledge about the phenomenon of the interaction between in-plane and out-of-plane forces in plane reinforced concrete elements in general and about the effect of transverse bending on the longitudinal shear resistance of beam-like elements in particular. A novel approach based on plane elastic-plastic stress fields is developed to this purpose. Applied to a unitary web segment it allows for a detailed insight into the behaviour of the stress field under the action of transverse bending as well as to identify parameters that play a major role in the overall interaction mechanism.

Several simplified equilibrium based models for the assessment of the effect of transverse bending in beam webs exist. They generally provide lower bound solutions according to the theory of plasticity, but simultaneous predict a very strong influence of the transverse moment on the shear resistance. These models are believed to give highly conservative predictions in some cases and to be non-representative of the actual behaviour of the web at failure. While safe estimates of the bearing capacity can be considered to be acceptable for the design of new structures, the assessment of existing structures may require more precise estimations of the actual resistance in order to avoid potentially unnecessary and costly reinforcement. This thesis investigates these models with respect to the proposed elastic-plastic stress field method which leads to the proposition of an enhanced simplified verification method for beam elements in practice.

As observed in the experiments on beams by Kaufmann and Menn [Kau76], the actual behaviour of the entire structural element cannot always be accurately predicted by simplified models that provide a local prediction of the shear resistance of a web segment. First of all, because in most real structural elements stress fields are not uniform and secondly, because other structural components (e.g. flanges) as well as other failure modes (e.g. yielding of longitudinal reinforcement) that are not considered in the simplified models might have a significant influence on the actual bearing capacity. Thus, to get a better understanding of the influence of out-of-plane actions on the in-plane resistance of more complex structural elements than panels, a general tool that is able to accurately assess the longitudinal (i.e. in-plane) as well as the out-of-plane behaviour of entire structural elements is required. To this purpose, a non-linear finite element program for the investigation of in-plane and out-of-plane actions on plane reinforced concrete elements is developed in this thesis.

1.3   Methodology and personal contributions

A literature review on the effect of out-of-plane actions on the in-plane resistance of plane reinforced concrete elements is performed in order to become familiar with the subject. Relevant models and experimental data are presented in Chapter 2. A particular attention

is payed to the shear transfer mechanism admitted in several rigid-plastic stress field (RPSF) interaction models for beam webs. Therefore the equilibrium based methods by Thürlimann [Thü77] and Menn [Men86] are investigated in detail and followed by a critical review on the main assumptions, in particular the stress field inclination and the concrete strength reduction factor. The analysis allowed as well illustrating that the rigid-plastic (RP) models predict a very strong in-plane shear transverse bending interaction leading thereby in theory to substantial losses in the shear resistance, already for small transverse bending moments. A kinematic and static compatible model presented by Marti [Mar80] (exact solution according to the theory of plasticity) however shows that the influence is less pronounced. Chapter 2 also introduces the theoretical basis of the elastic-plastic stress field (EPSF) method [Fer07] that is later used to develop enhanced analysis tools.

Chapter 3 presents a novel multi-layered elastic-plastic stress field approach (ML-EPSF) in order to overcome certain limitations of the existing interaction models. The multi-layered stress fields are not only in equilibrium with the in-plane forces and transverse bending moments but they result as well from a kinematically consistent model for in-plane and out-of-plane behaviour. While simultaneously respecting the plastic strength of the material, they eventually lead to an exact solution at failure (according to the theory of plasticity). The ML-EPSF approach is applied to the case of beam webs in order to analyse the phenomenological behaviour of the stress field that develops under the action of transverse bending. This analysis has been presented and rewarded at the *fib* International PhD Symposium in Canada [Bac14]. The predictions are later compared to the existing interaction models and the out-come of these observations is used to propose an enhanced simplified verification method for beam elements, published in [Mut16]. The ML-EPSF approach is as well the basis of the proposed non-linear finite element program. The main personal contributions regarding the topic of combined membrane and bending actions in plane reinforced concrete elements are enlisted hereafter:

- Development of a general ML-EPSF approach to establish stress fields that are statically as well as kinematically compatible with in-plane actions (membrane and shear) and transverse bending in plane reinforced concrete elements.

- Development of a ML-EPSF panel element to analysis the in-plane shear transverse bending interaction in a web segment and of a procedure to establish explicit interaction diagrams for the ultimate limit state resistance (exact solution according to the theory of plasticity). Compared to existing models, it provides a continuous transition between pure in-plane shear and pure transverse bending behaviour and it does not require assumptions regarding the stress field inclination and the concrete strength reduction factor because they are determined automatically from the kinematic compatibility conditions of the ML-EPSF approach.
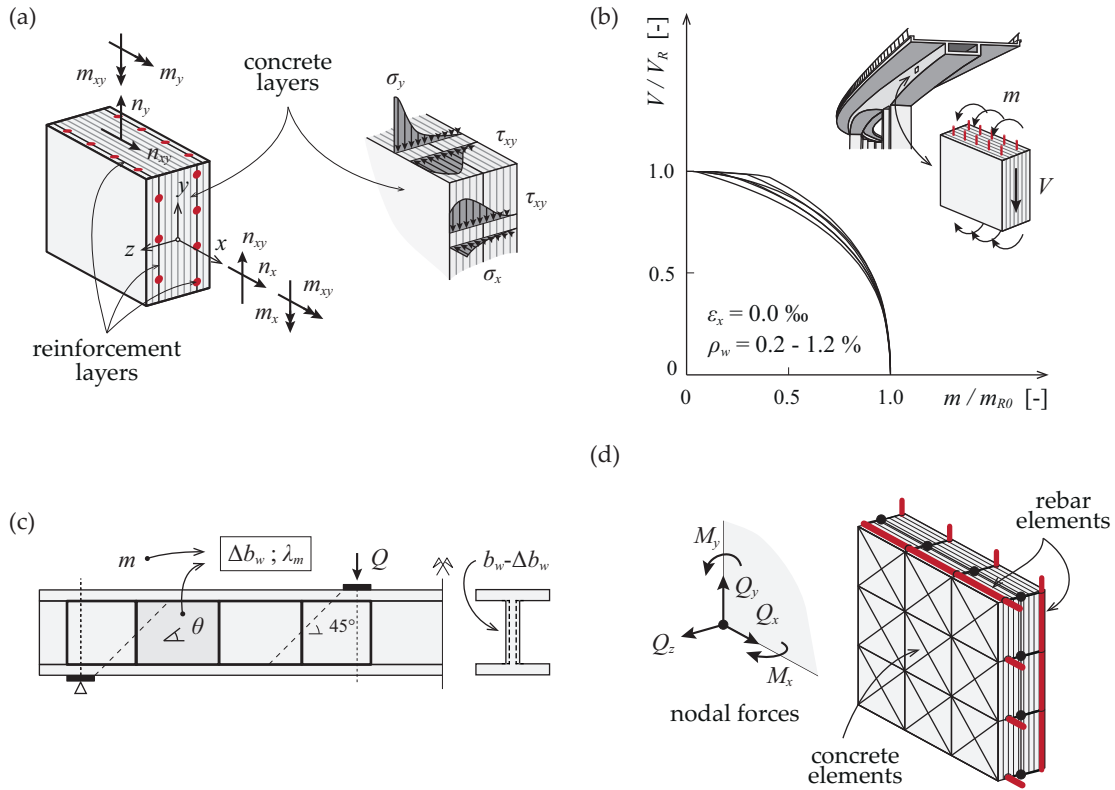
Figure 1.2 Application of the elastic-plastic stress field method to the reinforced concrete elements under in-plane and out-of-plane actions: (a) multi-layered elastic-plastic stress field approach; (b) in-plane shear transverse bending interaction in a beam web segment according to the ML-EPSF panel element; (c) simplified verification method for beams with transverse bending in the web and (d) non-linear finite element method for plane reinforced concrete elements subjected to in-plane actions and out-of-plane actions (forces and moments).

- Validation of the main principles of the shear transfer mechanisms admitted in the rigid-plastic stress field interaction models by comparison to the kinematic compatible ML-EPSF predictions. The model proposed by Menn [Men86] was found to be the most consistent with the actual behaviour of the web segment.

- Confirmation that the effect of transverse bending on the in-plane shear resistance is less pronounced than predicted with RP interaction models, especially in the range of small transverse bending moments.

- It is pointed out that the RP models are very strong simplifications of the actual stress fields that develop under transverse bending, which are highly non-uniform in the transverse direction of the web (inclination, distribution of stresses, concrete strength reduction factor) and additionally strongly depend on the intensity of the acting transverse bending moment.

5

- It is shown that moderate compression due to bending has a favourable effect on the stress field and thereby reduces the loss of shear resistance caused by the transverse bending moment (average stress field inclination and effective concrete compressive strength increase).

- It is found that the longitudinal deformation of the web, not accounted for in former interaction models, has a substantial influence on the ultimate resistance under combined action of in-plane shear and transverse bending.

- Proposition of a simplified method for the verification of beam-like elements in practice. The plane EPSF finite element method is used to predict the actual longitudinal behaviour of a beam element under in-plane actions (shear and longitudinal bending), meanwhile the effect of the transverse bending moment is accounted for in a simplified manner. The simplified verification method is validated with the experiments on beam elements by Kaufmann and Menn [Kau76].

- It is shown that the influence of the transverse bending moment on the bearing capacity of beams is probably significantly smaller than predicted by sectional analysis tools like the proposed ML-EPSF panel element or the RP interaction models from the literature. But more experimental data on beam elements is required to corroborate this observation and to quantify the actual effect of the transverse bending moment in these elements.

The analyses have shown that in order to advance in the knowledge about the effect of transverse bending on the shear resistance of beams, it is necessary to account for the behaviour of the entire structural element and in particular internal force redistributions. To this purpose and to provide as well a tool with a wider field of application, a non-linear finite element method based on the ML-EPSF approach is proposed in Chapter 4. The development of the finite element program included the conception and formulation of three novel finite elements for modelling the behaviour of concrete and reinforcing steel; the implementation of an appropriate solution procedure and convergence criteria for the non-linear problem, as well as the development of pre-processing and post-processing tools for modelling and analysis of the results. The finite element program is validated by means of benchmark tests and comparisons to experiential test data from the literature. Sensitivity analyses regarding modelling parameters such as the number of concrete layers, mesh fineness and element slenderness have also been performed. The personal contribution thus consists in the following:

- Proposition of non-linear finite element method for the assessment of reinforcement concrete structural elements subjected to in-plane (normal and shear) and out-of-plane (bending and shear) actions.

Chapter 2   State of the art

Experimental tests on beams [Kup73, Kau76, Ewa77 and Gas03] and shell elements [Kir86, Pol94] have shown that the membrane state-of-stress resulting from in-plane shear can be significantly disturbed by the presence of out-of-plane bending moments. This led to a reduced shear resistance, especially in cases where brittle failure due to crushing of concrete was expected. Consequently, neglecting the interaction and performing independent analyses for longitudinal shear and transverse bending, and then summing the required shear reinforcement, is not consistent with the actual behaviour of the web at failure. Furthermore, it potentially leads to excessive amounts of reinforcement and to inconsistent and unsafe superposition of concrete compressive stresses.

For the assessment of beam webs under the combined action of in-plane shear and transverse bending a number of consistent design approaches that are grounded on the lower bound theorem of the theory of plasticity are proposed in the literature [Thü77, Men86, Stu90 and Gas03]. In the latter, the shear-transverse bending interaction is investigated by means of equilibrium based models that assume rigid-perfectly plastic behaviour for concrete and steel. The models are based on the classical rigid-plastic stress field (RPSF) approach (basis of the Swiss code SIA262 [SIA13] and illustrated in [Mut97]) that is then adapted to account for transverse bending. The principle consists essentially in shifting the resultant of the inclined compression field in the web towards the bending compression side of the web width and by this equilibrating a transverse bending moment. This approach leads to an additional equilibrium condition (for the transverse bending moment) that then allows formulating a rigid-plastic (RP) interaction model for in-plane shear and transverse bending. Section 2.1 gives an overview on different RP interaction models and investigates two of them in detail.

Alternatively, the design of reinforced concrete members subjected to membrane and bending actions can be performed using sandwich models, as for instance indicated in the *fib* Model Code 2010 [FIB13] and Eurocode 2 [CEN05]. Sandwich models, as for example proposed by Marti [Mar90], Mancini et al. [Fan95], Figueiras [Lou95] and Seelhofer [See09] are useful tools for the ultimate limit state design of reinforced concrete slabs or elements with predominant out-of-plane loading. They are however less adapted for the analysis of beam webs where high membrane loads (due to in-plane shear) are expected. Sandwich models normally neglect the contribution of the sandwich core in the load transfer of membrane actions, which leads to safe but conservative estimates of the combined resistance for in-plane shear and transverse bending (see Mancini et al. [Gio99] and Seelhofer

[See09]). Furthermore, the sandwich model approach assumes that the stresses that result from in-plane shear and normal forces are carried by the two outer layers of the sandwich model. This is however not consistent with the behaviour observed in experimental tests, where the stress field in the concrete only acts on one side in the element thickness, in order to a counterbalance the transverse moment. The sandwich models are not appropriate to represent this behaviour accurately; consequently they are not further investigated in this research project.

The RPSF approaches provide lower bound estimates of the strength of a member [Mut97]. An approach to investigate the in-plane shear – transverse bending interaction on the basis of a kinematically compatible stress field has been proposed by Marti [Mar80]. Marti's model that lead to an exact solution according to the theory of plasticity is presented in section 2.3. A more general procedure for automatic development of stress fields that is based on the elastic-plastic stress field (EPSF) method proposed by Fernández Ruiz and Muttoni [Fer07] and that is the basis of the proposed advanced interaction model as well as the finite element method developed in this thesis is presented section 2.4.

2.1 Rigid-plastic stress field interaction models

The issue of longitudinal shear and transverse bending in beam webs was early addressed by Kupfer in 1969 (as cited in [Ewa77]). Kupfer assumed that under the action of a transverse bending moment the compression field in the web inclines towards the bending compression side. For a given shear load Kupfer computed a maximum admissible concrete compressive stress at the web-flange section which allowed him to formulate a limitation for the transverse bending moment (in the uncracked state). In 1973 (as cited in [Ewa77]), Jungwirth and Baumann adopted his principle, i.e. that the transverse bending moment can be resisted by the vertical component of the inclined compression forces (due to longitudinal shear) that is eccentric relative to the web axis. They additionally proposed a formulation for supplementary vertical bending reinforcement. Although the equilibrium of forces and moments is fulfilled at the considered web section, the assumptions are not, or only poorly, consistent with the actual behaviour of web at failure. Additionally, no effect of the transverse bending moment on the actual shear strength is considered.

In engineering practice, the design of reinforced and prestressed concrete members is generally performed using a stress field approach and in particular the rigid-plastic stress field (RPSF) method, which constitutes the basis of the Swiss code SIA 262:2013 [SIA13]. In 1977, Thürlimann [Thü77] extended the classical RPSF approach for longitudinal shear, bending and torsion to the case of additional transverse (out-of-plane) bending and deduced from this an interaction relationship between the in-plane shear resistance and the acting transverse bending moment. In Thürlimann's model, similarly to Kupfer's idea, the inclined compression field for shear is shifted towards the exterior face of the web such that the transverse bending moment is resisted by the vertical component of the eccentric concrete
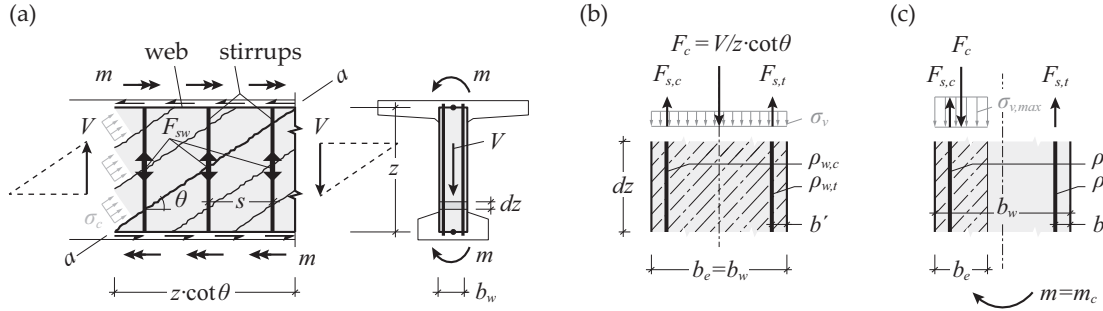
Figure 2.1 The RPSF method for in-plane shear and transverse bending [Thü77]: (a) web elevation with inclined compression field and web cross section with internal forces; equilibrium of forces in a web segment cross section (b) in pure shear and (c) with a moderate transverse bending moment.

compressive stress resultant (figure 2.1). Thürlimann's model allows carrying supplementary transverse bending moments by rearranging the tensile forces between the stirrups on both sides of the web. This approach that is grounded on the lower bound theorem of the theory of plasticity (static theorem) was later adopted and extended by several authors. In the following, the basic principle of the rigid-plastic (RP) interaction model as well as various extensions developed different authors such as Thürlimann [Thü77], Menn [Men86], Stucchi [Stu90] and Gaspar [Gas03] will be developed in particular.

2.1.1 The main principle

The rigid-plastic interaction models for in-plane shear and transverse bending are direct applications of the RPSF method, thus they have to satisfy the equilibrium of forces and the yield conditions of the materials. According to the usual approach for beam design, the beam is split into a tension chord, a web and a compression chord. The analysis of the in-plane shear transverse bending interaction is then performed on a shear panel representing the web of a reinforced concrete beam or box girder element failing in shear due to yielding of the shear reinforcement.

The rigid-plastic stress field that develops in the web at failure is shown in figure 2.1a. It is in equilibrium with the internal forces: the in-plane shear force V and the out-of-plane bending moment m. The stress field that is composed of an inclined compression field in the concrete and the stirrup forces F_{sw} is a licit solution according to the theory of plasticity (together with the top and bottom tension cord, not represented in this figure). The state-of-stress is defined as follows.

The compressive stresses in the concrete σ_c due to shear are inclined at an angle θ and are assumed to be constant in the depth of the web (uniform stress block).

$$\sigma_c = \frac{V}{b_w \cdot z \cdot \sin\theta \cdot \cos\theta} \tag{2.1}$$

$$\tau_c = \frac{V}{b_w \cdot z} \tag{2.2}$$

The stirrups forces due to shear are determined along a section $a - a$ parallel to the compression field (see figure 2.1a). The stirrup force F_s per unit length of the beam is expressed as follows, where F_{sw} is the force per stirrup and s the stirrup spacing.

$$F_s = \frac{F_{sw}}{s} = \frac{V}{z \cdot \cot\theta} \tag{2.3}$$

The stirrup force F_s is always in equilibrium with vertical component of the compression field F_c (per unit length), see equilibrium of a web section in the figures 2.1b-c, where $F_{s,t}$ and $F_{s,c}$ are the stirrup forces on each side of the web.

$$F_c = F_s = F_{s,t} + F_{s,c} = \frac{V}{z \cdot \cot\theta} \tag{2.4}$$

In pure shear condition, figure 2.1b, the vertical components σ_v of the compressive stresses σ_c are uniformly distributed over the entire web width b_w and the stress resultant F_c is centred.

$$\sigma_v = \frac{F_c}{b_w} = \frac{V}{b_w \cdot z \cdot \cot\theta} = \tau_c \cdot \tan\theta = \sigma_c \cdot \sin^2\theta \tag{2.5}$$

A transverse bending moment m can then be resisted by shifting the resultant F_c towards the bending compression side of the web, figure 2.1c. The inclined compression field is acting on a reduced section of the web width ($b_e < b_w$). The compressive stress distribution σ_v, respectively σ_c, is again approximated by a uniform stress block over the width b_e. No changes in the stirrup forces are required (compared to the state-of-stress for $m = 0$, figure 2.1b). The equilibrium of vertical forces, equation 2.4, is still verified and the equilibrium of moment is expressed as follows:

$$m = \frac{1}{2} \cdot F_c \cdot (b_w - b_e) \tag{2.6}$$

The maximum moment m_c that can be equilibrated by this procedure is limited by the minimum web width b_e required to resist the shear force V, i.e. when the stresses in the shear strut reach the maximal allowable stress for concrete in shear. At limit state, the two equilibrium conditions for vertical forces (eq. 2.4) and transverse moments (eq. 2.6) thereby allow for the establishment of an explicit interaction model for in-plane shear and transverse bending ($m - V$).

It should be noted that in such RP interaction models, the eccentricity relative to the web axis of the inclined compression due to shear generates additional torsion and bending
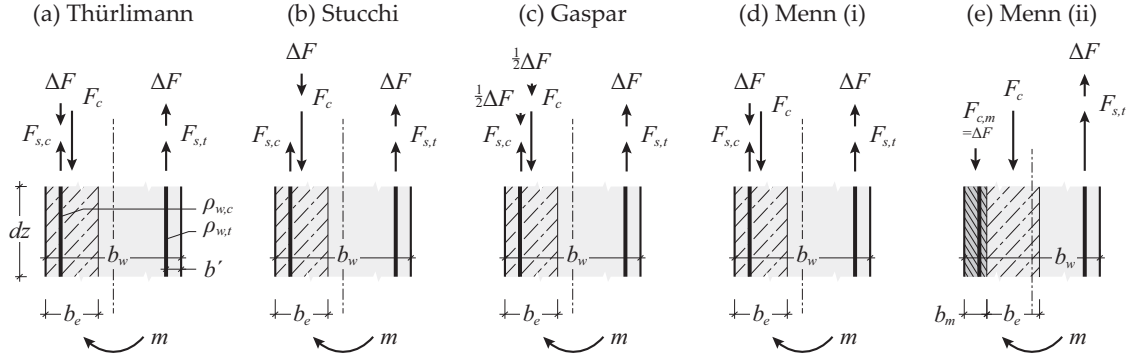
Figure 2.2   Schematics of the transverse equilibrium of a web segment subjected to a high transverse bending moments. RPSF models according to: (a) Thürlmann [Thü77]; (b) Stucchi [Stu90]; (c) Gaspar [Gas03] and (d-e) Menn [Men86].

moments in the longitudinal direction of the web (about the vertical axis). They are considered as generalized reaction forces and they potentially lead to a slight modification of the stress distribution in the upper and lower flanges of the beam before being transferred to the transverse supports of the structural element.

2.1.2   Various equilibrium based solutions

In the rigid-plastic stress field solution presented in the previous section (figure 2.1) the transverse bending resistance is exclusively provided by the eccentricity of the compression field. Some authors propose different modifications of this model in order to increase the predicted resistance in case of higher levels of transverse bending moments ($m > m_c$).

Thürlimann [Thü77] assumes that the supplementary transverse moment $\Delta m = m - m_c$ can be resisted by changing the stirrup forces by ΔF while preserving the equilibrium of forces, figure 2.2a. Stucchi [Stu90] recommends increasing the force in the stirrups on the flexural tension side by ΔF. The equilibrium of forces is maintained by applying an equivalent compression force ΔF on the shear strut, figure 2.2b. The tensile force $F_{s,c}$ in stirrups on the bending compression side remains unchanged.

In order to account for a more realistic kinematic bending behaviour of the web cross section, Gaspar [Gas03] combines the previous ideas by Thürlimann and Stucchi, figure 2.2c. Gaspar's model equilibrates the addition tensile force ΔF, due to Δm, at the same time by an increase of the concrete compression force on the shear strut F_c and a reduction of the stirrup force $F_{s,c}$ on the bending compression side.

Menn [Men86] proposes to distinguish between two different regimes: (i) predominant shear and (ii) predominant transverse bending. In the first situation, the additional moment Δm is balanced by variations in the stirrup forces, figure 2.2d. This is equivalent to Thürlimann's proposal, but it is only applicable as long as the stirrups on the bending compression side are still in tension, $F_{s,c} > 0$. For higher transverse bending moments (situation
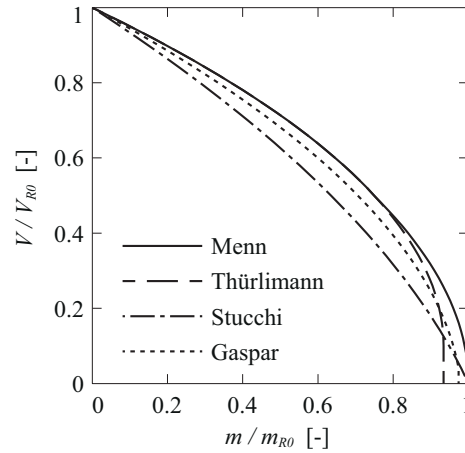
Figure 2.3 Rigid-plastic in-plane shear V - transverse bending m interaction models according to Thürlimann [Thü77], Menn [Men86], Stucchi [Stu90] and Gaspar [Gas03], evaluated for a typical case: $\theta = 30°$, $k_c = 0.55$, $f_{cd} = 20$ MPa, $f_{sd} = 435$ MPa, $\rho_w = 0.6\%$, $\rho_{w,c}/\rho_{w,t} = 1.0$ and $b'/b_w = 0.1$.

(ii)), the tensile force $F_{s,c}$ vanishes and is replaced by a compressive force $F_{c,m}$ acting on the outer layer of the flexural compression faces of the web. As a consequence, the resultant of the concrete compressive force due to shear F_c shifts towards the centre of the web, figure 2.2e.

A comparison of the different rigid-plastic interaction models by means of a shear-transverse bending ($m - V$) diagram is shown in figure 2.3. The overall behaviour of the models is very similar; with increasing transverse bending moment the predicted shear resistance of the web decreases rapidly. Stucchi's model is the most conservative, whereas Thürlimann's and Menn's models are more favourable, especially for larger bending moments. Gaspar's model, that is a combination of Thürlimann's and Stucchi's model, is consequently predicting a behaviour mid-way between the previous models.

In general, the effect of the transverse bending moment m on the in-plane shear strength V is significant. For example, in case of a transverse moment of 30% of the pure flexural strength m_{R0} of the web, the models predict a loss of up to 20% of the initial in-plane shear strength V_{R0}.

A more detailed examination of this phenomenon, presented later in this report on the basis of a multi-layered elastic-plastic (ML-EP) panel element, will show that RP approaches potentially have a high level of conservatism and that the actual interaction is less pronounced. Out of all the lower bound solutions, the models by Thürlimann and Menn predict the highest combined resistance, therefore these models are chosen for further investigations of the RP interaction models. An elaborate description of these two models and the corresponding design procedures is presented in section 2.1.3 and 2.1.4. They are followed by a detailed discussion on the main hypotheses leading to the previously mentioned ex-
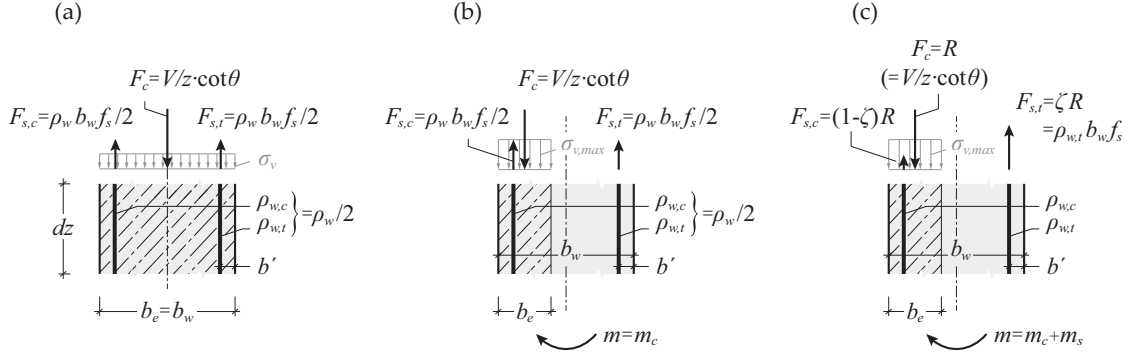
Figure 2.4 Equilibrium of a web segment at ultimate limit state according to Thürlimann: (a) in pure shear condition; (b) with a transverse bending moment in case of symmetrical reinforcement and (c) the general case: for higher levels of transverse bending and/or asymmetrical reinforcement layout.

tremely safe $(m - V)$ interaction predicted by the RPSF approaches, section 2.2.4. Later, the methodology of the ML-EP approach will be presented and discussed in chapter 2.3. Comparisons between the ML-EP approach and the RPSF approaches are presented in section 2.3.4.

2.1.3   Interaction model by Thürlimann

The work presented by Thürlimann in 1977 [Thü77] was a supplement to the new Recommendation 34 of the SIA162:1976 [SIA76] at the time. The SIA162, as well as the CEB Model Code (1976) [CEB76], had introduced new design rules based on the RPSF method for reinforced concrete beams under longitudinal shear, bending and torsion. Thürlimann proposed to extend the analysis to cases with out-of-plane, i.e. transverse, bending in order to obtain a consistent RP design procedure that is conforming to the new recommendations.

In his work, Thürlimann focuses on the interaction of in-plane shear and transverse bending in the web of reinforced concrete beams failing in shear due to yielding of the shear reinforcement. He does not consider other failure mechanisms that could lead to an early failure of the beam. In 1980 Marti [Mar80] extends Thürlimann's model for general cases in order to account for potential failure due to yielding of the longitudinal reinforcement (not developed in this report).

In a first approach, Thürlimann studied the effect of the location of the compression field in the width of the web on the transverse bending resistance. Later, he formulated a more general expression allowing for changes in the stirrup forces and asymmetric shear reinforcement layouts. He validates his model by comparing it to a series of tests performed by Kaufmann and Menn [Kau76].

The eccentricity of the compression field

The presence of an out-of-plane bending moment m in the shear wall requires a modification of the initial state-of-stress in order to ensure the equilibrium between external and internal forces. A possible solution that is proposed by Thürlimann [Thü77], as already illustrated in section 2.1.1, consists in shifting the inclined compression field and thus also its vertical resultant F_c towards the bending compression side within the web width, figure 2.4a to figure 2.4b.

In order to determine the maximum eccentricity of F_c relative to the web axis and by this the capacity of the web to resist a transverse bending moment m, the minimum width b_e required to resist the shear force has to be determined first. At this point, it must be stressed that Thürlimann established his model according to the recommendation at the time, i.e. SIA162:1976 [SIA76]. According to SIA162:1976, the concrete shear resistance of a beam is expressed in terms of nominal tangential stresses (τ_c) that should not exceed the maximal allowable stress τ_{max}. In comparison to recent codes (SIA262:2013 [SIA13]), the value of τ_{max} is approximately equivalent to the shear strength of concrete ($V_{R,c}$) when the inclination of the compression field is set to $\theta = 45°$. Thürlimann then computes the minimum width b_e while referring to the stress field in figure 2.4a-b, where $F_c = b_w \cdot \sigma_v = b_e \cdot \sigma_{v,max}$ and with $\sigma_{v,max} = \tau_{max} \cdot \tan\theta$ (from eq. 2.5).

$$\frac{b_e}{b_w} = \frac{\sigma_v}{\sigma_{v,max}} = \frac{\tau_c}{\tau_{max}} = \frac{2 \cdot V}{z \cdot b_w \cdot k_c \cdot f_{cp}},$$ (2.7)

$$\text{with} \quad \tau_{max} \cong \frac{V_{R,c,\text{SIA262:2013}}\,(\theta = 45°)}{z \cdot b_w} = \frac{1}{2} \cdot k_c \cdot f_{cp}.$$

At ultimate limit state the shear reinforcement is assumed to be yielding, thus the stirrup forces are known. In the case of a symmetrical reinforcement layout ($\rho_{w,t} = \rho_{w,c} = \rho_w/2$), the tension forces on each side of the web are identical $F_{s,t} = F_{s,c} = \rho_w/2 \cdot b_w \cdot f_s$.

The equilibrium equations for vertical forces (eq. 2.4) and transverse bending moments (eq. 2.6) can then be expressed as follows, with b_e according to equation 2.7.

$$F_c = \frac{V}{z \cdot \cot\theta} = F_{s,t} + F_{s,c} \quad = \rho_w \cdot b_w \cdot f_s$$

$$m = m_c = \frac{1}{2} \cdot F_c \cdot (b_w - b_e) \quad = \frac{1}{2} \cdot \rho_w \cdot b_w^2 \cdot f_s \cdot \left(1 - \frac{2 \cdot V}{z \cdot b_w \cdot k_c \cdot f_{cp}}\right)$$ (2.8)

The equation 2.8-2 constitutes an explicit expression of the $(m - V)$ interaction in a beam webs at ultimate limit state. It is however not very general since it assumes that the shear reinforcement layout is symmetrical ($\rho_{w,t} = \rho_{w,c}$) which is often not the case in existing structures. Additionally, only the contribution of the compression field in the transverse bending resistance ($m = m_c$) is accounted for, although the tensile forces in the shear rein-

forcement could greatly contribute to equilibrate m and thus to the combined $(m - V)$ resistance.

General shear-transverse bending interaction model

The $(m - V)$ relation presented in equation 2.8-2 allows to get a first impression of the effect of transverse bending on the in-plane shear strength. However, as pointed out by Thürlimann in [Thü77], this relation does not cover the general case where the shear reinforcement of the web cross section is not symmetrical ($\rho_{w,t} \neq \rho_{w,c}$).

Furthermore, in particular if m is high, the model should consider the possibility that only the shear reinforcement on the bending tension side reaches its yielding strength, while the reinforcement on the bending compression side only carries the remaining shear load. Based on these reflections, Thürlimann [Thü77] proposes a more general formulation for the rigid-plastic stress field, figure 2.4c. The new stress field respects the equilibrium of forces and the plastic strength of material (static theorem of the theory of plasticity) and can hence be used to determine a lower-bound value of the failure load.

The equilibrium of Thürlimann's general rigid-plastic stress field are defined as follows, where R designates the resultant of both stirrup forces.

$$R = F_{s,t} + F_{s,c} = F_c = \frac{V}{z \cdot \cot \theta}$$

$$m = m_s + m_c = \left(F_{s,t} - F_{s,c}\right) \cdot \left(\frac{b_w}{2} - b'\right) + R \cdot \left(\frac{b_w}{2} - \frac{b_e}{2}\right)$$

$$(2.9)$$

In the present model, the bars on the bending tension side are assumed to be yielding whereas those on the compression side carry the remaining load in order to ensure the equilibrium of forces (eq. 2.9-1).

$$\begin{cases} F_{s.t} = \zeta \cdot R & = \rho_{w,t} \cdot b_w \cdot f_s \\ F_{s,c} = (1 - \zeta) \cdot R & \leq \rho_{w,c} \cdot b_w \cdot f_s \end{cases}$$

$$(2.10)$$

$$\zeta = \frac{F_{s,t}}{R} \qquad \text{with} \quad \frac{1}{2} \leq \zeta \leq 1$$

$$(2.11)$$

The parameter ζ that designates the percentage of the total vertical load carried on the tension side, allows to control the ratio between the tension forces $F_{s,t}$ and $F_{s,c}$ and by this the contribution of the shear reinforcement to transverse bending resistance (eq. 2.9-2). Thürlimann allows to vary ζ between ½ and 1. The lower bound ($\zeta = ½$) represents the symmetrical case, where the stirrups on the bending tension and bending compression side carry the same amount of load, $F_{s,t} = F_{s,c} = R/2$. When $\zeta = 1$, the entire shear load is carried by the reinforcement on the bending tension side, $F_{s,t} = R$ and $F_{s,c} = 0$. This configuration will lead to the highest transverse bending moment resistance. Thürlimann does not account for

the cases where $\zeta > 1$, since he considers that the contribution of the compression force $F_{s,c} < 0$ to the transverse bending moment resistance is negligible.

The $(m - V)$ interaction can then be expressed as a function of the parameter ζ by substituting $F_{s,t}$ and $F_{s,c}$ (eq. 2.10), R (eq. 2.11) and b_e (eq. 2.7) into the equilibrium equation 2.9-2.

$$m = m_s + m_c$$

$$= \frac{\rho_{w,t} \cdot b_w^2 \cdot f_s}{2\zeta} \cdot \left[(2\zeta - 1) \cdot \left(1 - \frac{2b'}{b_w} \right) + \left(1 - \frac{2 \cdot V}{z \cdot b_w \cdot k_c \cdot f_{cp}} \right) \right] \leq \overline{m} \tag{2.12}$$

The model is limited to $\overline{m} = \rho_{w,t} \cdot b_w^2 \cdot f_s \cdot (1 - 2b'/b_w)$ in case of very small shear forces ($\tau/\tau_{max} = b_e/b_w \leq 2b'/b_w$) and $V \leq V_{max} = \tau_{max} \cdot z \cdot b_w = \frac{1}{2} \cdot k_c \cdot f_{cp} \cdot z \cdot b_w$ [Thü77].

The general expression for the $(m - V)$ interaction in equation 2.12 (see also eq. 2.9-2) shows two main components in the equilibrium of moments. The second term in the brackets denotes m_c, the transverse bending moment generated by the eccentricity of the compression field. The first term in the brackets is m_s, the contribution of the shear reinforcement to the transverse bending moment. This term shows the beneficial effect of higher tensile forces on the bending tension side than on the bending compression side. The transverse bending resistance can thus be considerably increased by rearranging a symmetrical reinforcement layout (where $\rho_{w,t} = \rho_{w,c}$ i.e. $\zeta = \frac{1}{2}$) into a asymmetrical layout, or by adding reinforcement on the bending tension side, such that $\rho_{w,t} > \rho_{w,c}$ ($\zeta \geq \frac{1}{2}$).

The $(m - V)$ interaction diagrams resulting from equation 2.12 are represented in figure 2.5 (solid lines). The linear relation between m and V indicates a rapid reduction of the shear resistance due to the presence of a transverse bending moment. An asymmetrical reinforcement layout ($\zeta > \frac{1}{2}$) allows increasing the shear resistance for a given moment, but the interaction itself will be even stronger (steeper slop).

Design and assessment procedures

Thürlimann [Thü77] also proposes design and assessment procedures.

In a first step, symmetrical shear reinforcement is designed to carry the design shear load. The inclination of the compression field is selected according to general shear design recommendations (SIA162 [SIA76] $30° \leq \theta \leq 60°$; SIA262 [SIA13] $30°(25°) \leq \theta \leq 45°$). The width of the web b_w should be selected larger than the minimum width b_e, especially if the transverse bending moment is important. The transverse bending resistance of the web is then verified by computing the bending resistance according to equation 2.12, or by reading it directly from the interaction diagram along the curve $\zeta = \frac{1}{2}$. If the bending strength is insufficient, Thürlimann proposes to redesign the shear reinforcement for a one-sided reinforcement layout. The stirrups on the bending tension side carry the entire shear load and the required amount of shear reinforcement on the tension side, $\rho_{w,t}$ is doubled com-
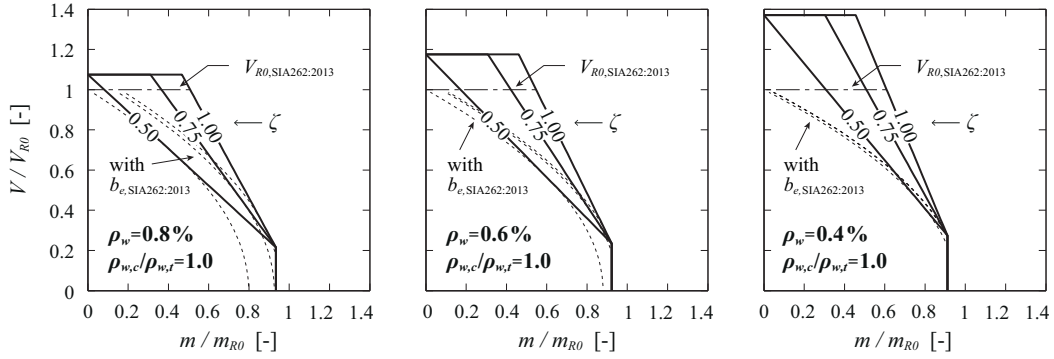
Figure 2.5 Original interaction diagrams by Thürlimann [Thü77] (solid lines) and adaptation to the SIA262:2013 [SIA13] (dashed lines) for $f_s = 435$ MPa, $f_c = 20$ MPa, $k_c = 0.55$ and $b'/b_w = 0.1$.

pared to the previous situation. If the bending strength with $\zeta = 1$ is still insufficient, the cross section of the web has to be increased. If the required bending strength lays between the two previous values (for $\zeta = \frac{1}{2}$ and $\zeta = 1$), the reinforcement on the tension side only needs to be partially increased (compared to $\rho_{w,t}$ for $\zeta = \frac{1}{2}$). In the next iterations the parameter ζ is progressively increased (from $\zeta = \frac{1}{2}$), the reinforcement $\rho_{w,t}$ increases while $\rho_{w,c}$ decreases, until the computed bending strength corresponds to the design moment.

For the assessment of existing structures, the web cross section, the shear reinforcement and the loads are known. First the total reinforcement force R have to be determined from V and θ (eq. 2.9-1). Next, it is assumed that the reinforcement on the tension side is yielding. The parameter ζ is then computed from equation 2.11. The transverse bending strength of the cross section can thus be read from the interaction diagram, respectively computed from equation 2.12.

Thürlimann's model according to today's standards

Thürlimann's original formulation (eq. 2.12) derives the required web width b_e by assuming that the nominal tangential stress in the strut has reached the maximum tangential stress according to SIA162:1976 [SIA76], $\tau = \tau_{max}$ (eq. 2.7). This potentially leads to unsafe estimates of the combined shear resistance, since the shear strength of the concrete strut is independent of the actual inclination of the compression field ($V_{R,c,max} = \tau_{max} \cdot z \cdot b_w =$ cst.). Figure 2.5 also indicates the maximum shear strength according to SIA262 [SIA13], which shows that the overestimation of the strength is especially pronounced for low reinforcement ratios ($V/V_{R0} > 1$).

The author adapted the original formulation by Thürlimann to the SIA262 [SIA13] recommendations by replacing the expression for the required web width b_e. The adapted ($m - V$) interaction (see development and explicit expression in Appendix A) is shown in figure 2.5 (dashed curves). In the range of small transverse bending moments, it is similar to

Thürlimann's original formulation. However, for high transverse bending moments, this formulation leads to an even more pronounced reduction of the shear strength.

In general, with both formulations (original and adapted) it is not possible to reach the plastic bending strength m_{R0} when no shear force is applied. This shows that the underlying RPSF is not appropriate for high transverse bending moments. Menn [Men86] has taken into account this issue when developing his interaction model (section 2.1.4).

2.1.4 Interaction model by Menn

Menn [Men86] clarifies again the fact that the superposition of the required reinforcement to resist each load (shear and transverse bending) separately is not consistent with the actual behaviour of the web at failure. The required reinforcement should be determined by a model that accounts for the effect of a combined load situation.

Menn grounds this statement on the results of an experimental campaign performed by Kaufmann and Menn [Kau76] on a series of beams subjected to a longitudinal shear load and a transverse bending moment in the beam web (see section 2.3). The tests clearly revealed a modification of the shear transfer action under the effect of transverse bending. In particular, it was observed that the resultant of the compressive force due to shear shifts towards the flexural compression side of the web and that the stresses in the two stirrup branches are not identical under the action of the transverse moment. The bending tension side usually had higher tensile stresses than the compression side of the shear reinforcement. For the beams that failed in shear with yielding of the shear reinforcement, it was observed that the stirrups on the bending tension side started yielding first, but at failure the stirrups on both sides had reached the yield strength. In beams that failed due to concrete crushing, the stirrups on the bending compression side did not yield.

Based on these observations, Menn [Men86] proposed a rigid-plastic stress field model that takes simultaneously advantage of the excess capacity of the web ($b_e < b_w$) and the resistance provided by varying the stirrup forces (figure 2.6b). Additional resistance can be provided by an increase of the total concrete compressive force in the web, in case of high transverse bending moments, figure 2.6c. Menn separates these two situations by formulating two distinct equilibrium expressions, one for predominant shear (case i) and one for predominant transverse bending (case ii).

The internal state-of-stress for the different equilibrium conditions is shown in figure 2.6. The stress field and the principle of equilibrating the transverse moment is very similar to Thürlimann's approach, except for case (ii). However, at the ultimate limit, the expression of the $(m - V)$ interaction models differe because Menn assumes, contrary to Thürlimann, that the inclination θ of the compression strut is known and that the forces in the stirrups on the tension and compression side adjust accordingly.
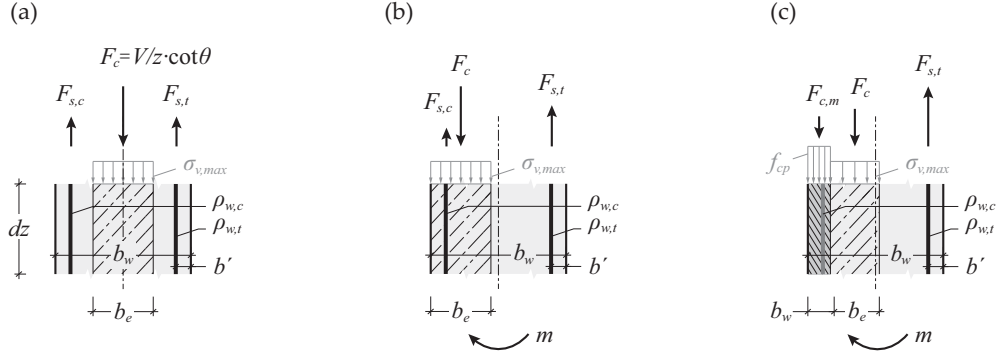
Figure 2.6 Equilibrium of a web segment at ultimate limit state according to Menn [Men86]: (a) in pure shear; (b) in case of predominant shear (case i) and (c) in case of predominant transverse bending (case ii).

Case (i) – Predominant shear

The equilibrium of a web segment subjected to a shear load V and a small transverse bending moment is established by shifting the resultant of the compression field in the concrete towards the bending compression side and by increasing the stirrup forces on the tension side and decreasing the tensile forces in the stirrups on the compression side (fig. 2.6b).

The equilibrium equations are identical to those of Thürlimann's model (eq. 2.9) and allow computing the stirrup forces as a function of V and m.

$$F_{s,t} = \frac{V}{z \cdot \cot \theta \cdot (b_w - 2b')} \cdot \left(\frac{b_e}{2} - b' \right) + \frac{m}{(b_w - 2b')}$$

$$F_{s,c} = \frac{V}{z \cdot \cot \theta \cdot (b_w - 2b')} \cdot \left(b_w - b' - \frac{b_e}{2} \right) - \frac{m}{(b_w - 2b')} \quad \geq 0$$

(2.13)

The minimum web width required to resist the shear force is computed hereafter. Menn's formulation, taken from the second edition (1990) of [Men86], used the reduced concrete compressive strength $f_{c,red}$ (SIA162 [SIA89]) which is replaced in the following by $k_c f_{cp}$, consistent to the notation of the SIA262 [SIA13].

$$\frac{b_e}{b_w} = \frac{V}{k_c \cdot f_{cp} \cdot b_w \cdot z \cdot \sin \theta \cdot \cos \theta}$$

(2.14)

The present state of equilibrium is only applicable if a net tensile force remains in the stirrups on the compression side ($F_{s,c} \geq 0$). If $F_{s,c}$ is negative, due to a high transverse bending moment or a small shear load, the internal forces have to be computed according to the rigid-plastic stress field for predominant transverse bending (case ii).

Case (ii) – Predominant transverse bending

In case of predominant transverse bending, it is assumed that the forces in the reinforcement on the compression side is equal to zero ($F_{s,c} = 0$) and instead an additional compressive force $F_{c,m}$ is applied to the web cross section. $F_{c,m}$ represents a pure bending compression force and is acting in the vertical direction at the outermost position of the web width. Therefore, the resultant of the inclined compression field due to shear (F_c) shifts towards the centre of the web cross section (no superposition of the bending compression and the stress field for shear). The equilibrium conditions can thus be established as follows:

$$\frac{V}{z \cdot \cot\theta} = F_{s,t} + F_{s,c}$$

$$m = m_s + m_c = F_{s,c} \cdot \left(b_w - b' - \frac{b_m}{2}\right) - \frac{V}{z \cdot \cot\theta} \cdot \left(\frac{b_e}{2} + \frac{b_m}{2}\right) \tag{2.15}$$

The unknown compressive force $F_{c,m}$ and the tension force in the shear reinforcement $F_{s,t}$ are then given by:

$$F_{s,t} = \frac{1}{b_w - b' - b_m/2} \cdot \left(\frac{V}{z \cdot \cot\theta} \cdot \frac{b_e + b_m}{2} + m\right)$$

$$F_{c,m} = \frac{1}{b_w - b' - b_m/2} \cdot \left(\frac{V}{z \cdot \cot\theta} \cdot \frac{b_e + b_m}{2} + m\right) - \frac{V}{z \cdot \cot\theta} \tag{2.16}$$

The width required to resist the compressive force $F_{c,m}$ is given by $b_m = F_{c,m}/f_{cp}$. Note that in this case no concrete strength reduction factor k_c intervenes (respectively $k_c = 1.0$).

Explicit expression for the in-plane shear transverse bending interaction

At ultimate limit state, the $(m - V)$ interaction can be expressed explicitly for a given amount of shear reinforcement ($\rho_{w,t}, \rho_{w,c}$) and a given inclination of the compression field θ. The transverse bending resistance is highest when the reinforcement on the tension side is yielding. In case of predominant in-plane shear, m can thus be expressed as function of V by substituting $F_{s,t} = \rho_{w,t} \cdot b_w \cdot f_s$ and b_e (eq. 2.14) into equation 2.9-2 . In a similar way the $(m - V)$ relation for predominant transverse bending can be derived from equation 2.15-2. The explicit expressions are shown hereafter.

Case (i) – predominant shear, if $V \geq V_{lim}$:

$$m = \rho_{w,t} \cdot b_w \cdot f_s \cdot (b_w - 2b')$$

$$-\frac{1}{2} \cdot \frac{V}{z \cdot \cot\theta} \cdot \left(\frac{V}{k_c \cdot f_{cp} \cdot z \cdot \sin\theta \cdot \cos\theta} - 2b'\right) \leq m_{lim} \tag{2.17}$$
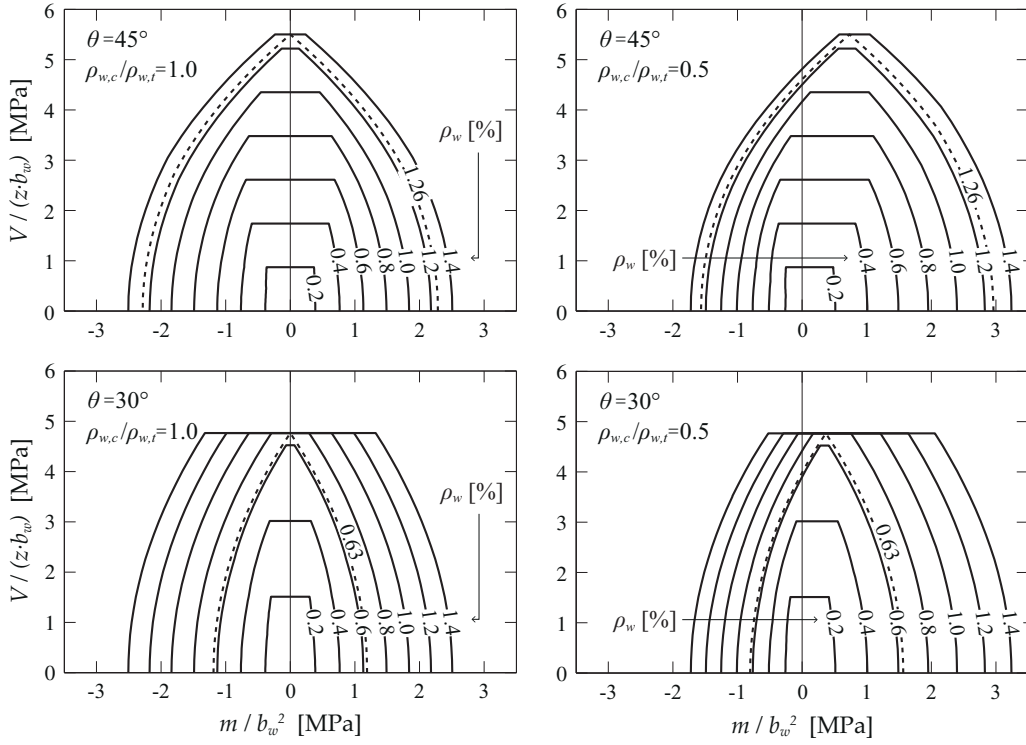
Figure 2.7 Rigid-plastic interaction diagrams by Menn [Men86] for symmetrical and unsymmetrical reinforcement layouts and different stress field inclinations, with $f_s = 435$ MPa, $f_c = 20$ MPa , $k_c = 0.55$ and $b'/b_w = 0.1$.

Case (ii) – predominant transverse bending, if $V \leq V_{lim}$:

$$m = \rho_{w,t} \cdot b_w \cdot f_s \cdot \left(b_w - b' - \frac{\rho_{w,t} \cdot b_w \cdot f_s}{2 f_{cp}} \right)$$

$$-\frac{1}{2} \cdot \left(\frac{V}{z \cdot \cot\theta} \right)^2 \cdot \left(\frac{1}{k_c \cdot f_{cp} \cdot \sin^2\theta} - \frac{1}{f_{cp}} \right) \quad \geq m_{lim} \tag{2.18}$$

The condition associated to the situation of predominant in-plane shear ($F_{s,c} > 0$) permits to define the limit state (m_{lim} and V_{lim}) between the two cases. They are obtained from the equilibrium equations 2.9 when $F_{s,c} = 0$.

$$V_{lim} = \rho_{w,t} \cdot b_w \cdot f_s \cdot z \cdot \cot\theta$$

$$m_{lim} = \rho_{w,t} \cdot b_w \cdot f_s \cdot \left(b_w - b' - \frac{1}{2} \cdot \frac{\rho_{w,t} \cdot b_w \cdot f_s}{k_c \cdot f_{cp} \cdot \sin^2\theta} \right) \tag{2.19}$$

Design procedure

The design of the shear reinforcement for the combined action of in-plane shear and transverse bending can be performed by using pre-established $(m - V)$ interaction diagrams (example in fig. 2.7 obtained from eqs. 2.17-2.19) or by directly applying the expressions for $F_{s,t}$ and $F_{s,c}$. In this case, the tensile forces in the reinforcement are first computed for the case of predominant shear. If the stirrups on the bending compression side are in compression ($F_{s,c} < 0$), the reinforcement has to be designed according to the case for predominant transverse bending. The latter requires some interactions in order to determine the necessary width b_m for the bending compression force $F_{c,m}$.

2.1.5 Main observations and conclusions

All the models proposed in the literature are RP equilibrium solutions that tailor the stress field in the transverse direction in order to account for the out-of-plane bending moment. They are ground on the same basic principle that consists in arranging the compression field on a minimum web width and then shifting it to the bending compression side. Differences in the models are observed when regarding the forces in the stirrups and for high levels of transverse bending.

The investigations performed on the basis of the models by Thürlimann and Menn show that the RPSF approach is an elegant method to illustrate the shear transfer action under transverse bending and to identify the key factors in the assessment of the maximum combined shear-transverse bending resistance, which are the reserve capacity of the web width ($b_w > b_e$) and the potential difference between the forces in the stirrups on the bending compression and the bending tension side ($\Delta F = F_{s,t} - F_{s,c} \geq 0$, resp. $\rho_{w,t} \geq \rho_{w,c}$).

Further advantages of the RP interaction models are that they can be easily adapted for any specific case (shear reinforcement and location, web geometry etc.) and that simple to use in practice, due to the explicit interaction formulas or diagrams.

However, the previously presented models predict a very strong interaction between in-plane shear and transverse bending which leads to a substantial loss in shear strength. Particularly in the range of small transverse moments, the effect on the in-plane shear strength is surprisingly high. For some models, a bending moment of 30% of m_{R0} (pure bending resistance) leads to a loss of up to 20% of the initial shear strength (fig. 2.3). While this safe estimate of the shear strength could be acceptable for the design of new structures, it might be too penalizing when assessing the shear strength of existing structures and consequently leading to costly and probably unnecessary strengthening.

It should be kept in mind that the rigid-plastic interaction models by Menn [Men86] and Thürlimann [Thü77], as any other models based on the RPSF approach, make a number of hypotheses that affect the shear strength prediction of the web. In the present context the most arguable assumptions are made regarding the inclination of the compression field θ

and the concrete strength reduction factor k_c. Firstly, from simple extrapolation of the classical rigid-plastic stress field approach, it is assumed that the inclination θ and the factor k_c are constant over the entire web width. Secondly, the values for θ and k_c are chosen according to recommendations for reinforced concrete members subjected to in-plane shear only.

Although, as shown in the previous sections, the stress field is subjected to significant modifications, the stress field parameters (k_c, θ) have not been revised in order to account for the mostly beneficial effect of the transverse bending moment (i.e. due to bending compression θ ↗, k_c ↗). The RP interaction models could thus potentially be improved, but this raises the questions on how to correctly assess the superposition of the bending compression with the inclined shear field and to what extent the value of k_c and θ should be adapted. Some effort in this direction has been made by Menn [Men86] (additional bending compression zone) and Stucchi [Stu90] (bending compression partially added to vertical component of the shear force) but the effect on the overall resistance was not significant, see figure 2.3.

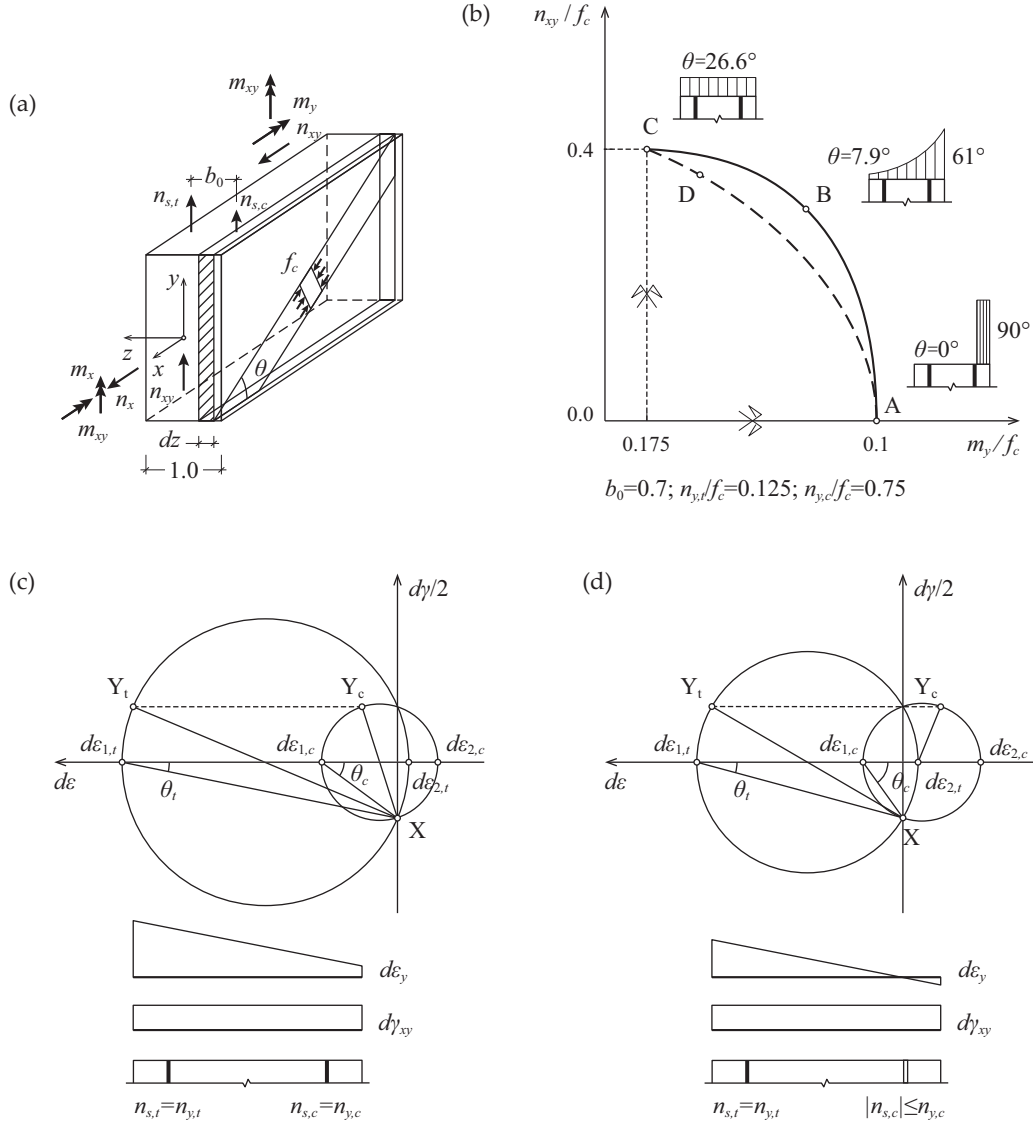## 2.2 An exact solution according to the theory of plasticity

The theory of plasticity is a widely spread tool to investigate the behaviour of reinforced concrete structures. Cookson [Coo79] and Marti [Mar80] both studied the case of in-plane shear and transverse bending on the basis of plane reinforced concrete panel elements subjected to membrane and bending actions. The derived yield criterions are exact solutions according to the theory of plasticity and illustrate that the previous RP interaction models, which correspond to lower bound solutions, provide strongly conservative estimates of the ultimate resistance. Figure 2.8b shows a schematic representation of the static solution by Thürlimann (dashed line) and the exact solution proposed by Marti (solid line). In the following, Marti's model is presented in detail. It is identical to the one proposed by Cookson.

Interaction model by Marti

To develop the exact solution, Marti starts from the kinematic theorem of the theory of plasticity which he applies to the general case of plates subjected to membrane and bending actions. In order to determine the yield condition for the reinforced panel, Marti uses the Jacob-Bernoulli hypothesis of plane sections to determine the in-plane deformations that result from out-of-plane bending. The in-plane strain increments $\{d\varepsilon_x,\ d\varepsilon_y,\ d\gamma_{xy}\}$ are thus varying linearly over the element thickness and are entirely defined by the generalized strain increments $\{d\varepsilon_{x0},\ d\varepsilon_{y0},\ d\gamma_{xy0},\ d\chi_x,\ d\chi_y,\ d\chi_{xy}\}$ (at the element mid-plane, similar to fig. 3.1b). Using Mohr's circle of strains, the principal strain increments $\{d\varepsilon_1,\ d\varepsilon_2\}$, as well as their orientation, are known for every point in the element thickness.

By using the Mohr-Coulomb yield criterion for concrete in a plane stress state (tensile strength neglected, fig. 2.13c), Marti can then determine a consistent stress state for every non-zero strain increment at every position in the element thickness ($\sigma_{c,i} = 0$ if $d\varepsilon_i > 0$, $\sigma_{c,i} = -f_c$ if $d\varepsilon_i < 0$, with $d\varepsilon_1 \geq d\varepsilon_2$). The reinforcement in the plane of the element is admitted to be yielding in compression or tension, depending if the deformation increment in the plane of the reinforcement is positive or negative. The energy dissipated by the reinforced concrete plate is thus uniquely defined by the generalized deformation increments $\{d\varepsilon_{x0},\ \dots,\ d\chi_x,\ \dots\}$ and can be derived to define the yield surface in the six-dimensional space of the generalized stress $\{n_x, n_y, n_{xy}, m_x, m_y, m_{xy}\}$.

In [Mar80], Marti reduces the problem of the general panel element to the case of in-plane shear and transverse bending by assuming that the generalized deformations $d\varepsilon_{x0}$, $d\chi_x$, $d\chi_{xy}$ and the membrane force n_y are zero. The in-plane shear force n_{xy} and the transverse bending moment m_y are the remaining unknown forces of the problem, which allows deriving the yield condition and thus as well the exact solution for the in-plane shear transverse bending interaction. To establish the interaction curve in figure 2.8b, Marti additionally assumes the stress field illustrated in figure 2.8a in which the concrete is in an uniaxial stress state (point F in fig. 2.13c: $d\varepsilon_1 > 0$, $d\varepsilon_2 < 0$ thus $\sigma_{c,1} = 0$ and $\sigma_{c,2} = -f_c$) and the (shear) reinforcement is vertical. Contrary to the RP interaction models, the stress field de-

Figure 2.8   An exact solution according to the theory of plasticity by Marti [Mar80]: (a) assumed stress field with variable inclination; (b) in-plane shear transverse bending interaction diagram: static solution (dashed) and exact solution (solid); kinematical relationships: (c) in case the stirrups on both sides are yielding and (d) in case the stirrups on the bending compression side are not yielding.

velops over the entire element thickness and its inclination varies from the bending compression side (index "$_c$") to the bending tension side (index "$_t$"). The forces n_x, m_x and m_{xy} that result from the restrained deformations are considered as internal reactions forces.

The equilibrium of forces for n_{xy}, m_y and $n_y = 0$ can thus be expressed as a function of the inclination of the compression field θ and the forces $n_{s,c}$ and $n_{s,t}$ in the shear reinforcement:

$$n_{xy} = \frac{f_c}{2} \int_{-1/2}^{1/2} \sin 2\theta \, dz \quad ; \quad m_y = -f_c \int_{-1/2}^{1/2} z \sin^2 \theta \, dz + \frac{b_0}{2}\left(n_{s,t} - n_{s,c}\right)$$

$$n_y = -f_c \int_{-1/2}^{1/2} \sin^2 \theta \, dz + \left(n_{s,t} + n_{s,c}\right) = 0 \tag{2.20}$$

with $n_{s,c} \le n_{y,c} = \rho_{w,c} f_s$ and $n_{s,t} \le n_{y,t} = \rho_{w,t} f_s$.

Following the application of the static theorem of the theory of plasticity, Marti maximises the expression for the shear for n_{xy}, while taking m_y, $n_{s,c}$ and $n_{s,t}$ as constant parameters. In the general upper bound solution (kinematic theorem) Marti [Mar80] derived that $\cot(2\theta) = (d\varepsilon_y - d\varepsilon_x)/d\gamma_{xy}$. In the present application this means that $\cot(2\theta)$ varies linearly over the element thickness, which allows eliminating the unknown stress field inclination θ from the previous equilibrium equations. Eventually, Marti obtains the following transcendental expression for the in-plane shear transverse bending interaction:

$$\phi\left(n_{xy}, m_y\right) = \ln\left\{ \frac{2l\left[l + \sqrt{l^2 - k(1 - m^2)}\right]}{k(1 - m)^2} - \frac{1 + m}{1 - m} \right\}$$
$$- \frac{2l}{k(1 - m)}\left[l - \frac{k(1 - m)}{l + \sqrt{l^2 - k(1 - m^2)}}\right] = 0 \tag{2.21}$$

with,

$$k = \frac{\omega}{1 - \omega} \quad ; \quad l = \frac{n_{xy}}{f_c(1 - \omega)} \quad ; \quad m = \frac{2m_y - b_0\left(n_{s,t} - n_{s,c}\right)}{f_c \omega(1 - \omega)} \quad ; \quad \omega = \frac{n_{s,t} + n_{s,c}}{f_c}.$$

Equation 2.21 still has to be optimized for the forces in the stirrups $n_{s,c}$ and $n_{s,t}$. Marti distinguishes different cases as illustrated in figure 2.8b. Provided that the stirrups are yielding on both sides, the yield limits $n_{y,t}$ and $n_{y,c}$ are inserted into equation 2.21. The corresponding kinematic relationships are illustrated in figure 2.8c. In case the reinforcement on the bending compression side is not yielding, which occurs for a pure shear state of strain at the position of the reinforcement (fig. 2.8d, $d\varepsilon_y = 0$ at $z = -b_0/2$), the state of stress in the reinforcement is not fully defined and can thus take any value respecting $|n_{s,c}| \le n_{y,c}$. The interaction equation has to be evaluated for various levels of the stirrup force $n_{s,c}$, while maintaining $n_{s,t} = n_{y,t}$. The envelope of all the interaction curves then provides the in-plane shear transverse bending interaction diagram as shown in figure 2.8b. The kinematic compatibility conditions allow determining as well the corresponding stress field inclinations as illustrated in figure 2.8b. Detailed information regarding these developments can be found in [Mar80].

Figure 2.8b gives an example of an interaction curve for unsymmetrical shear reinforcement ($n_{y,t} \ne n_{y,c}$). The curve is symmetrical about the axes $n_{xy} = 0$ and $m_{xy} = b_0(n_{y,t} - n_{y,c})/2$. The stress field inclination θ is shown for three characteristic points A, B and C. In

point C, the stirrups on both sides are yielding and the stress field due to shear is uniformly distributed over the element width. At this point, the transverse bending resistance is provided only by the unsymmetrical shear reinforcement. In point B, the deformation increment $d\varepsilon_y$ varnishes at $z = -b_0/2$ (fig. 2.8d), such that the reinforcement on the bending compression side is not yielding ($0 < n_{s,c} < n_{y,c}$). The inclination of the stress field has increased towards the bending compression side, which significantly augments the contribution of the compression field in the concrete to the transverse bending resistance (compare to the static solution by Thürlimann, dashed line). The situation of pure transverse bending, point C, leads to a singularity in the model. Indeed, for $n_{xy} = 0$ the state of stress in the concrete is not uniquely defined by the theory of plasticity. Marti thus chooses the statically consistent stress field as illustrated in figure 2.8b point A, with $m_y = b_0 n_{y,t} + f_c(1 - b_0)^2/8$ and $n_{s,c} = f_c(1 - b_0)/2 - n_{y,t}$.

The exact solution proposed by Marti shows that contrary to the assumptions made in Thürlimann's and Menn's interaction models, the stress field inclination is not uniform over the element width and significantly differs from the conventionally admitted inclination angles for pure shear. The kinematic consistent model predicts as well a noticeable less strong interaction, especially in the range of small transverse bending moments, which leads to higher shear resistance and thus potentially less penalizing predictions for the design of new and the assessment of existing structures. However, as in Thürlimann's and Menn's model, the question regarding the appropriate choice for the concrete strength reduction factor k_c still remains unanswered and becomes even more uncertain due to the very different inclinations that the stress field adopts over the element width.

2.3 Experiments for in-plane shear and transverse bending interactions

This section presents some experiments that have been conducted on beams and panels under combined in-plane and transverse bending actions. Most of these tests had been performed to validate proposals for design recommendations. Only a few, in particular Kaufmann [Kau76] and Kirschner [Kir86], performed tests that aimed to investigate the actual interaction mechanism that develops under the combined membrane and bending actions. The following section presents a brief overview of the most important tests and their main outcomes. The experiments by Kaufmann and Menn that provide thorough and conclusive information about the observed behaviour are presented more in detail.

Test by Kupfer and Ewald

Kupfer and Ewald [Kup73] were interested in the behaviour of the webs of continuous box-girder bridges that are subjected to the combined action of in-plane shear and transverse bending. They considered that the most unfavourable combination of internal forces in the web is located above the intermediate support at the connection to the deck slab. To inves-
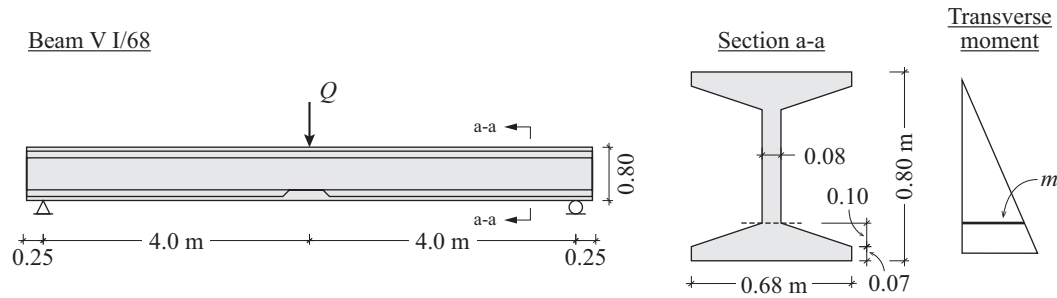
Figure 2.9 Experimental beam V I/68 tested by Kupfer and Ewald [Kup73].

tigate the behaviour of the web in that region they conducted an experimental test on a prestressed concrete beam in a scale 1:4 to a representative box-girder element. The test was conceived such that the transverse bending moment was varying linearly over the web height, with its maximum at the connection with the tension chord. Shear was introduced by a concentrated load at mid-span of the simply supported beam and the transverse moment was applied nearly uniformly over the entire beam length.

The test specimen was 8 meters long, 80 cm high and the web was 8 cm thick. The total amount of shear reinforcement was $\rho_w = 1.2\%$, with $\rho_{w,c}/\rho_{w,t} = 1.33$. The longitudinal reinforcement in the tension chord was composed of six prestressed tendons of 18.6 mm diameter ($\sigma_p = 392$MPa) and a passive reinforcement of ten bars of diameter 6 mm. The measured average concrete cylinder strength was $f_c = 43$ MPa and the yield limit of the reinforcing steel was $f_y = 473$ MPa.

During the testing procedure the shear load and transverse bending moment were progressively increased until a certain load level. This was performed by means of loading and unloading cycles in order to simulate the actual loading conditions in the bridge and to consolidate the crack pattern. Once the longitudinal reinforcement started yielding, the shear load was maintained constant and only the transverse bending moment was increased until eventually the yielding of the stirrups on the bending tension side was observed. Spalling of the concrete at the height of the web-flange connection on the bending compression side along the entire beam length indicated that the failure was imminent. Thereupon the beam was unloaded and then reloaded in pure shear (no transverse moment) until failure occurred. The latter was caused by a concrete compression failure in the web near the tension flange and led to a relative displacement (shear) between the web and the flange of three centimetres. The observed failure load ($Q_u = 550$ kN) was lower than the load of the previous load step ($Q = 598$ kN with $m = 16.48$ kNm/m). The authors thus concluded that the prior damage caused by the combined action of in-plane shear and transverses bending led to the reduction of the ultimate longitudinal bearing capacity.

Tests by Kaufmann and Menn

Kaufmann and Menn [Kau76] conducted a detailed study on the behaviour of beams which are subjected to the combined action of in-plane shear and transverse bending. The aim of the research project was to analyse questions regarding the design of the shear reinforcement and the upper limit of the admissible shear stresses in the concrete.

The test series comprised six I-shaped reinforced concrete beams with a span of 6 m (respectively 4 m), a height of 62 cm and a web width of 10 cm. The transverse bending was applied such that a constant moment developed over the entire web height and beam length, see figure 2.10. The experimental parameters were in particular the total amount of shear reinforcement, the relation between the shear reinforcement ratio on the bending compression and the bending tension side, the inclination of the compression strut and the intensity of the acting transverse bending moment, which was varied between 50% and 85% of the pure transverse bending resistance. More details are provided in table 2.1.

The beams were tested in two different load configurations, LS I and LS II. To this purpose, each beam had a very different reinforcement design in the two investigated shear spans. In the load configuration LS I, the beams were conceived for a ductile failure mode with yielding of the shear reinforcement. In the subsequent test, in load configuration LS II, a brittle failure with crushing of the concrete strut was expected. In order that the shear failure mechanisms can develop over the entire length, the longitudinal reinforcement was adjusted to follow the tensile force diagram of the tension chord.

The load was step-wisely applied (shear then transverse bending) until the serviceability load level was reached. Several load cycles were performed at this load level before the transverse bending moment was increased to the predefined test value, meanwhile the shear load was kept constant. Then only the shear load was increased until failure occurred. Contrary to beams S1 to S5, beam S6 (LS II) was subjected to a constant shear load and the transverse bending moment was increased until failure of the element.

The overall behaviour of the beams in load configuration LS I can be described as follows. At 70% to 90% of the failure load, yielding of the shear reinforcement on the tension side was observed. After this onset of yielding, further load increments had to be carried by other mechanisms which led to an overall softer response of the beams. The rearrangement of the internal force equilibrium was especially well visible in beam S1, where the measured stirrup strains clearly showed that after the onset of yielding on the tension side, the stirrups on the compression side carried the entire load increase. The load could be increased until the shear reinforcement reached the yield limit on both sides, see figure 2.10c. Eventually, a local rupture of the longitudinal reinforcement occurred in all the beams of load configuration LS I (except beam S4, failure of the compression flange).

(a)

(b)

Beam	Stirrups P1 Ø[mm] / [mm]	Stirrups P2 Ø[mm] / [mm]	Concrete $f_{c,cube}$ [MPa]
S1	2x Ø8 / 200	2x Ø10 / 200	39
S2	2x Ø8 / 200	2x Ø10 / 100	41
S3	2x Ø8 / 200	2x Ø10 / 200	41
S4	Ø8 / 200 Ø10 / 200	Ø8 / 200 Ø10 / 200	33
S5	Ø8 / 200 Ø8 / 100	Ø8 / 100 Ø8 / 200	33
S6	2x Ø8 / 200	2x Ø8 / 200	30

Steel:
Ø8: f_s = 540 MPa
Ø10: f_s = 531 MPa

(c)
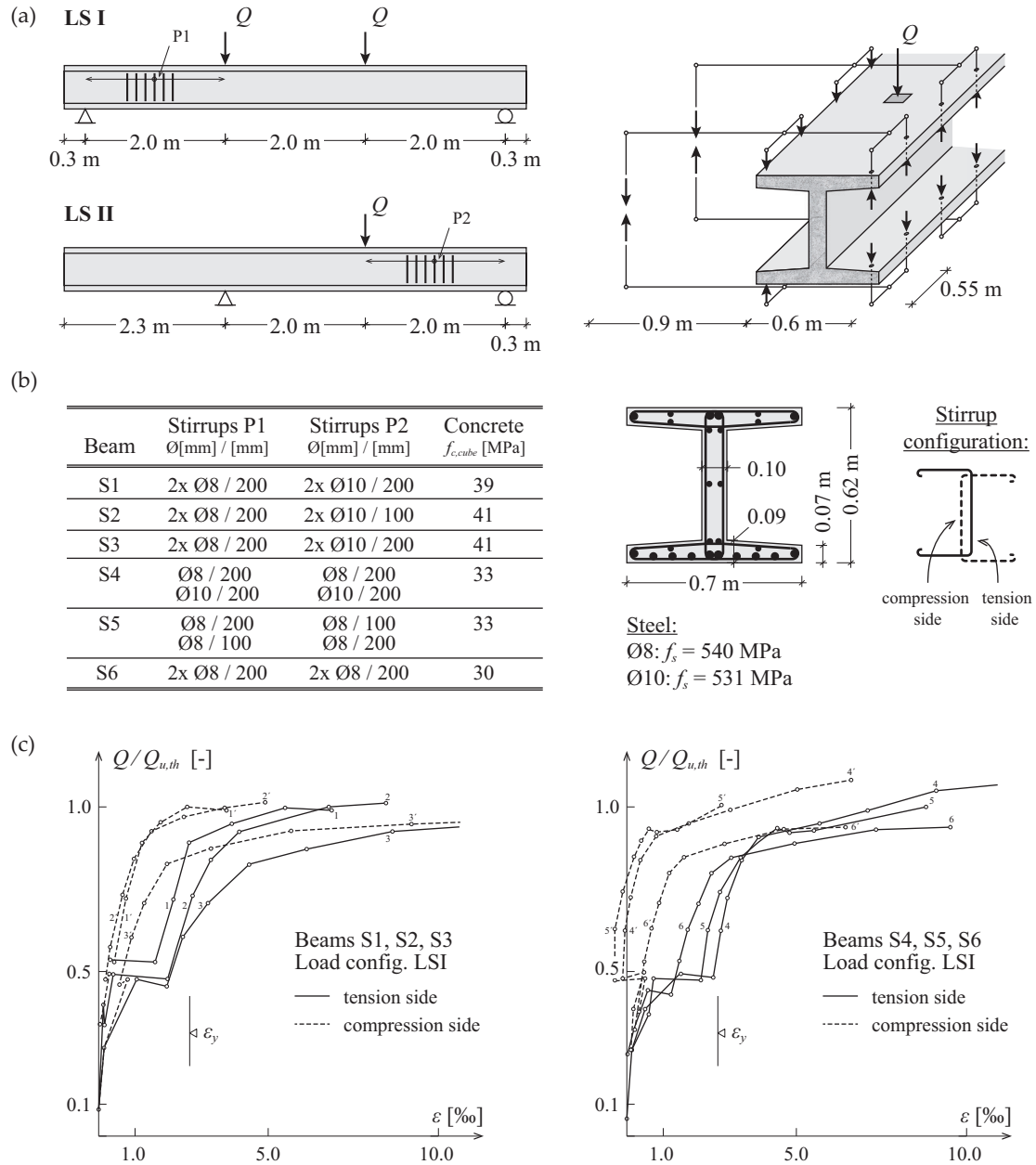
Figure 2.10 Experimental test campaign by Kaufmann and Menn [Kau76]: (a) Longitudinal load configuration LS I, LS II and application of the transverse moment; (b) shear reinforcement and material properties (c) average measured stirrup strains in load configuration LS I.

The specimens S1 to S5 in load configuration LS II showed no significant loss in rigidity during the loading process. At failure, substantial cracking and concrete spalling were observed. These signs, that are typical for a concrete strut failure, were especially visible in beams S1, S2 and S4. Simultaneously to the concrete failure in the web, yielding of the longitudinal reinforcement along the entire shear span was observed in all the beams, such that a longitudinal bending-shear failure mechanism developed. Regarding the shear rein-

forcement at failure, the tension side was fully yielding but not all the stirrups on the compression side. The authors thus concluded that for these beams, the shear reinforcement was not governing for the bearing capacity, especially for beams S1, S2 and S4 that were highly reinforced.

In the serviceability state, the measured reinforcement deformations on the tension side were lower than what would be expected by the superposition of the transverse bending moment and the in-plane shear force. The authors explained this by the fact that the shear strut in the concrete shifts towards the uncracked zone on the compression side and thereby counterbalances part of the applied transverse moment, which then reduces the tensile forces in the stirrups on the tension side. They suggested that the contribution provided by eccentric shear strut to the transverse bending resistance can be significant. It reduces the solicitation of the shear reinforcement due to bending and consequently as well the effect on the longitudinal bearing capacity. This behaviour was especially well visible in beam S6 LS II (loaded until bending failure), where the measured ultimate transverse bending resistance was about 30% higher than the theoretical pure transverse bending strength.

Under shear load, cracks are first inclined by 45° and the transverse bending moment caused additional horizontal cracks over the entire web height on the bending tension side. The progressive increase of the shear load (constant transverse bending) led to the formation of new cracks on the tension side with significantly lower inclination. The horizontal cracks did not further open and no substantial changes were overserved on the compression side. Only at the onset of yielding of the stirrups on the compression side, the

Table 2.1 Investigated parameters and measured failure loads of Kaufmann and Menn's beams [Kau76].

Beam	LS	Parameters					Failure load	
		$\dfrac{m_q}{m_{R0}}$	$\tan\theta$	$\dfrac{\tau_Q^{(*)}}{5\cdot\tau_r}$	$\dfrac{\rho_{w,c}}{\rho_{w,t}}$	ρ_w [%]	Q_{exp} [kN]	m_q [kNm/m]
S1	I	0.75	1.0	0.5	1.0	0.5	162.8	8.3
	II	0.56	0.6	1.29	1.0	0.785	334.5	9.4
S2	I	0.85	1.0	0.5	1.0	0.5	164.8	8.8
	II	0.56	1.5	1.03	1.0	1.57	290.4	17.4
S3	I	0.85	0.6	0.82	1.0	0.5	242.3	9.4
	II	0.85	0.6	1.29	1.0	0.785	332.6	14.3
S4	I	0.85	1.0	0.63	0.64	0.643	214.8	14.2
	II	0.56	0.6	1.05	0.64	0.643	297.7	10.9
S5	I	0.85	1.0	0.74	0.50	0.75	241.3	17.7
	II	0.56	0.6	1.24	0.50	0.75	316.4	13.5
S6	I	0.5	1.0	0.5	1.0	0.5	159.4	5.4
	II	1.0	0.6	0.82	1.0	0.5	124.6	15.8 [**]

[*] τ_Q nominal shear stress due to design shear load;

    $5\cdot\tau_r$ maximal nominal shear stress according to recommendation SIA162/34 [SIA76];

[**] m_{exp} increase of the transverse bending moment till failure.

number and width of the shear cracks increased significantly.

The authors concluded that the transverse bending moment has no influence on the ultimate shear resistance of beams sufficient ductile behaviour, i.e. if the resultant of the shear stresses can shift towards the bending compression side in order to maintain the equilibrium of internal forces in the web cross section. The authors say that in this case, a full interaction between shear and transverse bending takes place and that it is sufficient to design the shear reinforcement for the governing of the two actions. Additionally, the cracking behaviour in the serviceability limit state can be improved by using asymmetric shear reinforcement or by admitting an inclination of 45° (or higher) of the concrete strut.

Regarding the brittle failure modes (as for LS II), the authors claim that a significant loss of the shear resistance is to be expected as far as the transverse bending moment exceeds the cracking moment. They assumed that the reduction of the shear resistance is caused by the superposition of the compressive stresses resulting from the compression strut and the transverse bending moment in the compression zone of the web. The authors thus suggest that in these cases the maximum admissible shear stress in the concrete has to be reduced. They propose that the shear stress should not exceed 60% of the upper limit for pure shear given by design recommendation at the time (SIA 162/34 [SIA76]).

The design proposals provided by Kaufmann and Menn on the basis of this experimental campaign may however be questionable. First, because no reference test under pure shear load had been conducted and second, because for most of the brittle failures no pure shear failure mechanism was observed, since simultaneously the longitudinal reinforcement was yielding over the entire shear span.

Tests by Swann

Swann [Swa75] tested four post-tensioned I-shaped beams of micro-concrete. The small scale elements (span 1.34-2.11 m, height 25 cm, web thickness 3.8 cm) were tested similarly to Kaufmann and Menn's beams, with a concentrated load at mid-span and a constant transverse bending moment over the web height. The shear reinforcement consisted in 3.25 mm half-stirrups (one branch on the bending tension side) that were spaced by 12.5 to 100 mm.

Each beam was loaded simultaneously in longitudinal bending and transverse bending so that, at any load stage, all three internal forces were at the same percentage of their expected ultimate value. All four beams failed due to longitudinal bending and crushing of the compression flange could be observed in all cases. The failure load thus corresponded to the expected pure longitudinal bearing capacity. However, no meaningful conclusion can be drawn because the tests are very poorly documented (e.g. no reinforcement strains) and are furthermore not very representative of actual reinforced concrete box-girder elements.

Figure 2.11 Schematic representation of the experimental beams by Gaspar and Stucchi [Gas03].

Tests by Gaspar and Stucchi

Gaspar and Stucchi [Gas03, Gas13] conducted tests on two I-shaped reinforced concrete beams in order to validate their proposition for a rigid-plastic interaction model (presented in section 2.1.2). They tested two simplify supported beams subjected to a concentrated load in the mid-span and self-balancing load acting on one side of the flanges in order to introduce a constant moment over the height of the web. The geometry of the beams and a schematic presentation of the load introduction system are presented in figure 2.11. The two beams had very different amounts of shear reinforcement in order to investigate a brittle failure mode by crushing of the concrete shear struts in beam Nr°1 ($\rho_w = 1.3\%$) and a ductile failure mode with high levels of plastic deformation in the reinforcement in beam Nr°2 ($\rho_w = 0.38\%$). For both tests, first the shear load is introduced to a predefined level and then the transverse bending moment is applied and increased until failure of the element.

In beam Nr°1, the failure occurred for a transverse moment of $m = 23.3$ kNm/m (with $Q = 692$ kN). The authors observed that the concrete was close to failure and that the shear reinforcement on the bending compression side had entered into compression (probably the tension side was yielding, not clear in the documentation). The authors suggested that the transverse bending moment was mainly resisted by the shear reinforcement since the shear strut in the concrete could not shift towards the compression side because the whole web width was required to resist the longitudinal shear force.

In beam Nr°2 the transverse moment was increased until excessive stirrup deformation and cracking on the tension side was observed, for $m = 20.4$ kNm/m (with $Q = 392$ kN). Thereupon the authors increased the shear load until concrete crushing occurred which caused the element to fail (no significant increase of the load ~10 kN, exact value not documented). Strain measurements on the stirrups indicated that the initial transverse moment was mainly carried by the compression strut that shifts towards the bending compression side (only little deformation of the stirrups on the tension side). For a higher transverse moment the reinforcement strain on the tension side then started increasing rapidly ($\varepsilon_s > 1.0\%$ at ultimate load). At the ultimate load, only the stirrups on the tension side were yielding.

It should be noted that the way the transverse bending moment was applied induced a non-negligible vertical compression force in the web, which has an influence on the overall behaviour of the elements and most likely as well as on the interpretation of the observations. A more profound analysis of these tests is though difficult because of a very poor documentation of the test results.

Tests by Kirschner

Kirschner [Kir86] performed an experimental campaign on six reinforced concrete panel elements in order to verify the performance of the new *Shell Element Tester* built at the University of Toronto. Kirschner additionally used these tests to validate a numerical model of the modified compression field theory that he had extended for tri-axial stress states in the concrete.

The test series that comprised six panel elements of 1.524 x 1.524 x 0.285 m subjected to combinations of in-plane shear n_{xy} and transverse bending m_x are the first experiments conducted on shell elements involving this kind of loading, figure 2.12. The investigated parameters are the amount of reinforcement in the y-direction and the ratio between in-plane shear and transverse bending. Regarding the in-plane shear transverse bending interaction, only the specimens SE1, SE7, SE4 and SE3 are considered in the following, because they were tested for increasing moment-shear ratios ($m_x/n_{xy} = \{0, 0.13, 0.5, \infty\}$, [m]) and had the same amount of reinforcement ($\rho_x = 2 \cdot 1.465\%$, $\rho_y = 2 \cdot 0.489\%$). Figure 2.12a-b provides a summary of the main panel characteristics.

During testing procedure, the load was applied such that the predefined moment-shear ratio was respected at every load level and that all other stress resultants (n_x, n_y, m_y, m_{xy}) were zero. Since the transverse moment m_x was inclined by 45° to the horizontal axis of the test setup, it has been applied by a combination of bending moments in the horizontal and vertical direction and a torsion moment. The latter was produced by eight of the *Shell Element Tester*'s out-of-plane cylinders. The in-plane shear force n_{xy} was introduced by horizontal membrane tension and vertical membrane compression. For the investigated cases, Kirschner found that the coexistence of a transverse bending moment has a significant in-
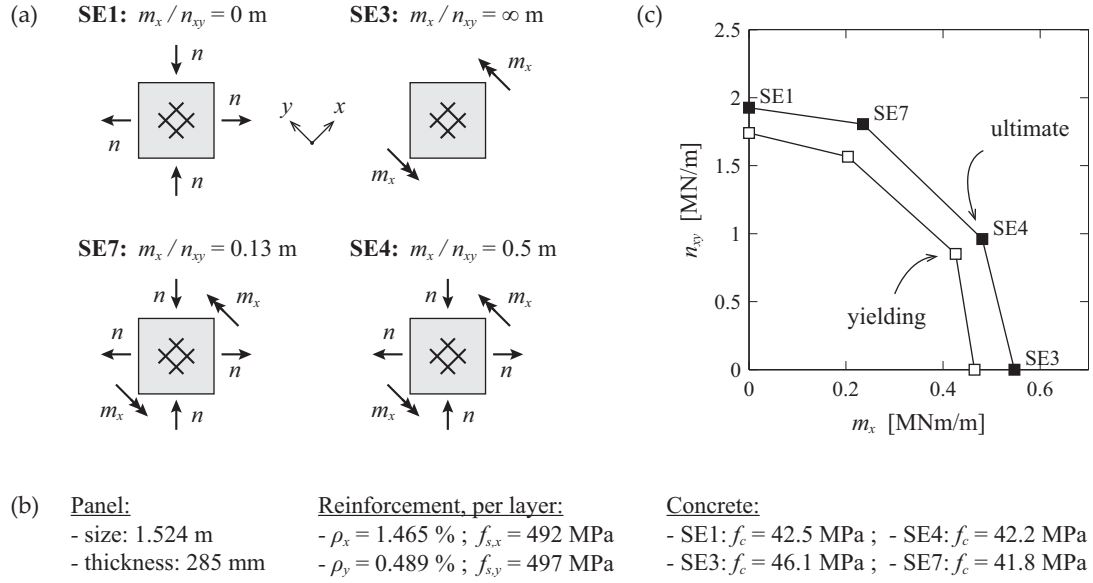
Figure 2.12 Panel tests by Kirschner [Kir86]: (a) specimens with load configuration; (b) specimen and material characteristics and (c) measured yielding and failure loads represented in a transverse bending m_x - in-plane shear n_{xy} diagram.

fluence on the shear response of the panel. In panel SE4, that was subjected to the combined actions, a reorientation of the crack direction on the tension face was observed after the x-reinforcement started yielding. For a smaller moment, as in panel SE7, this was less pronounced. The representation of the measured failure loads in figure 2.12c suggests as well that there is a strong interaction between these two types of loads. The author did though no further investigations regarding this phenomenon.

Tests by Polak and Vecchio

Polak and Vecchio [Pol94] conducted four tests on reinforced concrete panel elements by means of the *Shell Element Tester* at the University of Toronto. The goal was to validate tension stiffening models for membrane elements and to provide additional experimental data regarding the bending behaviour of shell elements that are subjected to a combination of membrane and bending loads. The test campaign mainly focused on the influence on the reinforcement orientation and the amount of membrane action on the out-of-plane bending behaviour and resistance. The authors observed a significant influence of the membrane action on the bending behaviour, especially if the principal stress directions were not in-line with the reinforcing directions. However, because of the chosen experimental parameters (load configuration, bending-shear ratios), the experiments provide only little information regarding the actual in-plane shear transverse bending interaction that develops in beam-like elements, where shear is predominant. These experiments are thus not further investigated in this section, but they are later used to validate the proposed finite element method (Chapter 4), where more information is presented.

2.4   Elastic-plastic stress field method

The stress field method is widely used for the design, assessment and detailing of structural concrete in practice. Stress fields result from a direct application of the theory of plasticity to reinforced concrete elements and are based on its static (lower bound) theorem. The first application proposed by Drucker [Dru61] as well as following developments of the stress field method (e.g. Marti [Mar80], Muttoni [Mut90]) rely on the assumption of rigid-plastic material laws and neglect the concrete tensile strength. This provides a great freedom for the choice of the load-bearing actions that develop in the cracked concrete, but may lead to inappropriate behaviour for some solutions. A general method for developing stress fields in a systematic way and thereby considering also the behaviour in the serviceability state has been proposed by Muttoni [Mut97] (choice of load-bearing action + control of critical crack). Although this method is completely general, selecting the most suitable load-carrying actions still remains a trial and error process and requires a certain level of experience. Other difficulties that arise from the rigid-plastic assumption are the evaluation of the effective concrete compressive strength (affected by cracking) as well as the appraisal of the actual ductility of the reinforced concrete member.

The automatic method for developing stress fields proposed by Fernández Ruiz and Muttoni [Fer07] overcomes the aforementioned limitations of the rigid-plastic stress field method. Concrete and steel are modelled by elastic-plastic constitutive relationships (bi-linear), which allows considering the actual state of deformation in the process of determining a statically consistent stress field. This approach called elastic-plastic stress field (EPSF) method is implemented into a finite element (FE) procedure in order to establish stress fields that respect the equilibrium condition as well as the compatibility of deformations inside a structural element. Contrary to RPSF, where the stress field inclination is chosen to respect equilibrium with external loads and to avoid concrete crushing, the EPSF derive the principal stress directions directly from the local deformations and additionally account for the effect of cracking on the effective concrete compressive strength by knowing the acting transvers strains.

The EPSF-FE thus consistently accounts for the actual kinematic behaviour of the entire structural element in which the state-of-strain may be variable over the element height and length and thereby seizes the influence of kinematically dependent actions or phenomena (e.g. effect of prestressing, variable stiffness or variable cross sections, internal forces redistribution in the non-linear regime and/or in hyperstatic structures etc.). Due to the respected kinematic compatibility condition, the EPSF-FE method leads to a licit failure mechanism when the load approaches the ultimate bearing capacity of the element. It can thus be considered that the EPSF method yields exact solutions according to the theory of plasticity, for which a statically consistent stress field that respects the plastic condition of materials (lower bound) simultaneously corresponds to a kinematically consistent failure mechanism (upper bound), [Mut15, Nie11].

The EPSF method is a practical and reliable tool to investigate the behaviour of reinforced concrete elements [Fer07, Fer08, Kos09, Mut15]. This is particularly true if the basic assumptions of the stress field method are respected of which the most important is the presence of a minimal reinforcement for crack control that allows the elements to reach the plastic behaviour [Mut97, Fer07]. The method has been thoroughly tested by comparing EPSF predictions to experimental test results of various types of structural elements. On the overall, EPSF provide excellent predictions of the failure loads as well as the failure mechanisms [Mut16]. The EPSF allows as well to investigate prestressed elements with low amount of shear reinforcement [Rup14] and critical details of existing structures such as dapped-end beams, Gerber-joints, crossed walls, insufficient anchorage and concrete cover spalling [Arg14, Mut16]. Campana [Cam13] showed that ESPF method can even provide good results in cases without minimum transverse reinforcement, if no localisation of the deformations occurs.

2.4.1 Constitutive laws

In contrast to other finite element methods for the non-linear analysis of reinforced concrete elements, the EPSF method [Fer07] is characterized by the fact that concrete and reinforcing steel behaviour are modelled by only two material parameters that have a clear physical meaning and are relatively well defined: the uniaxial compressive strength and the modulus of elasticity.

The reinforcement is modelled using an elastic-plastic material law for tension and compression, figure 2.13a. The material law is defined by the yield strength f_s and the elastic modulus E_s of steel. If necessary, strain hardening can be considered by introducing an appropriate hardening modulus E_h.

The constitutive relationship for concrete is admitted to be elastic-perfectly plastic in compression. The tensile strength is completely neglected, see figure 2.13b. The effective concrete compressive strength $f_{cp,eff}$ is determined from the equivalent plastic strength f_{cp} that is corrected by the factor η_ε to account for transverse strain:

$$f_{cp,eff} = \eta_\varepsilon \, f_{cp} \tag{2.22}$$

The factor η_ε (see following subsection and eq. 2.25) depends on the acting state-of-strain such that the effective compressive strength has to be evaluated individually for each concrete finite element. The equivalent plastic strength of concrete is defined according to Muttoni [Mut90]:

$$f_{cp} = \eta_{f_c} \cdot f_c \tag{2.23}$$

where f_c is the cylinder compressive strength of concrete and η_{f_c} a correction factor to account for brittle behaviour of higher strength concrete (see following subsection and eq. 2.24).
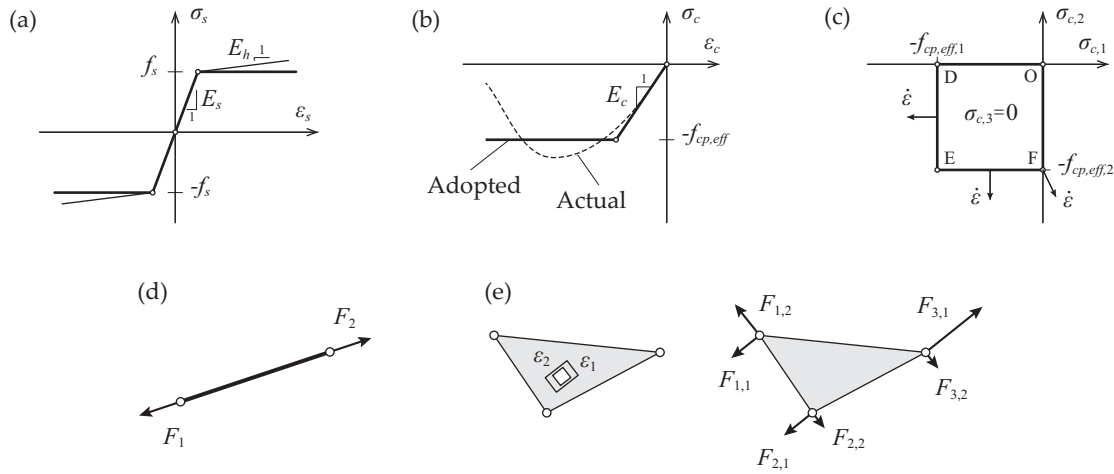
Figure 2.13 Elastic-plastic stress fields [Fer07]: constitutive laws for (a) steel; (b) concrete and (c) Mohr-Coulomb yield surface for concrete in plane stress state with neglected tensile strength; (d) finite element for reinforcing bars and (e) constant strain triangle for modelling concrete.

In accordance with works by Vecchio et al. [Vec94] and Belarbi and Hsu [Bel95], the EPSF method admits a constant secant modulus E_c for concrete in compression. It should be noted that a consequence of this assumption is that the deformation for which the concrete reaches the effective compressive strength $f_{cp,eff}$ is not always the same, since the latter is influenced by the acting transverse strain.

Regarding the behaviour of concrete in a biaxial stress state, the EPSF method [Fer07] assums that the principal stress directions are parallel to the principal strain directions (Wagner's tension field assumption [Wag29]) and that the principal stresses are directly obtained from the principal strains by means of the previously presented constitutive law. This behaviour corresponds to a Mohr-Coulomb yield surface with a tension cut-off as shown in figure 2.13c. The influence of the transverse strains on the concrete compressive strength ($\eta_\varepsilon \leq 1.0$) can be interpreted as shrinkage of the yield surface with respected to a positive transverse strain increase.

Influence of brittle behaviour of higher strength concrete

The assumption of a plastic resistance for steel agrees relatively well with the actual material behaviour, this is however not the case for concrete that shows a non-negligible softening behaviour after reaching the peak strength. Furthermore, it has been shown (e.g. [Pop73]) that with increasing compressive strength, concrete develops a pronounced brittle behaviour that leads to an important and rapid loss of the resistance once the peak strength is reached. In order to still be able to model the behaviour of concrete by means of a plastic (resp. elastic-plastic) constitutive law (fig. 2.13b), the concrete compressive strength f_c is reduced by the factor η_{f_c} to account for the brittle behaviour of higher strength concrete.

The EPSF method [Fer07, Mut16] generally adopts the formulation of η_{f_c} according to the development by Muttoni [Mut90] (as well adopted in design recommendations [SIA13, FIB13]):

$$\eta_{f_c} = \left(\frac{30}{f_c}\right)^{1/3} \leq 1.0 \tag{2.24}$$

where the uniaxial cylinder compressive strength f_c is introduced in [MPa]. It should be noted that in the FE method, the reduction factor η_{f_c} has to be introduced manually by setting the concrete compressive strength in the material properties equal to the corresponding plastic strength f_{cp}.

Influence of transverse strain

Another factor that influences the effective concrete compressive strength is the tensile strain (ε_1) that acts perpendicular to the principal compressive stress direction. Such strains are naturally present during the cylinder test and eventually cause failure of the concrete. In structural elements transverse tensile strains can have several origins and can be higher, such that the measured cylinder compressive strength can generally not be reached. In structural concrete, significant tensile strains are typically introduced by the elongation of reinforcing bars that are inclined compared to principal compressive stress directions in the concrete. The imposed tensile deformations induce cracking and lead to a similar concrete strain softening behaviour as observed in the post-peak behaviour under uniaxial compression. The concrete compressive strength has thus to be reduced in order to account for the influence of transverse strains. Regarding this subject, several studies have been conducted and led to various models but are generally providing similar results [Vec86, Bel95, Kau98]. A commonly used formulation is the one proposed by Vecchio and Collins [Vec86] that has been developed in the context of the modified compression field theory. The empirical formulation of concrete strength reduction factor η_ε is a function of the first principal strain ε_1:

$$\eta_\varepsilon = \frac{1}{0.8 + 170 \, \varepsilon_1} \leq 1.0 \tag{2.25}$$

In order to estimate the effect of cracking on the compressive strength of concrete, a representative tensile strain has to be determined, which requires a strain-based analysis tool. The EPSF-FE is thus able to evaluate the effective concrete compressive strength based on the realistic and kinematically compatible deformation of the entire structural element, whereas in RPSF approach, the reduction factor that accounts for cracking can only be estimated based on experimental observations and experience, as proposed in [Mut97].

2.4.2 Finite element implementation

The following section present a brief description of the finite element concept of the EPSF method proposed in [Fer07]. Detailed information regarding the FE formulations is presented in the Chapter 4 where the proposed ML-EPSF is developed.

Starting from the displacement field over a continuum, the EPSF-FE method determines the deformation in the concrete and of the reinforcement. To this purpose, the two materials are modelled by distinct finite elements: constant strain triangles (fig. 2.13e) and bar elements (fig. 2.13d). It is assumed that reinforcement and the surrounding concrete are perfectly bonded (no relative displacement), such that the two elements have identical deformations in the direction of the bar element.

The behaviour of concrete is modelled by constant strain triangles. The displacement of the three nodes allows determining the state-of-strain of the concrete (ε_x, ε_y, γ_{xy}). Using Mohr's circle of strains, the principal strains (ε_1, ε_2) and the principal strain direction are obtained. Due to the assumption that principal stresses are parallel to the principal strains, concrete stresses can be directly computed by means of the elastic-plastic constitutive law. The constant stresses are then integrated over the element surface in order to obtain the corresponding nodal forces.

The behaviour of the reinforcing steel is modelled by bar elements. The strains are determined in the direction of the element axis, the corresponding stresses are obtained from the constitutive relationship. The element nodal forces are eventually computed from the stress by multiplying with the rebar cross-section surface of the analysed element. An additional assumption of the EPSF method is that the rebar elements only carry axial forces, i.e. dowel action is neglected. If required, the bar elements allow as well to implement prestressing by imposing an initial self-induced strain in the element.

The nodal forces of each concrete and steel finite element are assembled according to classical finite element technique. If the nodal forces of the FE model are in equilibrium with the applied forces, a static and kinematic valid solution has been found. If residual forces exist in the model, the FE program implemented by [Fer07] applies an iterative solution procedure based on a tangent stiffness matrix and a full Newton-Raphson algorithm to solve the non-linear problem. The basic principal is to determine an improved displacement field by means of the residual forces and the tangent stiffness matrix. This displacement field is again applied to the FE model and the nodal forces are re-evaluated. The iterative procedure is repeated until the equilibrium condition is satisfied.

Chapter 3   Elastic-plastic stress field models for membrane and bending interactions

The present chapter introduces a novel multi-layered elastic-plastic stress field (ML-EPSF) approach to investigate plan reinforced concrete element subjected to membrane and transverse bending actions. The ML-EPSF approach is applied to the case of a web segment in order to study the in-plane shear and transverse bending interaction mechanism. For the application in practice, an enhanced simplified verification method for beams elements with transverse bending is proposed and validated by a comparison to experimental test results from the literature.

3.1   Multi-layered elastic-plastic stress field approach

This section presents a method to establish stress fields that are in equilibrium with the external loads and that simultaneously accounts for the actual kinematics of a reinforced concrete element subjected to a combination of in-plane forces and out-of-plane bending moments.

To this purpose, the EPSF method by Fernández Ruiz and Muttoni [Fer07], that has proven to be a powerful tool for the assessment and design of reinforced concrete members in a plane stress-state, is extended to a multi-layered model by assuming appropriate kinematic relationships for out-of-plane deformations.

The advantage of using the EPSF method is that it provides detailed information about the internal state-of-stress in the concrete and the reinforcement, which makes it a valuable tool to investigate the in-plane shear transverse bending interaction mechanism. Additionally, at failure, the EPSF method yields exact solutions according to the theory of plasticity by bringing together the upper and lower bound theorem. This leads to a more accurate and thus less conservative estimation of the actual combined in-plane shear transverse bending resistance of reinforced concrete segments.

The present section introduces the general formulation of the proposed multi-layered elastic-plastic stress field method. In section 3.2 it is then applied to the practical case of in-plane shear and transverse bending in beam webs.

3.1.1 Concept and kinematics of the layered model

The ML-EPSF, as the EPSF, is a displacement-based procedure, where the stresses are derived from the strains by means of material laws and then integrated to obtain the internal forces.

The deformation of the layered model is entirely defined by a set of six generalized strains: the three in-plane strains at the mid-plane of the element ($\varepsilon_{x0}, \varepsilon_{y0}, \gamma_{xy0}$) and the three out-of-plane curvatures ($\chi_x, \chi_y, \chi_{xy}$). The state-of-strain in a plane located at a distance z from the mid-plane is obtained by assuming the Bernoulli-Navier hypothesis of plane sections:

$$\varepsilon_x = \varepsilon_{x0} - z \cdot \chi_x \qquad \varepsilon_y = \varepsilon_{y0} - z \cdot \chi_y \qquad \gamma_{xy} = \gamma_{xy0} - z \cdot \chi_{xy} \tag{3.1}$$

The reinforced concrete element is divided over its width into a finite number of concrete layers (n_c) which each behave according to the EPSF method, figure 3.1a. Additional layers are introduced for steel at the location of the reinforcement. The deformation of each layer i is defined by a separate strain field ($\varepsilon_{x,i}, \varepsilon_{y,i}, \gamma_{xy,i}$), figures 3.1d-e. In the concrete layers the principal strains ($\varepsilon_{1,i}, \varepsilon_{2,i}$) and their orientation (θ_i) are determined using Mohr's circle of strains. The concrete principal stresses are then computed from the principal strains assuming that the principal strain directions coincide with the principal stress directions and it is admitted that concrete and steel behave according to elastic-plastic material laws [Fer07]. Additionally, the plastic strength of concrete f_{cp} is reduced individually in each layer using the reduction factor $\eta_{\varepsilon,i} = f(\varepsilon_{1,i})$ (of that layer) to account for the effect of cracking. The resulting stresses in the concrete and reinforcement layers (figures 3.1f-g) are then integrated over the element width to obtain the stress resultants, figure 3.1c.

3.1.2 Concrete and reinforcement layers

The ML-EPSF model distinguishes between two layer types: concrete layers and reinforcement layers. Their definition and behaviour, i.e. state-of-strain, constitutive models and state-of-stress, are presented in the present section. As in the ESPF method, it is assumed that concrete and steel behave according to elastic-perfectly plastic constitutive laws as presented in section 2.4.1.

Concrete layers

The element width is divided into n_c concrete layers of equal width (b_w/n_c). The location of the i-th layer relative to the element mid-plane is indicated by $\bar{z}_i$ (centre of the layer). The state-of-strain in each concrete layer ($\varepsilon_{x,i}, \varepsilon_{y,i}, \gamma_{xy,i}$) is then obtained from the kinematic relationships (eq. 3.1) when $z = \bar{z}_i$. The principal strains $\varepsilon_{1,i}$ and $\varepsilon_{2,i}$ (with $\varepsilon_{1,i} \geq \varepsilon_{2,i}$) of the layer are computed using Mohr's circle of strains. The angle θ_i indicates the inclination of the principal compressive strain $\varepsilon_{2,i}$ relative to the x-axis, see figure 3.2a.
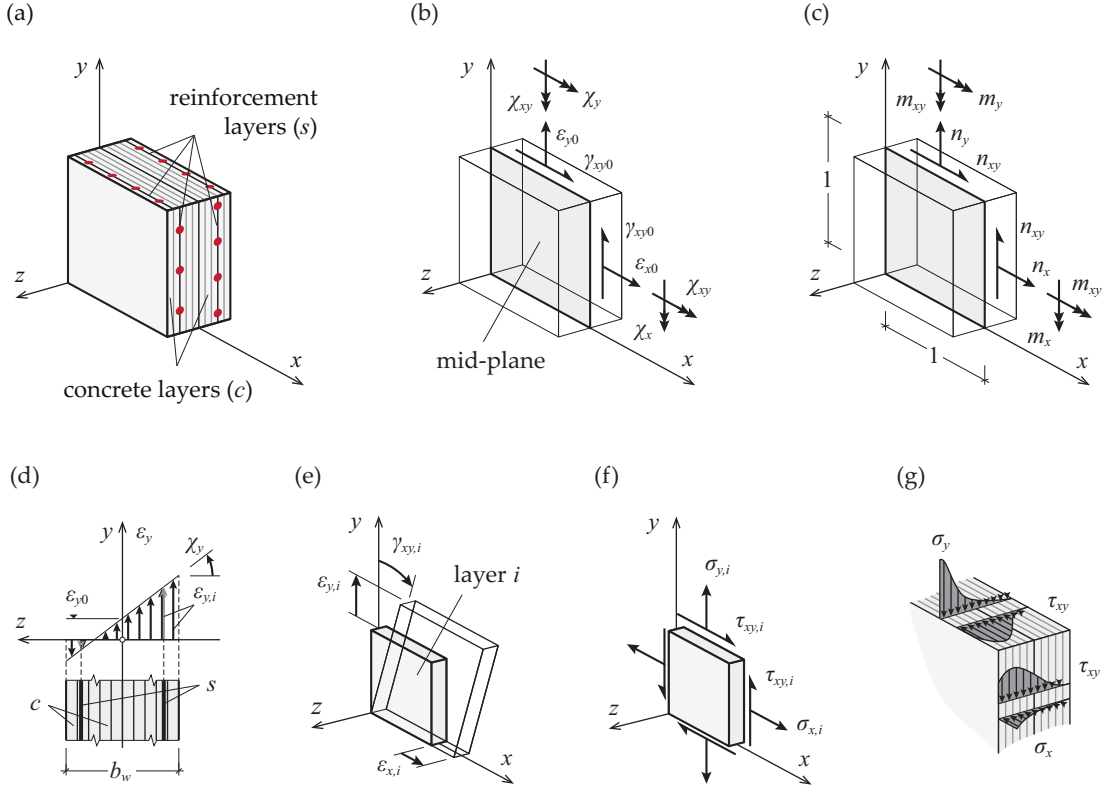
Figure 3.1 Concept of the ML-EPSF model: (a) concrete and reinforcement layers; (b) generalized in-plane and out-of-plane deformations; (c) generalized internal forces; (d) deformation of the cross section; (e) state-of-strain of a layer; (f) state-of-stress of a layer and (g) example of a stress profile across the element width.

$$\tan \theta_i = \frac{\varepsilon_{y,i} - \varepsilon_{x,i} - \sqrt{\left(\varepsilon_{x,i} - \varepsilon_{y,i}\right)^2 + \gamma_{xy,i}^2}}{\gamma_{xy,i}} \tag{3.2}$$

$$\varepsilon_{1,i} = \varepsilon_{x,i} - \frac{1}{2} \cdot \gamma_{xy,i} \cdot \tan \theta_i \qquad \varepsilon_{2,i} = \varepsilon_{y,i} + \frac{1}{2} \cdot \gamma_{xy,i} \cdot \tan \theta_i \tag{3.3}$$

It is assumed that the directions of principal stresses are parallel to the directions of principal strains [Fer07]. Thus the concrete principal stresses $\sigma_{1,i}$ and $\sigma_{2,i}$ (with $\sigma_{1,i} \geq \sigma_{2,i}$) are computed directly from the principal strains using the elastic-plastic constitutive law for concrete. The compressive stress in each layer is limited to the effective compressive strength $f_{cp,eff,i} = \eta_{\varepsilon,i} \cdot f_{cp}$, where the concrete strength reduction factor $\eta_{\varepsilon,i}$ is evaluated separately for each layer based on the acting transverse strain $\varepsilon_{1,i}$ (eq. 2.25).

$$\sigma_{1,i} = E_c \cdot \varepsilon_{1,i} \qquad \text{with} - f_{cp} \leq \sigma_{1,i} \leq 0$$

$$\sigma_{2,i} = E_c \cdot \varepsilon_{2,i} \qquad \text{with} - \eta_{\varepsilon,i} \cdot f_{cp} \leq \sigma_{2,i} \leq 0 \tag{3.4}$$
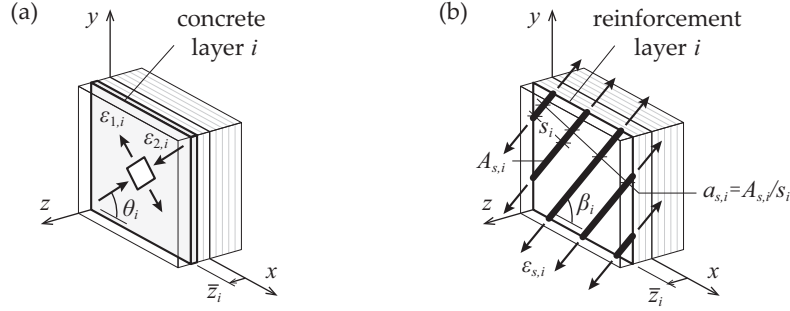
Figure 3.2 State-of-strain in the layers: (a) principle strains in a concrete layer and (b) axial strains in a reinforcement layer.

The concrete strength reduction factor is only applied to the compressive strength of the second principal direction (eq. 3.4-2) and doesn't affect the concrete's Young modulus E_c. In fact, two distinct factors could be computed, one for each principal direction: $\eta_{\varepsilon 1,i} = f(\varepsilon_{2,i})$ and $\eta_{\varepsilon 2,i} = f(\varepsilon_{1,i})$ that define respectively $f_{c1,eff,i}$ and $f_{c2,eff,i}$. However, $f_{c1,eff,i} < f_{cp}$ is never governing for $\sigma_{1,i}$. Indeed, if $\varepsilon_{1,i} \geq 0$ the stress $\sigma_{1,i} = 0$ (tensile strength neglected) independently of the value of $f_{c1,eff,i}$ and if $\varepsilon_{1,i} < 0$ the second strain $\varepsilon_{2,i}$ is negative too ($\varepsilon_{1,i} \geq \varepsilon_{2,i}$) which leads to $\eta_{\varepsilon 1,i} = 1.0$ and $f_{c1,eff,i} = f_{cp}$. Consequently, only the reduction for the second principal direction needs to be computed, $\eta_{\varepsilon,i} = \eta_{\varepsilon 2,i}$.

The concrete principal stresses are expressed in the global $x - y$ coordinate system, where $\sigma_{cx,i}$ and $\sigma_{cy,i}$ are the concrete compressive stresses and $\tau_{cxy,i}$ are the concrete tangential stresses in each layer (figure 3.1f).

$$\sigma_{cx,i} = \sigma_{1,i} \cdot \sin^2 \theta_i + \sigma_{2,i} \cdot \cos^2 \theta_i$$

$$\sigma_{cy,i} = \sigma_{1,i} \cdot \cos^2 \theta_i + \sigma_{2,i} \cdot \sin^2 \theta_i \qquad (3.5)$$

$$\tau_{cxy,i} = \left(\sigma_{2,i} - \sigma_{1,i} \right) \cdot \sin \theta_i \cdot \cos \theta_i$$

Reinforcement layers

The reinforcement layers (figure 3.2b) are placed at the actual position $\bar{z}_i$ of the reinforcement in the width of the element (independently of position of the concrete layers). The state-of-strain ($\varepsilon_{x,i}, \varepsilon_{y,i}, \gamma_{xy,i}$) in the i-th reinforcement layer is given by equation 3.1 when $z = \bar{z}_i$. It is assumed that the reinforcement bars carry only axial forces (dowel action is neglected [Fer07]). The rebar strains $\varepsilon_{s,i}$ are thus expressed in the direction of the rebar axis that is indicated by β_i (measured from the x-axis, fig. 3.2b).

$$\varepsilon_{s,i} = \varepsilon_{x,i} \cdot \cos^2 \beta_i + \varepsilon_{y,i} \cdot \sin^2 \beta_i + \gamma_{xy,i} \cdot \sin \beta_i \cdot \cos \beta_i \qquad (3.6)$$

The rebar stresses $\sigma_{s,i}$ are computed using the elastic-plastic constitutive law for steel presented earlier:

$$\sigma_{s,i} = E_s \cdot \varepsilon_{s,i} \qquad \text{with } |\sigma_{s,i}| \leq f_s \tag{3.7}$$

The state-of-stress of each reinforcement layer in $x - y$ coordinates according to figure 3.1f is finally given by:

$$\sigma_{sx,i} = \sigma_{s,i} \cdot \cos^2 \beta_i$$

$$\sigma_{sy,i} = \sigma_{s,i} \cdot \sin^2 \beta_i \tag{3.8}$$

$$\tau_{sxy,i} = \sigma_{s,i} \cdot \sin \beta_i \cdot \cos \beta_i$$

3.1.3 Generalized internal forces

The generalized internal forces (n_x, n_y, n_{xy}, m_x, m_y, m_{xy}) in figure 3.1c that result from the imposed set of generalized deformations (ε_{x0}, ε_{y0}, γ_{xy0}, χ_x, χ_y, χ_{xy}) are obtained by integrating the layer stresses (fig. 3.1g) over the element thickness. Since the stresses are constant over the width of each layer, the integration is performed by summation over the n_c concrete layers and the n_s steel layers. The stress resultants are expressed per unit length.

The in-plane forces in x and y direction, n_x and n_y, and the in-plane shear force n_{xy}:

$$n_x \quad = n_{cx} + n_{sx} \quad = \frac{b_w}{n_c} \cdot \sum_{i=1}^{n_c} \sigma_{cx,i} + \sum_{i=1}^{n_s} a_{s,i} \cdot \sigma_{sx,i}$$

$$n_y \quad = n_{cy} + n_{sy} \quad = \frac{b_w}{n_c} \cdot \sum_{i=1}^{n_c} \sigma_{cy,i} + \sum_{i=1}^{n_s} a_{s,i} \cdot \sigma_{sy,i} \tag{3.9}$$

$$n_{xy} \quad = n_{cxy} + n_{sxy} \quad = \frac{b_w}{n_c} \cdot \sum_{i=1}^{n_c} \tau_{cxy,i} + \sum_{i=1}^{n_s} a_{s,i} \cdot \tau_{sxy,i}$$

The out-of-plane moments, m_x and m_y, and the torsional moment, m_{xy}, are given by:

$$m_x \quad = m_{cx} + m_{sx} \quad = -\frac{b_w}{n_c} \cdot \sum_{i=1}^{n_c} \bar{z}_i \cdot \sigma_{cx,i} - \sum_{i=1}^{n_s} \bar{z}_i \cdot a_{s,i} \cdot \sigma_{sx,i}$$

$$m_y \quad = m_{cy} + m_{sy} \quad = -\frac{b_w}{n_c} \cdot \sum_{i=1}^{n_c} \bar{z}_i \cdot \sigma_{cy,i} - \sum_{i=1}^{n_s} \bar{z}_i \cdot a_{s,i} \cdot \sigma_{sy,i} \tag{3.10}$$

$$m_{xy} \quad = m_{cxy} + m_{sxy} \quad = -\frac{b_w}{n_c} \cdot \sum_{i=1}^{n_c} \bar{z}_i \cdot \tau_{cxy,i} - \sum_{i=1}^{n_s} \bar{z}_i \cdot a_{s,i} \cdot \tau_{sxy,i}$$

3.2 Assessment of the in-plane shear transverse bending interaction in beam webs

The objective of the present section is to investigate the phenomenological behaviour of a beam web segment subjected to the combined action of in-plane shear and out-of-plane bending and to propose an enhanced model for the evaluation of the web resistance.

To this purpose a multi-layered panel element, based on the previous ML-EPSF approach, is developed. It allows a detailed investigation of the stress field and its parameters (inclination, concrete strength reduction factor) under combined action of in-plane and out-of-plane moment. Additionally, the panel element, that actually represents a small segment of the beam web, is used to establish enhanced in-plane shear transverse bending interaction diagrams for the assessment of the web resistance.

The observations on the ML-EPSF panel element are compared to the previously investigated RP interaction models. In particular the assumption on the stress distribution, the concrete strength reduction factor and the inclination of the compression field are examined. A comparison of the resulting interaction diagrams shows that the ML-EPSF panel element leads to a potentially more accurate and thus less conservative estimation of the combined resistance than rigid-plastic interaction models.

3.2.1 ML-EPSF panel element

The multi-layered elastic-plastic stress field panel presented in this section is an application of the previously presented general ML-EPSF approach to the practical case shown in figure 3.3. The panel element represents a unitary segment of a beam web subjected mainly to in-plane shear V and out-of-plane bending m. Transverse shear forces are neglected.

The panel element, of unit size ($l_x = 1, l_y = 1$) and width b_w, is divided into n_c concrete layers and has two reinforcement layers ($n_s = 2$) that are placed at the location of the actual shear reinforcement (on each face of the web), figure 3.3c. It is assumed that the orientation of the shear reinforcement is vertical ($\beta_1 = \beta_2 = 90°$). The panel deformation (fig. 3.3b) is defined by the following equations:

$$\varepsilon_x = \varepsilon_{x0} \qquad \varepsilon_y = \varepsilon_{y0} - z \cdot \chi_y \qquad \gamma_{xy} = \gamma_{xy0} \tag{3.11}$$

The shear deformation γ_{xy} and the transverse curvature χ_y will allow computing the in-plane shear force V and the transverse bending moment m. The longitudinal deformation of the web ε_x is assumed to be constant over the width ($\chi_x = 0$). The vertical deformation at the mid-plane of the web ε_{y0} defines, together with χ_y, the strain profile across the web width.

In the present case, no external vertical forces (as for example vertical prestressing) are acting on the web cross section, thus the vertical component of the concrete compression field
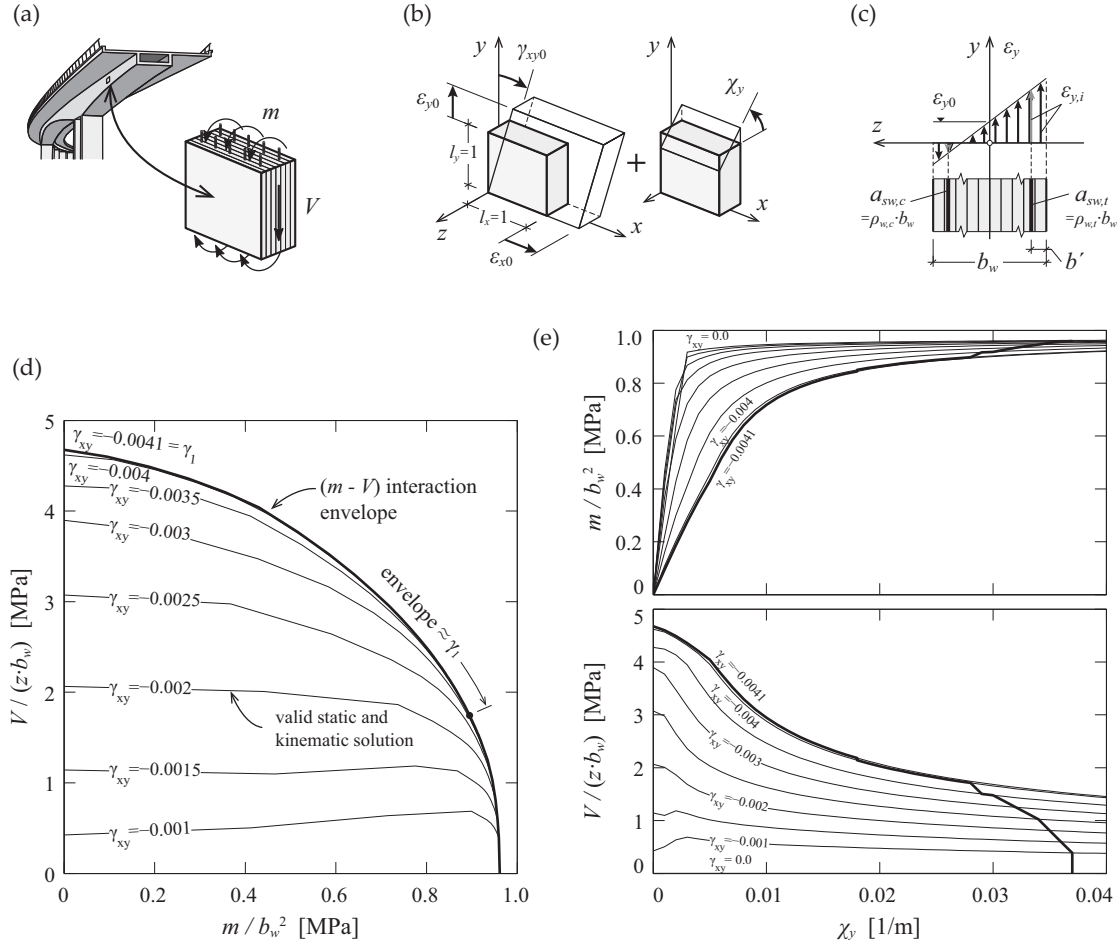
Figure 3.3 Multi-layered panel element and $(m - V)$ interaction diagram for beam webs: (a) investigated forces; (b) assumed panel kinematics; (c) layered web cross section with vertical deformation; (d) example of constructing the interaction diagram for $f_s = 435$ MPa, $f_{cp} = 20$ MPa, $\rho_w = 0.5$ %, $\rho_{w,t} = \rho_{w,c}$, $b'/b_w = 0.1$ and $\varepsilon_x = 0.5$ ‰: and (e) transverse bending moment and in-plane shear force as a function of the imposed transverse curvature along the $(m - V)$ interaction diagram.

has to be in equilibrium with the reinforcement forces. This leads to the following equilibrium condition:

$$n_y = n_{cy} + n_{sy} = \frac{b_w}{n} \cdot \sum_{i=1}^{n_c} \sigma_{cy,i} + \sum_{i=1}^{n_s} a_{s,i} \cdot \sigma_{sy,i} \quad = 0 \tag{3.12}$$

The shear force V and the transverse bending moment m that result from γ_{xy} and χ_y are computed according to the iterative procedure illustrated in figure 3.4 (light grey shaded area). For given panel characteristics (geometry, material, longitudinal deformation) and the imposed deformations (γ_{xy}, χ_y), the state-of-stress fulfilling the equilibrium of forces has to be determined. To do this, the initially unknown vertical deformation ε_{y0} is varied until the condition $n_y = 0$ (eq. 3.12) is fulfilled.

During the iterative procedure, the state-of-strain in each layer given by equation 3.11 allows computing the concrete and reinforcement stresses according to the ML-EPSF approach presented earlier. Once ε_{y0} satisfying the equilibrium condition of vertical forces is found, the resulting stress field is in equilibrium and the internal forces V and m are given by:

$$
\begin{aligned}
V = -l_y \cdot n_{xy} \quad &= -l_y \cdot \frac{b_w}{n_c} \cdot \sum_{i=1}^{n_c} \tau_{cxy,i} \\
m = m_c + m_s \quad &= -\frac{b_w}{n_c} \cdot \sum_{i=1}^{n} \bar{z}_i \cdot \sigma_{cy,i} - \sum_{i=1}^{n_s} \bar{z}_i \cdot a_{s,i} \cdot \sigma_{sy,i}
\end{aligned}
\tag{3.13}
$$

Longitudinal deformation ε_{x0}

The panel deformation ε_{x0} that is representing the longitudinal deformation of the web is assumed to be a property of the web. It allows considering the actual boundary conditions of the web as well as the effect of a possible longitudinal prestressing. Typical values for the average longitudinal strain are for example: $\varepsilon_{x0} = 0.5‰$ for normal beams and $\varepsilon_{x0} = 0.0‰$ for prestressed beams.

Number of layers n_c

The web width is divided into a finite number of concrete layers n_c. This number that has to be chosen by the user in advance of the computations has a certain influence on the precision of the predicted results. A smaller number of layers will speed up the computational time but will lead to less precise results; the obtained interaction curve will not be smooth and the predicted resistance slightly more conservative. In order to consider a representative stress distribution in the concrete cross section and to obtain meaningful predictions for the combined resistance, a minimum number of twenty layers should be used. In the following examples, the web width is divided into hundred layers in order to avoid that the interpretation of the results could be affected by numerical issues.

Establishing the $(m - V)$ interaction diagram

The objective of the $(m - V)$ interaction curve for the assessment of beam webs is to provide an estimation of the ultimate load carrying capacity under the combined action of in-plane shear and transverse bending. In the ML-EPSF approach, this curve is given by the envelope of all possible combinations of the internal forces m and V that respect the static and kinematic compatibility conditions, see figure 3.3d.

The interaction curve is obtained in an iterative procedure that is detailed in the flowchart in figure 3.4. The procedure consists in three main parts:

Part 1: Compute m and V for different curvatures χ_y while the shear deformation γ_{xy} is maintained constant (fig. 3.3d and fig. 3.3e thin lines);
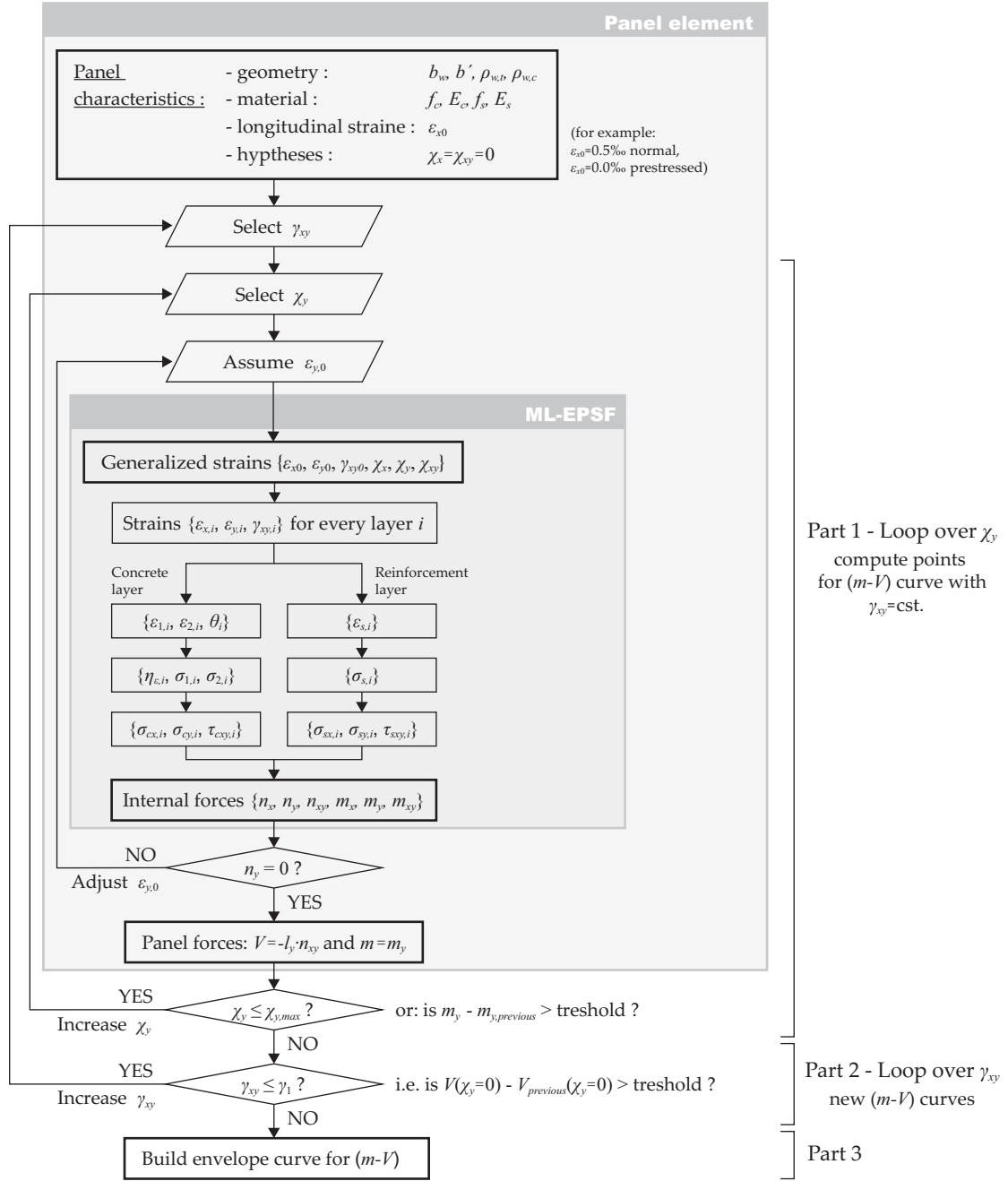
Figure 3.4 Flowchart for the development of the $(m - V)$ interaction diagram according to the ML-EPSF panel element.

Part 2: Increase the shear deformation and repeat Part 1;

Part 3: Determine the envelope curve of the previous results (fig. 3.3d bold line).

In Part 1, the ML-EPSF panel element is solved for different transverse curvatures ($0 \leq \chi_y \leq \chi_{max}$) and a constant shear deformation (γ_{xy}). After each computation, the curvature is increased and the shear force and transverse moment corresponding to the new panel

deformation are computed. This operation is repeated until the increase of the transverse moment between two iterations is negligible or the deformation in a reinforcement or concrete layer reaches the ultimate deformation of the material ($\varepsilon_{s,i} = \varepsilon_{su}$ or $\varepsilon_{2,i} = \varepsilon_{cu} = -3.0‰$).

Part 2 consists in a loop over the shear deformation with $0 \leq \gamma_{xy} \leq \gamma_1$. When the maximum curvature is reached the shear deformation is increased and Part 1 is repeated. The iterations are stopped when $\gamma_{xy} = \gamma_1$, where γ_1 is defined as the shear deformation that leads to the highest initial shear force V (i.e. when $\chi_y = 0$). For higher shear deformations no significant improvement of the final $(m - V)$ interaction curve (envelope) was observed.

From figure 3.3e it can be seen that the shear force increases with increasing shear deformation and decreases with increasing curvature. The transverse moment however shows the opposite behaviour. Thus, in order to determine the ultimate resistance of the web both diagrams are combined in the shear transverse bending diagram in figure 3.3d. The envelope of all the curves for constant shear deformation is the $(m - V)$ interaction curve defining the ultimate resistance of the investigated web section (bold line in fig. 3.3d).

Figure 3.3e shows that the envelope curve (in bold) intercepts multiple curves, for small curvatures $\gamma_{xy} = \gamma_1$ is governing, but with increasing curvature the envelope is obtained for smaller shear deformations. In general, it has been found that the curve for $\gamma_{xy} = \gamma_1$ is a good approximation of the envelope curve. However, it is not covering the entire range of interaction diagram (fig. 3.3d), since it is limited by the ultimate deformation of the material. For higher transverse bending moments (approximately $m > 0.8 \cdot m_{R0}$) the envelope curve has to be used.

3.2.2 Investigation of the interaction

The following section investigates the in-plane shear transverse bending interaction as predicted by the ML-EPSF panel element. The overall behaviour is analysed based on the $(m - V)$ interaction diagrams of various web cross sections, the multi-layered stress field and its parameters are discussed.

Overall $(m - V)$ interaction relationship

The $(m - V)$ interaction curves for various shear reinforcement ratios (ρ_w) and different longitudinal deformations (ε_x) are shown in figure 3.5. In general, it can be observed that the transverse bending moment leads to a significant reduction of the initial in-plane shear strength. However, the results show as well that the interaction is much weaker in the range of small transverse moments where the shear strength is only slightly reduced. For example, a transverse bending moment m of 30% of m_{R0} causes a reduction of the initial shear strength by 10% (at most) which is significantly less than what has been predicted with the RP interaction models for comparable cross sections (see detailed comparison between the RPSF and ML-ESPF interaction models in section 3.2.3).
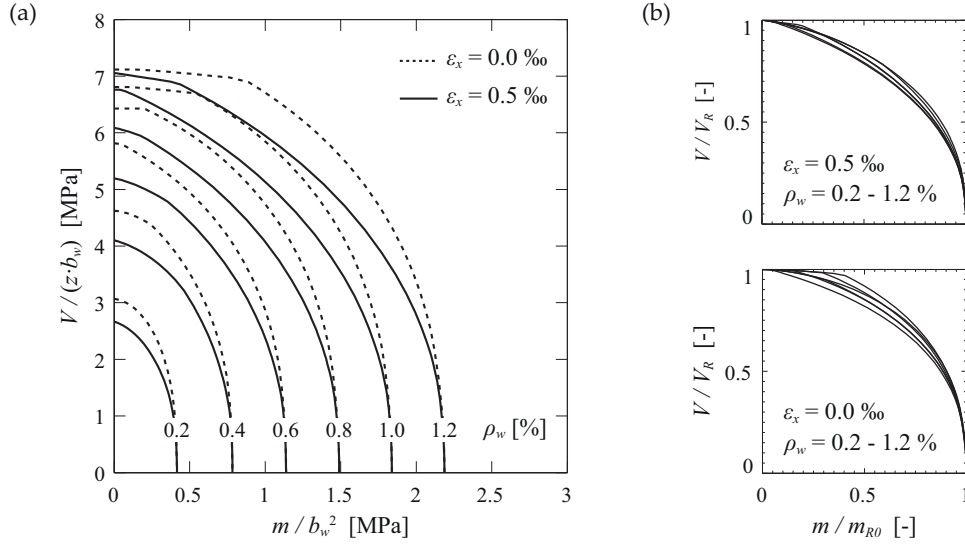
Figure 3.5 In-plane shear transverse bending interaction diagrams according to the ML-EPSF panel element ($f_c = 20$ MPa, $f_s = 435$ MPa $\rho_{w,t} = \rho_{w,c}$, $b'/b_w = 0.1$) for (a) different reinforcement ratios and (b) normalized diagrams for $\varepsilon_x = 0.5$‰ and $\varepsilon_x = 0.0$‰.

For high shear reinforcement ratios, the $(m - V)$ interaction curves presented in figure 3.5a show a horizontal plateau in the range of small transverse bending moments. In this region, the shear resistance is limited by the concrete strength ($V_{R,c} < V_{R,s}$); the shear reinforcement is not yet yielding (see fig. 3.6c for $\rho_w = 1.2\%$), which allows the cross section to carry a transverse bending moment by changes in the stirrup forces with no or only little loss of shear resistance. This phenomenon is more pronounced for reduced longitudinal strain ($\varepsilon_x = 0.0$‰).

When the in-plane shear force goes to zero, the transverse bending resistance computed with the ML-EPSF panel element is equal to the bending strength m_{R0} calculated using a stress bloc with strength f_c (Appendix A.2.2).

The effect of longitudinal strain ε_x

The interaction diagrams in figure 3.5 show, that the longitudinal strain ε_x has a non-negligible effect on the overall resistance of the element. In elements with no or only limited longitudinal deformation (for example prestressed beams $\varepsilon_x \approx 0$) the predicted initial shear strength (when $m = 0$) is significantly higher than for normal beams ($\varepsilon_x = 0.5$‰). This is mainly due to the fact that a restrained deformation ε_x can lead to a significant increase of the concrete strength reduction factor η_ε (up to 1.0), whereas in the RP approach this factor is assumed constant (SIA262 [SIA13]: $k_c = 0.55$, or $k_c \leq 0.65$ in case of a refined analysis). Besides its effect on the initial shear strength, ε_x also positively influences the overall shape of the interaction curves making thereby the in-plane shear strength less sensitive to the transverse bending moment, compare the curves in figure 3.5b.
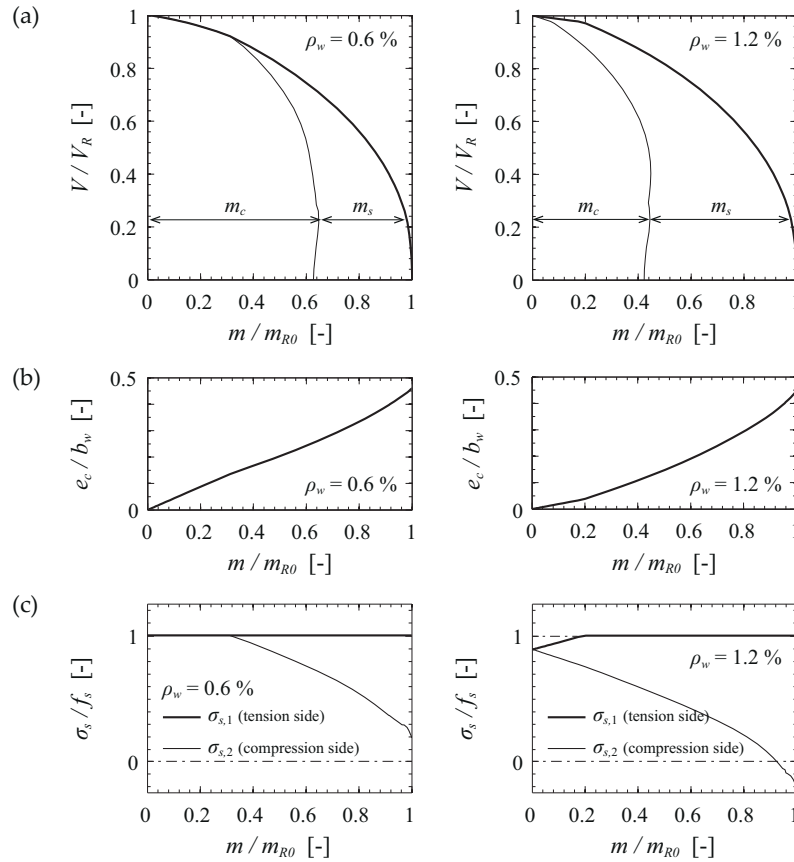
Figure 3.6 Contribution of the concrete and of the shear reinforcement to the transverse bending moment resistance: (a) shares of the moment equilibrated by compression field in the concrete m_c and the stirrup forces m_s; (b) eccentricity e_c of the compression field resultant n_{cy} and (c) stresses in the stirrups on both sides of the web.

Steel (m_s) and concrete (m_c) contribution to the transverse bending resistance

The transverse bending moment is resisted by the combination of two mechanisms: the eccentric compression field in the concrete and the asymmetrical forces in the shear reinforcement. The share of the moment that is resisted by each of them depends on the mechanical properties of the web cross section (especially the ρ_w and $\rho_{w,t}/\rho_{w,c}$) and the proportion between shear load and transverse bending moment.

In case of predominant shear load with small transverse bending moments, the stirrups on both sides are generally yielding (fig. 3.6c left). The transverse moment is then resisted entirely by the stress field in the concrete that shifts towards the bending compression side of the web (see figure 3.6a left: $m = m_c$ and $e_c = m_c/n_{cy}$ in figure 3.6b left). For higher levels of transverse bending, the stirrup stresses on the compression side ($\sigma_{s,2}$) decrease (fig. 3.6c left) and thereby contribute to equilibrate the transverse bending moment (see $m = m_c + m_s$ in figure 3.6a left).

The web behaviour is slightly different in case of high shear reinforcement ratios where the reinforcement is initially not yielding because the concrete strength of the web is governing (fig. 3.6c right). Thus small transverse moments are first mainly resisted by changes in the stirrup forces ($\sigma_{s,1}$ ↗ and $\sigma_{s,2}$ ↘) and an only small contribution of the compression field in the concrete (e_c in fig. 3.6b right increases much slower). Once the yield limit is reached on the tension side the behaviour is similar to the previous case. This initial reserve capacity of the shear reinforcement leads to a plateau in the $(m - V)$ interaction diagrams and thereby significantly increases the combined resistance of the web. A similar behaviour is observed for unsymmetrical shear reinforcement layouts ($\rho_{w,c} \neq \rho_{w,t}$).

The state-of-stress in the concrete under the influence of m

The $(m - V)$ interaction diagrams are compact representations of the highly non-linear behaviour a web segment subjected to a combination of in-plane and out-of-plane loads. The analysis of the multi-layered elastic-plastic stress field that governs them helps to interpret correctly such diagrams. Figure 3.7 shows the state-of-stresses in the web cross section of the previously investigated interaction curve for $\rho_w = 0.6\%$ and $\varepsilon_x = 0.5\text{‰}$ (fig. 3.5a). Since the stress field in the concrete varies significantly along the interaction curve, it is represented for different levels of transverse bending ($m/m_{R0} = \{0, 0.3, 0.8, 0.98 \text{ and } 1.0\}$), which allows illustrating several particularities of the ML-EPSF and the interaction phenomenon in general.

For small transverse bending moments (for example $m/m_{R0} = 0$ to 0.3) the behaviour of the element is still close to a pure shear behaviour (fig. 3.7); the shear stresses τ_{cxy} are relatively uniformly distributed over the entire web width and the stress field inclinations θ are almost constant.

The ML-EPSF panel elements show that for higher transverse bending moments, the stress distribution on the cross section is not uniform anymore; the concrete compressive stresses (σ_2 and σ_{cy}) and the shear stresses (τ_{cxy}) increase towards the bending compression side. At the same time, the width for the compression field diminishes. Indeed, some of the layers on the bending tension side are subjected to a pure tensile state-of-strain ($\varepsilon_1 > \varepsilon_2 > 0$) for which no concrete stresses can develop (concrete tensile strength being neglected in the EPSF method). Additionally, the multi-layered panel element confirmations that the inclination of the compression field θ in the outer layers increases significantly for higher transverse moments, reaching up to 90° (vertical) in some layers.

Finally, for very high levels of transverse bending (see fig. 3.7 for $m/m_{R0} = 0.98$ to 1.0), the results of the ML-EPSF panel show that the web stress profile resembles more and more a typical plastic bending stress distribution. The outer concrete layers on the compression side, together with the stirrups on the tension side, behave as in pure flexion: the compression field is concentrated in a narrow segment and it's inclination approaches 90° (vertical), the compressive stresses σ_2 reach the plastic strength of concrete f_{cp} ($\eta_\varepsilon \to 1.0$) and the rein-
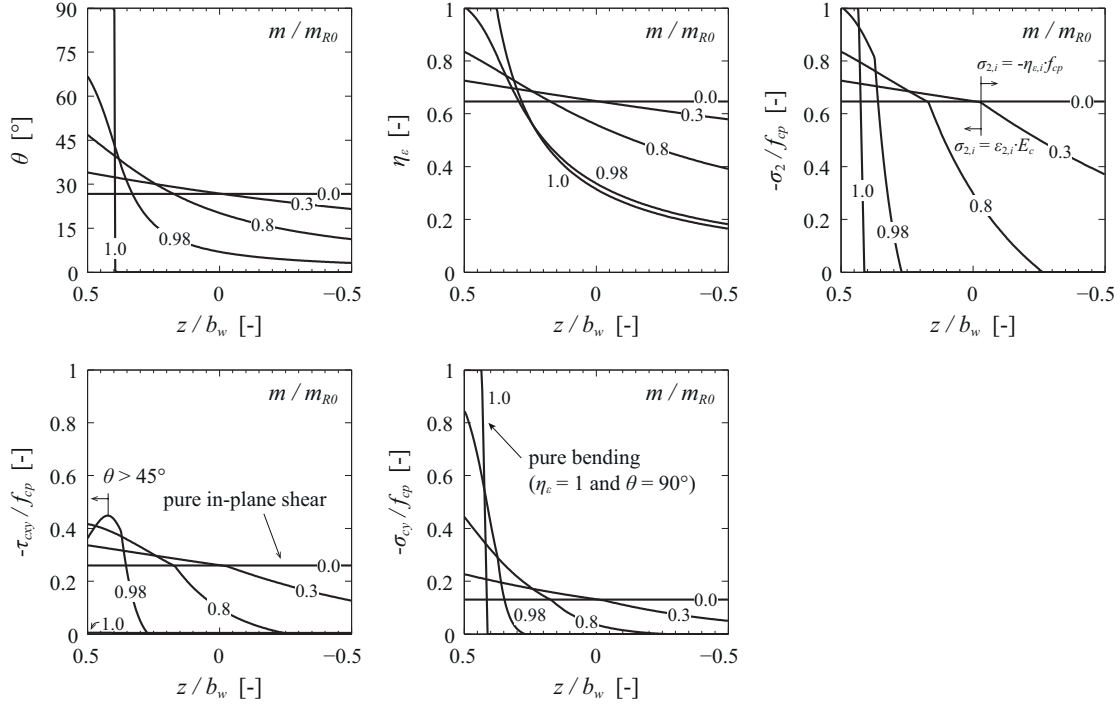
Figure 3.7 State-of-stress in the concrete layers of the web cross section for different levels of transverse bending moment of the $(m - V)$ interaction curve for $\varepsilon_x = 0.5\%_0$ and $\rho_w = 0.6\%$, with $f_c = 20$ MPa, $f_s = 435$ MPa, $\rho_{w,t} = \rho_{w,c}$, $b'/b_w = 0.1$.

forcement on the bending tension side is yielding ($\sigma_{s,1} = f_s$ in fig. 3.6c left). At the same time, only a small shear force V is still resisted by the web, of which most is carried by inner concrete layers, see τ_{cxy} for $m/m_{R0} = 0.98$ in figure 3.7. The outermost layers mostly only contribute to resist the transverse bending moment; their compression field inclination exceeds 45° such that they can only carry a very small amount of the shear force but significant bending compression forces. When the transverse moment eventually reaches the plastic bending strength m_{R0} the entire compression field is vertical and no shear stresses are transferred by the concrete layers.

Concrete strength reduction factor η_ε

A particular attention should be paid to the concrete strength reduction factor η_ε. It plays a significant role in the evaluation of the shear strength in general [Fer07] and thus as well in the assessment of the combined in-plane shear transverse bending resistance of the web cross sections.

In the ML-EPSF approach the factor η_ε is computed as a function of the state-of-strain in each layer, the latter is derived directly from the panel kinematic compatibility conditions. Figure 3.7 shows that the reduction factor decreases rapidly towards the bending tension side (where the principal tensile strains ε_1 increase due to χ_y) and increases towards the

bending compression side (where the ε_1 decrease due to χ_y) when the transverse moment becomes higher. Close to the pure bending strength (meaning χ_y high and thus ε_1 very small) the reduction factor $\eta_\varepsilon = 1$ in the outermost layers on the compression side.

The effect of η_ε on the concrete compressive stress σ_2 ($\sigma_2 \leq -\eta_\varepsilon f_{cp}$) and consequently as well on the entire stress field (σ_{cy}, τ_{cxy}) is clearly visible in the graphs of σ_2 in figure 3.7. The sudden change in the stress profile indicates in which layers the compressive stress is limited to the local effective compressive strength $f_{c,eff,i} = -\eta_{\varepsilon,i} f_{cp}$ (towards the bending tension side). The non-uniform distribution of η_ε and the stress field inclination θ thus largely contributes to the non-linear distribution of shear stresses and the vertical compressive stresses on the web cross section.

Due to the variable nature of the reduction factor and the kinematic compatibility conditions (especially the variable stress field inclination) it is possible to establish a continuous transition between pure in-plane shear behaviour (η_ε and θ uniform over the web width) and pure bending behaviour ($\eta_\varepsilon = 1$ and $\theta = 90°$ on a limited web width segment), which is one of the major issues encountered by most rigid-plastic interaction models.

Additionally, the reduction factor is generally higher than what is typically assumed for conventional rigid-plastic stress fields where no out-of-plane moment is considered (in the present example $\eta_\varepsilon \approx 0.65$ compared to $k_c = 0.55$ [SIA13]). This stays true for predominant shear load cases with small transverse bending moments. Consequently, the ML-EPSF leads to higher in-plane shear strength as conventional RPSF methods (see also comparison to RPSF in fig. 3.8a where $V_{ML-EPSF} > V_{R0}$), which is consistent with observations made with the classical elastic-plastic stress field method (for in-plane loading) by Fernández Ruiz and Muttoni [Fer07].

3.2.3 Comparison to the rigid-plastic interaction models

Shear transfer action under out-of-plane bending

The observations made on the basis of the proposed multi-layered elastic-plastic stress field panel element allow validating the basic principles and ideas of the rigid-plastic interaction models presented earlier:

- The out-of-plane bending moment that is acting on the transverse web cross section causes the shear force resultant to shift towards the flexural compression side in order to maintain the equilibrium of moments (F_c in fig. 2.2c and e_c in fig. 3.6b).

- Additional transverse bending resistance is obtained by changes in the stirrups forces between the bending compression and the bending tension side (ΔF in fig. 2.3, σ_s and m_s in fig. 3.6a,c).

- Furthermore, the ML-EPSF approach confirms Menn's model for predominant transverse bending (fig. 2.3e) that assumes the presence of a pure compression zone (where $k_c = 1$ and $\theta = 90°$) in the outermost layers of the web (compare to σ_{cy} and η_ε in fig. 3.7).

Although the ML-EPSF approach leads to very similar in-plane shear transverse bending interaction mechanisms, the actual stress fields, as well as the predicted strength, differ significantly. These differences result naturally from the different types of stress fields used: equilibrium based rigid-plastic stress fields that lead to a lower bound solutions; static and kinematic compatible elastic-plastic stress fields that lead to an exact solution at failure, according to the theory of plasticity.

Stress fields and assumptions

In the RPSF interaction models, the transverse stress distribution is tailored to equilibrate m and concrete stresses are admitted to act as a uniform stress bloc with $\sigma_c = k_c f_{cp}$ (effective compressive strength of concrete). The stress field parameters (θ, k_c) are chosen based on recommendations for RPSF that had been established for in-plane shear loads only, typically $k_c = 0.55$ and $30° \leq \theta \leq 45°$ [SIA13]. They are assumed constant over the width of the web and their value does not depend on the intensity of the transverse bending moment. These hypotheses are however very different from what is observed when computing the stress field with respect to kinematic compatibility conditions.

The ML-EPSF panel element shows that the inclination of the compression field is variable over the web width and changes with the intensity of the acting transverse moment (see θ in fig. 3.7). The inclination can reach up to 90° in the outer layers in case of important transverse bending. For close to pure shear behaviour, the ML-EPSF method (as EPSF in general) yields inclinations that are lower than the code recommendations. Similar observations are made for the concrete strength reduction factor η_ε (i.e. k_c) that varies strongly, depending on the intensity of the moment and the position in the web width (see η_ε in fig. 3.7).

The most significant difference in the overall stress field profile between the models is observed for small transverse bending moments. The compression field of the RPSF is already concentrated on a minimum web width and shifted until the web face on the bending compression side. Whereas, in the ML-EPSF approach, the compression field is still developed over the entire width of the web and the stress distribution is only slightly effected by the transverse bending moment (σ_{cy} and τ_{cxy} close to uniform for $m/m_{R0} = 0.3$ in fig. 3.7). With increasing transverse bending the ML-EPSF approaches the uniform stress distribution of the RPSF, but with different maximum stresses (due to the different values for k_c resp. η_ε).
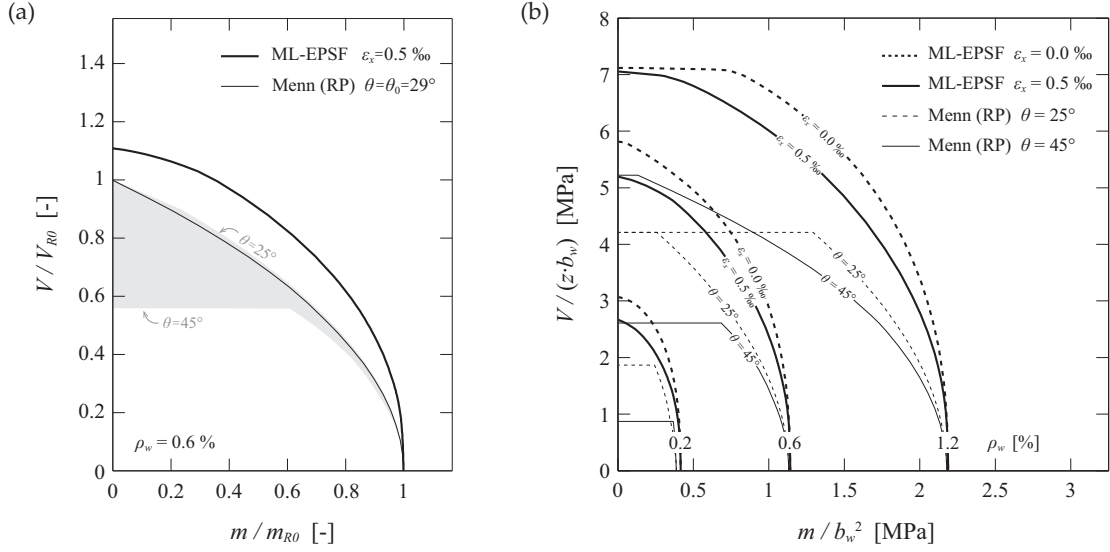
Figure 3.8 Comparison of $(m - V)$ interaction diagrams according to the RP model by Menn [Men86] and the proposed ML-EPSF panel element for $f_c = 20$ MPa, $f_s = 435$ MPa, $\rho_{w,t} = \rho_{w,c}$, $b'/b_w = 0.1$: (a) normalized diagram for $\rho_w = 0.6\%$, Menn with $\theta = \theta_0 = 29°$ and $k_c = 0.55$, ML-EPSF with $\varepsilon_x = 0.5‰$; (b) range of diagrams for various ρ_w.

These differences in the stress fields of the RPSF and the ML-EPSF approaches affect the predictions of the combined in-plane shear transverse bending resistance of webs, which is clearly visible in the resulting $(m - V)$ interaction diagrams presented in figure 3.8. The predictions differ especially in the range of small transverse moments because of the aforementioned reasons.

Predicted shear transverse bending interactions

The interaction diagrams in figure 3.8 show the predicted in-plane shear transverse bending resistance according to the RPSP approach by Menn [Men86] and the proposed ML-EPSF panel element.

The normalized diagrams in figure 3.8a show, that the ML-EPSF model predicts a substantially higher combined in-plane shear transverse bending resistance than the RPSF model. The two main reasons for this are:

- The overall interaction is weaker (weaker slope and higher curvature of the $(m - V)$ curve), especially in the range of small transverse bending moments.

- The initial shear strength (when $m = 0$) is remarkably higher.

As already mentioned earlier, the differences between these two interaction curves is a direct consequence of the different kinds of stress fields used and their respective hypotheses regarding the stress distribution, the concrete strength reduction factor and the stress

field inclination. Whereas these factors are chosen to be constant and on the safe side for the RPSF model, the ML-EPSF method computes them on the basis of a more realistic kinematical approach. This not only predicts more exactly the shear resistance due to a refined analysis tool, but the latter also accounts for the positive effect of the bending compression on the stress field and in particular on the strut inclination and the concrete strength reduction factor. Indeed, the latter increase due to the bending compression which slows down the loss of shear resistance caused by the transverse bending moment.

Besides the generally more favourable shape of the ML-EPSF interaction curve, the initial in-plane shear strength (when $m = 0$) also plays a major role for the overall resistance. The ML-EPSF method predicts substantially higher initial shear strength (+12% for $\rho_w = 0.6\%$, fig. 3.8a), which leads to a general increase of the shear strength under transverse bending (curve shifts upwards). This difference is again mostly due to the concrete strength reduction factor which is less penalizing in an EPSF approach (for example $\eta_\varepsilon = 0.65$ for $m = 0$ in fig. 3.8a) than for a RPSF method ($k_c = 0.55$). This effect becomes even more pronounced for high shear reinforcement ratios ($\eta_\varepsilon = 0.75$ for $\rho_w = 1.2\%$ and $m = 0$ in fig. 3.8b). For very low shear reinforcement ratios the concrete strength reduction factor for both methods (RP and EP) is very similar (~0.55), nevertheless the EPSF predicts higher initial shear strength (see fig. 3.8b $\rho_w = 0.2\%$) because, in these cases, the computed inclination of the compression field decreases below 25°, the inferior limit recommended by SIA262 [SIA13] for the rigid-plastic stress fields.

In the range of small transverse moments, which is probably the most important for most practical cases, the predicted shear strength shows thus little sensitivity to the transverse moment. As shown in the previous section, small transverse moments only slightly disturb the stress field distribution over the web cross section, which then causes just a little loss in shear resistance. The fact that the computed concrete strength reduction factor is still high contributes to the positive behaviour.

3.2.4 Synopsis

The sectional analysis performed with the ML-EPSF panel element leads to the following findings regarding the interaction of in-plane shear and transverse bending in beam webs:

- The ML-EPSF panel approach covers effectively the entire range of combined solicitations, from pure shear to pure transverse bending.

- The analysis confirms the existence of the in-plane shear transverse bending interaction, but indicates that is less pronounced than predicted by RP models.

- The model confirms the force transfer mechanism assumed in the RP models: shifting of the compression field to the bending compression sided; increase of the transverse bending resistance by changes in the stirrup forces.

- The stress field is highly non-linear in the transverse direction (inclination, distribution of stresses and concrete strength reduction factor) and strongly depends on the intensity of the transverse bending moment.

- The longitudinal deformation, not accounted for in the RP mode, has a substantial influence on the overall resistance.

- The effect of bending compression on the shear resistance is significant: it locally increases the compression field inclination and the effective concrete compressive strength, which has a favourable effect on the shear resistance.

- The interaction curve provided by the ML-EPSF approach is an exact solution according to the theory of plasticity, leading thereby to less conservative estimates of the combined in-plane shear transverse bending resistance than RP interaction models (lower bound solutions).

Compared to the RP interaction models, the ML-EPSF panel element is a refined analysis tool that provides more accurate estimates of the actual combined in-plane shear transverse bending resistance of beam webs. Nonetheless, it should be noted that the RP and ML-EPSF interaction models are both sectional analysis tools that inform about the resistance of small web segments. This is however only useful if the most critical section and the corresponding internal forces are known, but in case of more complex structural elements this might not be straight forward. It becomes even more complicated if redistributions of internal forces are to be expected, as for instance between different components of one element (e.g. between the web and the flanges of a beam) or in hyperstatic structural elements like for example multi-span beams.

In such cases a global analysis of the entire structural element is required, which is generally performed by a finite element analysis. To this purpose, a simplified method based on the well-established elastic-plastic stress field finite element method by [Fer07] for plane reinforced concrete elements is proposed (section 3.3). This tool is conceived for practical applications and provides a rapid and safe estimation of the shear resistance under the influence of transverse bending, while simultaneously accounting for the actual non-linear behaviour of the reinforced concrete element in the longitudinal direction.

3.3 Simplified plane EPSF verification method for beams with transverse bending moments

This section presents a simplified verification tool for reinforcement concrete elements subjected to in-plane shear and out-of-plane bending. The approach provides safe estimates of the actual longitudinal shear resistance of beams by using the plane elastic-plastic stress field method for in-plane loads in which the geometric beam properties are modified to simulate the effect of the transverse bending moment. The proposed method is validated by a comparison to a series of experimental test results.

The Swiss code SIA262 [SIA13] recommends assessing the shear strength of beams with stress field approaches. The elastic-plastic stress field method, which is implemented into a finite element method [Fer07], allows obtaining a more precise estimation of the ultimate strength of reinforced concrete members than the classical rigid-plastic stress field approach. Thus this method has been chosen as the basis for a simplified verification method that allows investigating the in-plane shear strength of beams and box girder beams subjected to out-of-plane bending moments in addition to the in-plane shear loading.

The EPSF method [Fer07] is conceived for plane stress fields, i.e. reinforced concrete members subjected to forces acting in the element plane, the transverse bending moment m can thus not be introduced explicitly in the FE model. The simplified approach for transverse bending makes use of the principles of the RP interaction models in order to account for the effect of m on the in-plane shear strength. Based on a pure equilibrium approach the following considerations are made:

- Reduction of the web thickness.

- Reduction of the shear reinforcement cross section. Only applied in case of very high transverse bending moments.

These two aspects are discussed in the following sections.

3.3.1 Reduction of the web width

From the previous analyses performed on the basis of the RPSF and the ML-EPSF panel elements it was found that the transverse bending moment leads the compression field to concentrate on a limited area on the bending compression side of the web cross section ($b_e \leq b_w$ in fig. 2.5 and σ_2 in fig. 3.7). Thus, only a part of the web width b_w is available to transfer the shear force when a transverse bending moment is acting at the same time. In order to account for this in the finite element model, the web width is reduced to an effective web width $b_{w,eff} = b_w - \Delta b_w$. The reduction of the web width Δb_w is computed as follows:
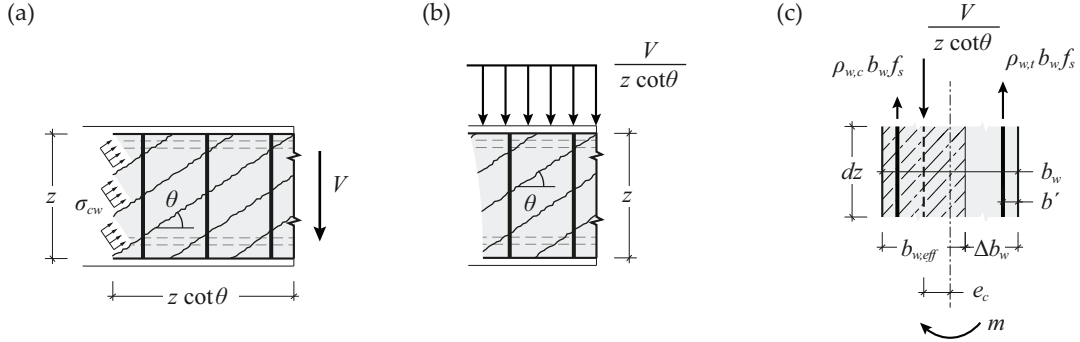
Figure 3.9 Simplified approach: (a) web elevation with in-plane shear and RP stress field with average inclination θ taken from the EPSF computation; (b) vertical component of the shear force per unit length; (c) transverse cross section of the web with equilibrium between the stirrup forces and the eccentric compression field.

$$\Delta b_w = 2e_c = 2z \cot\theta \frac{m_c}{V} \qquad \text{with,} \quad m_c = m - m_s \qquad (3.14)$$

where z is the lever arm, θ the average inclination of the compression field in the concerned region (obtained, by iteration, from the previous computation with the EPSF method), m is the transverse bending moment acting on the web, m_s the transverse bending resistance provided by the shear reinforcement and V the shear force acting in the plane of the web (accounting for the longitudinal shear force and the torsional moment in box girder cross sections, for instance according to SIA262 [SIA13]).

The equation 3.14 is derived from the equilibrium of a web segment subjected to a shear load and a transverse bending moment (fig. 3.9): the compression field is only acting on a limited width $b_{w,eff}$ on the bending compression side of the web width and its inclination θ is assumed constant over the width; the vertical component of the resultant of the compression field $V/(z \cot\theta)$ is acting at $e_c = (b_w - b_{w,eff})/2 = \Delta b_w/2$ from the web centre and consequently contributes to the transverse bending resistance by $m_c = V/(z \cot\theta) \cdot \Delta b_w/2$. At this point, it is assumed that the shear reinforcement on both sides of the web is yielding and the resisting moment is computed by $m_s = f_s(\rho_{w,t} - \rho_{w,c})b_w(b_w/2 - b')$. Knowing the acting transverse moment m and the resistance provided by the shear reinforcement m_s, the required resistance m_c can be derived (eq. 3.14) and by this the necessary eccentricity e_c of the compression field resultant. Consequently, the required effective width $b_{w,eff}$ and eventually the width reduction Δb_w are obtained according to equation 3.14.

Note that in this simplified verification approach, the required web width is computed based on equilibrium considerations only, whereas in the previous RP interaction models, the required width is determined on the basis of the shear resistance of the compression strut. In order to emphasize this difference, a different notation for the required web width was chosen, namely $b_{w,eff}$, compared to b_e in the RP models.

3.3.2   Reduction of the effective shear reinforcement

The width reduction Δb_w is reasonable for transverse bending moments up to the magnitude of m_s, but it is very conservative for higher transverse moments.

The RP interaction models presented in the literature (in particular Thürlimann [Thü77] and Menn [Men86]) suggest that, in case of high transverse bending moments, additional resistance is obtained when reducing the tensile force in the shear reinforcement on the bending compression side (if $\sigma_{s,c} \searrow$, $m_s \nearrow$). This behaviour is confirmed by the proposed ML-EPSF panel element, where the internal state-of-stress is computed with respect to the panel kinematics, see $\sigma_{s,2}$ in figure 3.6c. The reinforcement stress reduces with an increasing moment, which leads to a higher contribution of the shear reinforcement to the transverse bending resistance, see figure 3.6a: m_s increases with m.

The behaviour of the web is significantly improved when this additional bending resistance provided the shear reinforcement is taken into account. In the present simplified verification method this leads to a less penalizing reduction of the web width, but requires at the same time a reduction of the effective shear reinforcement area on the bending compression side. This is considered by the factors λ which represent the amount of reinforcement that is actually used (activated), relative to the available amount of shear reinforcement:

$$
\begin{aligned}
\rho_{w,t,eff} &= \lambda_t \, \rho_{w,t} = \lambda_t a_{sw,t}/b_w \\
\rho_{w,c,eff} &= \lambda_c \, \rho_{w,c} = \lambda_c a_{sw,c}/b_w
\end{aligned}
\qquad \text{with,} \qquad
\begin{aligned}
\lambda_t &= 1 \\
0 &\leq \lambda_c \leq 1
\end{aligned}
\tag{3.15}
$$

where $\rho_{w,c,eff}$ and $\rho_{w,t,eff}$ are the effective amount of shear reinforcement and $a_{sw,c}$ and $a_{sw,t}$ the available reinforcement area per unit length on the bending compression and tension side of the web. Thus the effective amount of shear reinforcement in the FE model is given by $\lambda_m a_{sw}$, where the reduction factor λ_m is given by :

$$
\lambda_m = \frac{\lambda_t \rho_{w,t} + \lambda_c \rho_{w,c}}{\rho_{w,t} + \rho_{w,c}} \leq 1.0
\tag{3.16}
$$

If the factor λ_c is selected smaller than 1.0, the transverse bending resistance provided by the shear reinforcement increases, $m_s = f_s(\lambda_t \rho_{w,t} - \lambda_c \rho_{w,c}) b_w (b_w/2 - b')$. Consequently, the moment that has to be resisted by the compression field m_c (eq. 3.14) decreases and with it the reduction of the web width Δb_w. However, since reducing λ_c means reducing the allowable tensile forces in the stirrups on the bending compression side, the available amount of reinforcement for the transmission of the shear force in the FE model has to be adjusted accordingly by applying the factor $\lambda_m \leq 1.0$.

This procedure (with $\lambda_c < 1$) leads to a more moderate reduction of the web width (i.e. higher concrete shear strength, $V_{R,c} \nearrow$), but simultaneously reduces the effective shear rein-

forcement ($V_{R,s}$ ↘). The optimal value for λ_c can be found by iteration in order to maximise the failure load (see example in figure 3.10b).

3.3.3 The simplified method relative to other methods

Effective web width

The stress field layout on the web cross section and the principle used to equilibrate the transverse moment in the simplified verification method is identical to the principles of the RP interaction models proposed by Thürlimann [Thü77] and Menn [Men86]. The approaches differ however in the way the required web width is computed, hence the use of different notations: b_e and $b_{w,eff}$. In the RPSF the width b_e is obtained based on resistance considerations, whereas $b_{w,eff}$ in the simplified verification method is obtained by equilibrium conditions only.

In the RPSF models, b_e is the minimum web width necessary to resist the in-plane shear force and thus is computed directly according to the shear strength of concrete ($V_{R,c} = k_c f_c b_e z \sin\theta \cos\theta$). This procedure however requires knowing the effective strength of concrete (i.e. k_c) and choosing an inclination θ for the compression field.

In the proposed simplified design procedure the width $b_{w,eff}$ is computed based on equilibrium considerations only that do not require hypotheses on the effective concrete strength and the inclination of the compression field (because taken from the EPSF calculation). The resistance of the element with the reduced web width $b_{w,eff}$ is then verified in a separate step using the EPSF finite element method, where the concrete strength reduction factors η_ε (equivalent to k_c in RPSF) and the inclinations of the compression field θ are computed automatically from the local state-of-strain at each point in web of the beam.

An enhanced lower bound solution

The simplified EPSF method, as the EPSF method [Fer07], generally leads to higher failure loads than the classical RP interaction models because the stress field parameters η_ε and θ are determined on the basis of a kinematically compatible strain field. However, in the present context, where both, the in-plane and out-of-plane actions, are considered, the EPSF method cannot yield an exact solution according to the theory of plasticity, since only in-plane kinematics are taken into account. Nonetheless, the simplified approach provides an enhanced lower bound solution compared to the RP interaction models, thereby leading to more realistic predictions for the actual shear resistance under the effect of out-of-plane bending.

Possible improvement of the simplified method

The web width reduction, as well as the amount of effective shear reinforcement, is derived from a RPSF, i.e. an equilibrium based, approach for which the stress field inclination and the concrete strength reduction factor are admitted constant over the web thickness. How-

ever, the experimental campaign by Kaufmann and Menn [Kau76] and the sectional analysis with the ML-EPSF panel element have shown that these parameters vary significantly over the web cross section and, additionally, are highly sensitive to the intensity of the applied transverse bending moment.

In order to account for this, the proposed simplified verification method could be used in combination with the ML-EPSF panel element, instead of the proposed RP approach. For a given shear force and transverse moment, the eccentricity e_c of the vertical stress resultant in the concrete (n_{cy}) and the stress in the reinforcement on the bending compression side $\sigma_{s,c}$ can be obtained from the ML-EPSF panel element. Knowing e_c, the web width reduction is then determined according to figure 3.9c, such that $\Delta b_w = b_w - 2e_c$. The amount of effective reinforcement on the compression side is given by $\lambda_c = \sigma_{s,c}/f_s$ and the reduction factor λ_m to apply in the FE model is computed according to equation 3.16. The longitudinal deformation ε_{x0} in the ML-EPSF panel is given by the average deformation in the concerned region, which is obtained, by iteration, from the previous computation with the EPSF method.

Using the ML-EPSF panel element could be particularly interesting in situations with very high levels of transverse bending for which the ML-EPSF showed that the stress field inclination is significantly influenced by the bending compression effect (θ locally reaching up to 90°). With the ML-EPSF approach a more accurate estimation of the web width reduction and the effective shear reinforcement ratio could be obtained.

Nevertheless, this verification method would remain a simplified approach leading to a lower bound solution of the shear strength under transverse bending, since the real kinematics of the web in the transverse direction cannot be represented with the plane EPSF method. An exact solution can only be obtained with a model that simultaneously respects the static and kinematic compatibility conditions of the theory of plasticity for both, in-plane and out-of-plane, actions. To this purpose, the ML-EPSF finite element method present in Chapter 4 has been developed.

3.4   Validation of the simplified verification method

The simplified verification method is compared to a test series by Kaufmann and Menn [Kau76] (described in section 2.3) performed on simply supported beams with concentrated vertical loads and a constant transverse bending moment in the web. Two categories of specimens were tested: LSI and LSII. Specimens LSI were designed to fail by yielding of the shear reinforcement (ductile failure) and specimens LSII by crushing of the concrete in the web due to shear (non-ductile failure).
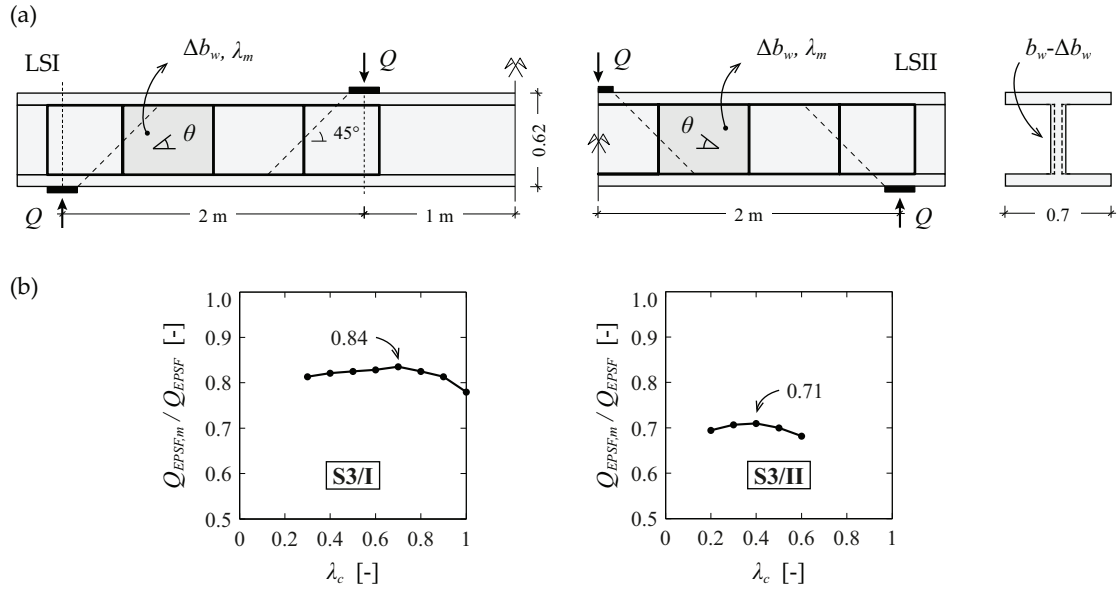
Figure 3.10 (a) Geometry of the finite element model for Kaufmann's beams [Kau76], with web regions for the determination of the width reduction factors Δb_w and (b) optimization of the reduction factor λ_c to maximize the failure load, example for beams S3 LSI and S3 LSII.

3.4.1 Model assumptions and optimisation process

A summary of the modelling parameters is given in table 3.1. The indicated shear reinforcement (ρ_w, A_{sw}) and web width (b_w) are the original values, later they are reduced (λ_m, Δb_w) to account for the effect of the transverse moment in the simplified EPSF approach. The amount of longitudinal reinforcement is the same as in the test specimens (step-wisely reducing towards the supports).

The model geometry is presented in figure 3.10a. In the shear span, the beam web is divid-

Table 3.1   Modelling parameters for the tests by Kaufmann and Menn [Kau76].

Tests	ρ_w	$\dfrac{\rho_{w,c}}{\rho_{w,t}}$	A_{sw}	s	f_s	$\eta_{fc} f_c$	b_w	$\dfrac{m}{V} \cdot 100$
	[%]	[-]	[mm²]	[mm]	[MPa]	[MPa]	[m]	[-]
S1 - LS I						31		5.10
S2 - LS I						32		5.34
S3 - LS I	0.5	1.0	100	200	540	32	0.1	3.88
S6 - LS I						24		3.39
S1 - LS II	0.785			200		31		2.81
S3 - LS II	0.785	1.0	157	200	531	32	0.1	4.30
S2 - LS II	1.57			100		32		5.99
S4 - LS I	0.643	0.64	129	200	535	26	0.1	6.61
S4 - LS II								3.66
S5 - LS I	0.75	0.50	75	100	540	26	0.1	7.33
S5 - LS II								4.27

ed into four regions, for each of them an individual web width reduction (Δb_w) and effective amount of shear reinforcement (λ_m) will be determined.

In the two central regions, the stress field is relatively uniform and the average inclination could be easily measured. However, in the support and load introduction regions, the stress fields develop in the shape of a fan. It has thus been chosen to take the numerical average of the inclination at each FE in these regions.

In a first step the ultimate failure load of the beams is determined without considering the transverse bending moment ($\Delta b_w = 0, \lambda_m = 1$). The obtained EPSF allows determining the average inclination of the stress field and shear force V in each web region. The web width reductions are then computed for the amount of effective shear reinforcement (λ_m) that had been chosen beforehand. The web regions in the FE model are updated with the new values for the effective web width and the failure load is re-evaluated. This procedure is repeated until the failure load stabilises.

In the present example it was assumed that the ratio between the applied transverse bending moment and the shear force remains constant during the iterations. The ratio m/V was chosen identical to the experimental values m_q/Q_{exp} (m_q applied transverse moment, Q_{exp} measured failure load). Additionally, the amount of effective shear reinforcement λ_m is assumed to be the same in all the web regions.

Each beam has been computed for several values of effective shear reinforcement. The researched failure load is then given by the calculation with the highest failure load, see example in figure 3.10b.

3.4.2 Comparison to experimental results

A resume of the failure load prediction with the simplified EPSF for transverse bending moments in beam webs is presented in table 3.2 and figure 3.11a.

In general, it can be observed that the simplified method gives stable and safe estimates of the failure load, without being overly conservative ($Q_{exp}/Q_{EPSF,m} = 1.17$ with COV $= 0.06$). Furthermore, the prediction of the failure mode of most beams is consistent with the experimental observations (except for the beam S3-LSI, see explanation below).

Table 3.2 also separates the results according to the observed failure modes: ductile (yielding) and non-ductile (concrete crushing). The simplified EPSF method seems to be more conservative for beams where a non-ductile failure (crushing of concrete) is to be expected, $Q_{exp}/Q_{EPSF,m} = 1.23$. In case of ductile failure, the predictions are significantly better $Q_{exp}/Q_{EPSF,m} = 1.11$. Probably, the EPSF method itself adds a little to this difference, because it generally tends to give a little more conservative predictions when the failure is not governed by yielding of the reinforcement [Mut16].

The predictions for specimens LSI show a very similar behaviour to the experimental observations (except for beam S3-LSI): close to failure the shear reinforcement is yielding and at ultimate load a longitudinal bending-shear failure mechanism develops, with local yielding of longitudinal reinforcement. For beam S3-LSI an early failure occurred that is caused by a combination of crushing of concrete in the web and yielding of the stirrups (longitudinal reinforcement is not yielded). This leads to a more conservative estimation of the actual failure load ($Q_{exp}/Q_{EPSF,m} = 1.21$) as for the other specimens LSI.

The failure modes of the specimens LSII correspond to the experimental observations. They show a very high level of concrete solicitation (high concrete stresses, $\sigma_2/\eta_\varepsilon f_{cp} \rightarrow 1.0$) leading to a shear failure by crushing of concrete in the web. Additionally, it is observed that at ultimate load the shear reinforcement is partially yielding. This is due to the artificially reduced amount of reinforcement in FE model (effective reinforcement, $\lambda_m < 1.0$) to account for the effect of the transverse moment. This does however not contradict with the experiments, where yielding of the stirrups on the bending tension side and partial yielding on the bending compression side was observed. Only beam S2-LSII failed in longitudinal bending, which led to a rather ductile behaviour at failure that could be very precisely predicted with the simplified EPSF method ($Q_{exp}/Q_{EPSF,m} = 1.01$).

Table 3.2   Resume of the failure load predictions of Kaufmann's beams [Kau76] according to: the simplified EPSF method for transverse bending ($Q_{EPSF,m}$) with the effective shear reinforcement ratio (λ_m), web width reduction (Δb_w) and failure mode; the plane EPSF method without considering the transverse bending moment (Q_{ESPF}).

Test	λ_m [-]	Δb_w[(*)] [mm]	failure mode	$\dfrac{Q_{exp}}{Q_{EPSF,m}}$	$\dfrac{Q_{exp}}{Q_{EPSF}}$	$\dfrac{Q_{EPSF}}{Q_{EPSF,m}}$
S1 - LS I	0.90	63	d	1.13	1.07	1.06
S2 - LS I	0.85	54	d	1.15	1.08	1.07
S3 - LS I	0.70	45	n-d [(**)]	1.21	1.01	1.20
S6 - LS I	1.00	47	d	1.06	1.05	1.01
S1 - LS II	0.80	58	n-d	1.20	0.97	1.24
S3 - LS II	0.65	34	n-d	1.32	0.94	1.41
S2 - LS II	0.80	30	d	1.01	0.92	1.10
S4 - LS I	0.69	49	d	1.18	1.07	1.10
S4 - LS II	0.81	28	n-d	1.22	1.00	1.22
S5 - LS I	0.70	46	d	1.16	1.03	1.12
S5 - LS II	0.77	20	n-d	1.20	1.00	1.19
			mean (all)	1.17	1.01	1.16
			COV	0.06	0.04	0.09
			mean (d)	1.11	1.04	1.07
			COV	0.05	0.04	0.03
			mean (n-d)	1.23	0.98	1.25
			COV	0.04	0.02	0.06

[(*)] - mean of the two span regions;   d - ductile failure mode;
[(**)] - not consistent with test result;   n-d - non-ductile failure mode.

Figure 3.11a shows the predicted failure loads with respect to the amount of shear reinforcement, reinforcement layout and intensity of the transverse bending moment. No significant trend is observed regarding the amount of shear reinforcement ρ_w in the beam. The small tendency that could be observed if beam S2-LSII is neglected is rather linked to the failure mode (ductile vs. non-ductile) than to the amount of shear reinforcement. The reinforcement layout ($\rho_{w,c}/\rho_{w,t}$) has no visible influence on the results; the simplified verification methods leads to equally good predictions of the failure loads for symmetrical and unsymmetrical shear reinforcement layouts. The proposed method shows a light tendency to be more conservative for higher transverse bending moments.

3.4.3 Influence of the transverse bending moment

The previous section investigated to what extent the proposed simplified verification method is able to predict the experimental failure loads. In the present section, the actual and predicted influence of the transverse moment on the shear resistance of beam elements is investigated. To this purpose, the experimental test results are first compared to EPSF predictions where the influence of the moment is neglected. This allows getting an idea of the real influence of the transverse moment. In a second analysis the EPSF prediction (without transverse moment) are compared to the prediction of the proposed simplified verification method (with transverse moment) in order to quantify the predicted effect of the transverse bending moment.

Shear failure loads according to EPSF without transverse bending moment

This section investigates Kaufmann's beams [Kau76] with the plane EPSF without considering the transverse bending moment in the FE model. The subsequent comparison to the experimental failure loads allows observing the influence of the transverse moments on the ultimate failure load.

The plane EPSF ultimate load predictions are shown in table 3.2 (Q_{exp}/Q_{EPSF}) and figure 3.11b. The average ratio of measure failure load to estimate failure load Q_{exp}/Q_{EPSF} is 1.01 with a coefficient of variation of 0.04, which indicates a rather weak influence of the transverse moment on the ultimate shear resistance.

By separating the results according to the type of failure mode (apart for beam S2-LSII the failure modes are identical to those observed in the simplified EPSF method, column four in table 3.2) we can see that the specimens with ductile failure modes give safe results ($Q_{exp}/Q_{EPSF} = 1.04$), whereas in case of non-ductile failure the predictions are a little unsafe ($Q_{exp}/Q_{EPSF} = 0.98$).

Indeed, in the experimental campaign on the specimens LSI (ductile failure), it was observed that, due to the transverse bending moment, the stirrups on the bending tension side started yielding first, but at failure both stirrups (on the bending compression and bending tension side) had reached their yielding strength. The ultimate load thus corre-

sponded to the expected conventional longitudinal shear resistance for beams. This explains why the EPSF predictions, where the transverse moment is neglected, give very good predictions of the experimental failure loads.

The EPSF predictions for the specimens LSII (designed for brittle failure by crushing of the concrete in the web) slightly overestimate the experimental failure load, which is not contradictory to the experimental observations. As in the experimental campaign, the EPSF predictions show that the concrete in the web is highly damaged ($\sigma_{c2}/\eta_\varepsilon f_{cp} \rightarrow 1$). But contrary to the test observations, at failure, the EPSF models can be loaded until the yield limit of the stirrups on both sides and consequently the full shear resistance of the beam is reached. However, in the experimental campaign, the transverse bending moment led to an earlier failure caused by concrete crushing in the web. At ultimate load, the stirrups on the bending tension side were fully yielding, whereas on the bending compression side only part of the reinforcement had reached the yield limit. Consequently the ultimate failure load was reduced compared to pure longitudinal shear resistance, which is confirmed by the EPSF prediction ($Q_{exp}/Q_{EPSF} = 0.98 < 1.0$).

In figure 3.11b the results are plotted against different parameters: the intensity of the applied transverse moment (m/m_{R0}), the total amount of shear reinforcement (ρ_w) and the ratio between the amount of shear reinforcement on the both web faces ($\rho_{w,c}/\rho_{w,t}$). No significant trend can be observed in the predictions with the plane EPSF method.

On the overall, the previous observations would lead to suggest that the influence of the transverse bending moment on the longitudinal shear resistance is very small. However, no definitive conclusion can be drawn because these observations are only based on a single series of test data. Additionally, during the testing, yielding of the longitudinal reinforcement was observed in several elements which might interfere with the interpretations regarding the in-plane shear transverse bending interaction. Nonetheless, some remarks regarding the overall behaviour can be made and allow thereby identifying some general tendencies.

Elements, as specimens LSII, that have only little reserve capacity in the concrete of the web, i.e. in pure shear the compressive stresses in the concrete are already high, the transverse bending moment seems to affect the ultimate shear resistance. Indeed, in these elements the compression field cannot shift efficiently towards the bending compression side to counterbalance the moment because almost the entire web width is already required to resist the longitudinal shear force. The additional transverse bending compression then eventually leads to the failure.

In elements that are conceived for ductile failure by yielding of the shear reinforcement, the compressive stresses in the concrete are generally not governing for the longitudinal shear resistance. The reserve capacity of the concrete web thus allows that at failure, the stress field in the concrete can concentrate on the bending compression side of the web (shift of
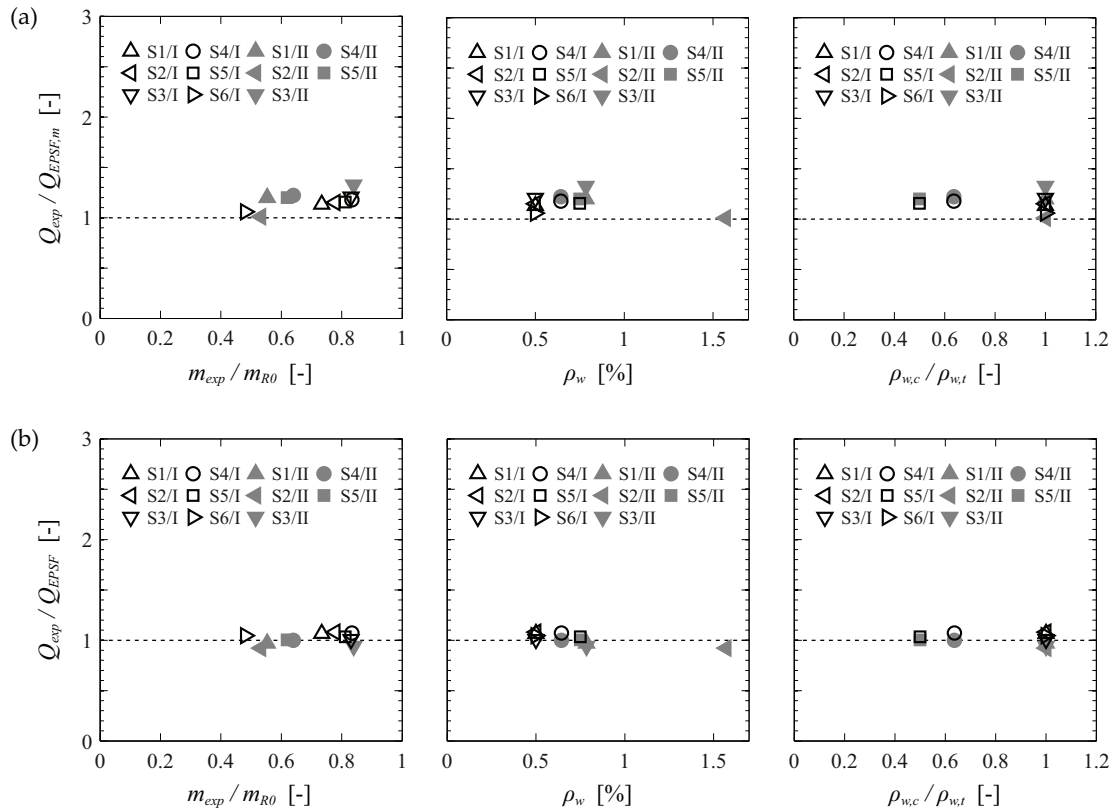
Figure 3.11 Ultimate load predictions for Kaufmann's beams [Kau76] according to: (a) the simplified EPSF method for transverse bending and (b) the plane EPSF method without considering the transverse bending moment.

the shear stress resultant) in order to counterbalance the acting transverse bending moment, while the shear reinforcement on both sides is yielding. Thus, in agreement with the observations performed by Kaufmann and Menn [Kau76], it can be concluded that if the shear resistance of the concrete $V_{R,c}$ is higher than the shear resistance of the reinforcement $V_{R,s}$, a certain amount of transverse bending (depending on the ratio m to $V_{R,c}$) can be resisted without affecting the bearing capacity of the beam.

Predicted effect of the transverse bending moment

The comparison between the predictions provided by the plane EPSF method (m neglected) and the predictions of the simplified EPSF method (m not neglected) is shown in table 3.2 column $Q_{EPSF}/Q_{EPSF,m}$. On average, the simplified method predicts a reduction of 16% of the initial shear resistance due to transverse bending, which is conservative but acceptable considering the fact that it is a simplified approach.

In case of ductile failure the predicted reduction is smaller (7%) than for beams failing by crushing of the concrete in the web (25%). This allows concluding that the overall behaviour of the simplified method is in agreement with the expectations. However the differ-

ence between the two failure modes is significantly higher than what has been observed in the previous analyses (Q_{exp}/Q_{EPSF}: ductile 1.04, non-ductile 0.98), which leads to the conclusion that simplified verification method might be overly conservative if concrete crushing is to be expected at failure.

This behaviour is probably caused by the fact that the simplified method does not account for the positive effect of bending compression on the inclination of the stress field and the concrete strength reduction factor (as observed with the ML-EPSF panel element). On the contrary, only the unfavourable effect of additional concrete solicitation due to the bending compression is considered by reducing the effective web width. Consequently, as already observed in section 3.4.2, the simplified method thus leads to more conservative estimates of the actual shear resistance in case of higher transverse bending moments.

3.4.4 Synopsis

A simplified verification method for reinforced concrete beam elements subjected to longitudinal shear loads and transverse bending in the web is introduced. The method bases on the EPSF method and accounts for the effect of the transverse bending moment by reducing the available amount of concrete and shear reinforcement in the beam web. It is explained that this is done by means of an equilibrium based approach inspired from RP interaction models. The method is compared to experimental test data and some general observations on the effect of transverse bending in beam elements are made. The main findings and conclusions are:

- The simplified verification method for the longitudinal shear resistance in case of transverse bending in the beam web is an efficient tool for practical applications. It provides an enhanced lower-bound solution on the basis of the well-established EPSF method.

- Compared to RP plastic interaction models, it does not require choosing a stress field inclination and concrete strength reduction factor. The latter are determined automatically based on the kinematic and static compatibility condition of the EPSF method.

- It permits to consider the actual longitudinal behaviour of beam elements during the verification of the in-plane shear – transverse bending interaction. Internal force redistribution as well as other failure modes (longitudinal bending) that could affect the overall resistance can thus be accounted for directly.

- A comparison to experimental test data showed that it yields safe but not overly conservation estimations of the actual shear resistance. This is especially true for ductile failure modes. In case of non-ductile failure modes caused by crushing of the concrete in the web, the predictions are a little more conservative.

- The predicted failure modes are in general consistent with the experimental observations.

- Comparisons of the experimental failure loads to predictions neglecting the influence of the transverse bending moment lead to suggest that the influence of the transverse bending moment on the shear resistance of beam elements is very small, especially in case of a ductile failure governed by yielding of the shear reinforcement.

3.5   Discussion and conclusion

The present chapter introduced a novel ML-EPSF approach for the establishment of consistent stress fields under combined membrane and bending actions. Additionally two methods that allow accounting for the effect of transverse bending on the longitudinal shear resistance of beam elements are proposed: a sectional analysis tool for the investigation of the phenomenological behaviour of the stress field under the influence of an out-of-plane moment and a simplified verification method for beam elements in practice. A detailed summary of the main findings and outcomes regarding these two methods was already presented in the respective sections (section 3.2.4 and section 3.4.4).

One of the important observations made by means of the ML-EPSF panel element is that the in-plane shear – transverse bending interaction is less pronounced than predicted by former models. Nonetheless, the model clearly indicates that the transverse moment has a negative influence on the shear resistance. However, an investigation on the experimental failure loads of beams with respect to EPSF predictions suggests that the effect of the transverse bending moment on the actual bearing capacity is almost negligible.

Even if these results seem somewhat contradicting, this mainly indicates that the shear transfer action under transverse bending in beam elements is more complex than what is considered in panel elements, like the proposed ML-EPSF panel element. Structural elements like beams have a higher potential for redistribution of internal forces and therefore, a stress field perturbation, as caused by the transverse bending moment, has less influence on the ultimate bearing capacity. An important factor in this may be the contribution of the girder flanges in the shear transfer action that develops in the cracked concrete. Even though the ML-EPSF panel element is a precious tool to understand the non-linear dependencies between transverse bending and longitudinal shear on a local level, it cannot (automatically) account for redistribution effects that develop at the structural level. Therefore, if it is used to evaluate the shear resistance of beams, it may overestimate the effect of the transverse bending moment on the actual bearing capacity of the element in some cases.

Nonetheless, the observations on the experimental beams predict an unexpected weak influence of the moment. Further comparisons and more experimental data on beam ele-

ments with transverse moments are required in order to confirm if and under which conditions the influence of the transverse bending moment is indeed almost negligible.

It can thus be concluded that the ML-EPSF panel provides valid information at a local level, this is however not always representative of the overall behaviour of a structural element. The proposed simplified verification method for beam elements in practice is able to account for redistributions at the structural level (the entire beam is modelled), but the effect of the transverse bending moment is considered on a similar basis and thus provides rather conservative predictions.

To represent the actual interactions, which develop in a structural element under in-plane and out-of-plane actions and the resulting consequences on the bearing capacity, internal forces redistributions in and out of the element plane, as well as along the entire element length must be considered simultaneously. This can only be achieved by an advanced analysis tool capable of representing the actual in-plane and out-of-plane kinematics of the entire structural element. To this purpose, the ML-EPSF approach is implemented into the non-linear finite element procedure presented in Chapter 4.

Chapter 4   Non-linear finite element method for in-plane and out-of-plane actions
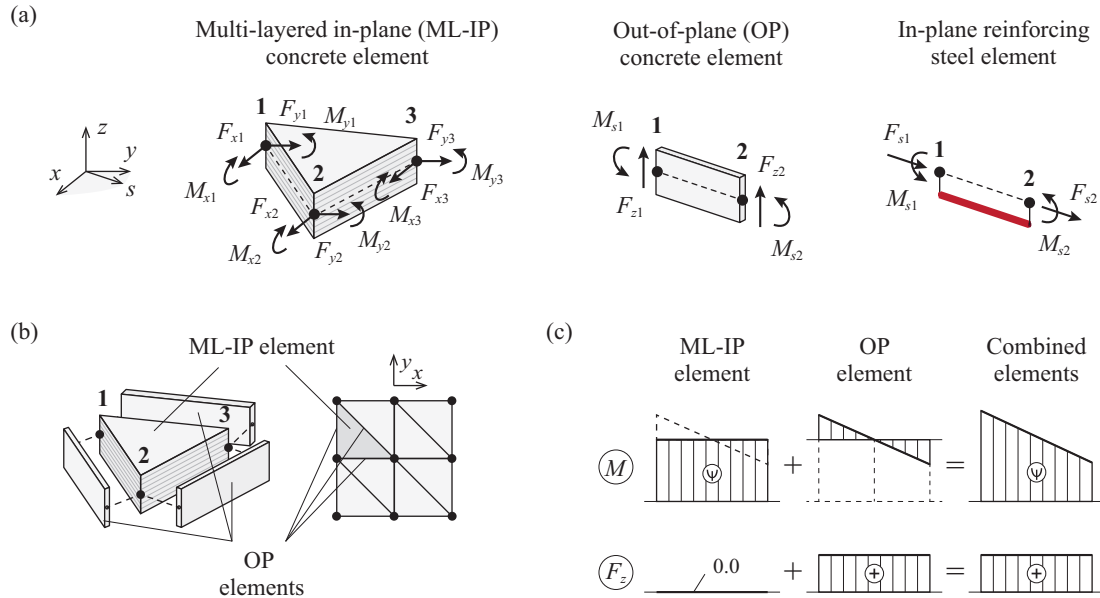
This chapter presents a non-linear finite element method that has been developed on the basis of the multi-layered elastic-plastic stress field approach presented earlier and that allows investigating reinforced concrete elements under in-plane and out-of-plane actions. First, a summary of the proposed finite element concept is presented, followed by the formulations of the different finite elements, the adopted solution procedure and the validation and sensitivity analysis of the method.

4.1   Outline of the proposed finite element method

The objective of the proposed finite element method is to provide a tool to investigate the behaviour of reinforced concrete shell elements that are primarily subjected to a combination of in-plane forces and out-of-plane bending moments. In many cases, out-of-plane bending is caused by actions normal to the element plane. The method accounts for this by means of appropriate equilibrium formulations. Consequently, the proposed finite element method allows studying the effect of out-of-plane forces and moments on the in-plane resistance as well as the influence of in-plane forces on the transverse bending resistance. Out-of-plane shear failure modes can however not be represented with this method.

The finite element method is based on the multi-layered elastic-plastic stress-field (ML-EPSF) approach presented earlier. It can be considered as an enhancement of the numerical implementation of the plane elastic-plastic stress field (EPSF) method by Fernández Ruiz and Muttoni [Fer07], extending thereby the range of structural elements and load combinations that can be studied with the stress field approach.

Similarly to the plane EPSF method, the ML-EPSF finite element method yields stress fields that are in equilibrium with the external actions and that respect the plastic condition of the material in every point. Since they are derived from kinematically compatible displacement fields, the resulting stress fields at failure are in agreement with a licit failure mechanism. Thus, they simultaneously fulfil the static and kinematic theorem of the theory of plasticity and consequently represent exact solutions according to the theory of plasticity. This clause is nevertheless limited to in-plane failure and out-of-plane bending failure modes.

(a)

Multi-layered in-plane (ML-IP)
concrete element

Out-of-plane (OP)
concrete element

In-plane reinforcing
steel element

(b)

ML-IP element

OP
elements

(c)

ML-IP
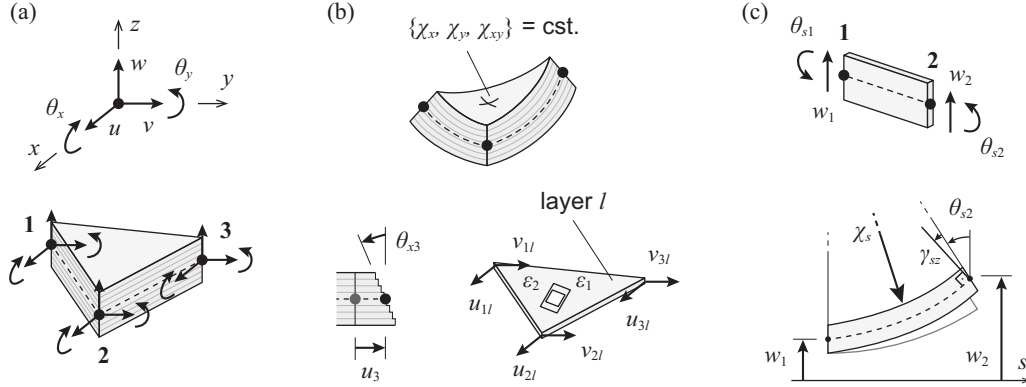element

OP
element

Combined
elements

Figure 4.1 Finite elements of the FEM: (a) FEs for concrete and steel; (b) the combined element for concrete and (c) concept of the combined concrete element (schematic representation).

Reinforced concrete members are modelled with different finite elements for concrete and steel, figure 4.1a. The concrete is modelled by two types of finite elements: the multi-layered in-plane (ML-IP) concrete element and the out-of-plane (OP) concrete shear element. Together, the two concrete elements ensure the transmission of in-plane forces (normal and shear), out-of-plane shear and out-of-plane bending moments.

The ML-IP element, in which each layer respects the conditions of the EPSF, carries the in-plane forces and the average out-of-plane bending moments (constant). It is completed at each face by an OP shear element that carries the out-of-plane shear force and the moment variation, figure 4.1b-c. The reinforcement is modelled with rebar elements which are placed with an eccentricity relative to the mid-plane of the concrete elements in order to account for the actual location of the rebars in the element thickness. As in the EPSF method [Fer07], the rebar element carries only axial forces (dowel action is neglected) and the bond with the concrete is assumed to be perfect (no slip).

The concrete ML-IP element is a degenerated flat shell element with three nodes and fifteen degrees of freedom: three translations $\{u, v, w\}$ and two rotations $\{\theta_x, \theta_y\}$ at each node (fig. 4.2a). Out-of-plane, the element deforms with a constant curvature and undergoes shear deformations in order to ensure C^0 continuity of displacements between elements (displacements are continuous across the boundary of elements but not necessarily its derivatives (slopes), [Ona13]). Consequently, each layer behaves like a constant strain triangle.

Figure 4.2   (a) Nodal membrane (u, v) and flexural (w, θ_x, θ_y) degrees of freedom; (b) deformed ML-IP element with constant curvature, derivation of layer strains and constant strain triangle; (c) OP shear element with shear deformation.

The constant curvature, figure 4.2b, is a fundamental hypothesis of ML-IP element that allows computing a constant strain field in each layer (no need for numerical integration points), which is the necessary condition for computing the plane stress states of each layer according to the EPSF method by [Fer07].

The ML-IP concrete element accounts for shear deformations according to the Reissner - Mindlin plate bending theory (plane sections remain plane but not necessarily normal to the mid-plane after deformations) [Rei45, Min51]. The shear deformation is an additional degree of freedom that is necessary to approximate the out-of-plane displacement by a constant curvature displacement field $w(x, y)$ defined by the three displacements (w, θ_x, θ_y) of each node. The shear deformation decouples the rotations from the out-of-plane translation which means that the displacement fields for rotations $\theta_x(x, y)$ and $\theta_y(x, y)$ are not only dependent on the translational displacement field $w(x, y)$, i.e $\theta \neq$ derivative of w.

Since Mindlin-type elements only require C^0 continuity for the displacement fields (see [Ona13]), the element membrane displacement fields and rotation fields are described using linear shape functions. Additionally, it is assumed that the shear deformation is constant along the element border. The out-of-plane displacement is then discretized by a quadratic polynomial function respecting the condition of constant curvature.

The strain fields defining the state-of-strain at any point inside the element are obtained from the previously described displacement fields and Mindlin plate kinematics. The in-plane strains that result from the membrane (elongation) and bending (curvature) effects are constant in each layer and concrete stresses (plane stress state) are obtained according to the ML-EPSF method presented earlier. Eventually, the stress resultants are integrated similarly to the method used in [Fer07] in order to obtain the element nodal forces $\{F_x, F_y, M_x, M_y\}$.

As a consequence of the aforementioned kinematic hypotheses, the ML-IP element does not carry out-of-plane forces ($F_z = 0$, figure 4.1a), this is why the element is completed by three OP shear elements. The latter deform identically to the ML-IP element border to which they are connected to, thus their out-of-plane deformation is a polynomial function of the second order with constant curvature and constant shear deformation, see figure 4.2c. This shear deformation is used to compute the out-of-plane shear force according to a Timoshenko beam approach [Ona13] and nodal moments are applied in order to ensure the equilibrium of forces.

The non-linear finite element problem is solved by applying an iterative secant stiffness procedure. The entire finite element method, as well as pre-processor and post-processor, have been coded in the MATLAB computing environment [MAT13].

4.2 Element formulations

Following sections present the formulations of the three finite elements: the multi-layered in-plane (ML-IP) concrete element; the out-of-plane (OP) concrete shear element and the rebar element for steel reinforcement.

4.2.1 Displacement fields and strain fields

The element formulations are based on the Reissner-Mindlin flat shell theory, an extension of the Reissner-Mindlin plate theory that combines flexural (bending and shear) and membrane behaviour. Flat shell elements are typically used to study folded plate structures such as box-girder or slab-beam bridges.

In plate theory, the 3D displacement fields are expressed in terms of displacements and rotations at the middle plane: (u, v) are the in-plane displacements, w the out-of-plane (transverse) displacement and (θ_x, θ_y) the rotations of the normal vector. The element middle plane is equidistant from the upper and lower faces and is the reference plane for the transverse direction ($z = 0$).

$$
\begin{aligned}
u_z(x, y, z) &= u(x, y) - z\theta_x(x, y) \\
v_z(x, y, z) &= v(x, y) - z\theta_y(x, y) \\
w_z(x, y, z) &= w(x, y)
\end{aligned}
\tag{4.1}
$$

Equation 4.1 expresses the displacement fields according to the Reissner-Mindlin theory [Rei45, Min51] that assumes that the thickness of the plate does not change during deformation (eq. 4.1-3) and that a straight line normal to the middle plane before deformation remains straight but not necessarily normal to the deformed middle plane (eq. 4.1-1-2).

The rotation of the normal vector is expressed as a sum of two terms: the slope of the middle plane and an additional rotation ϕ accounting for the lack of orthogonality, see
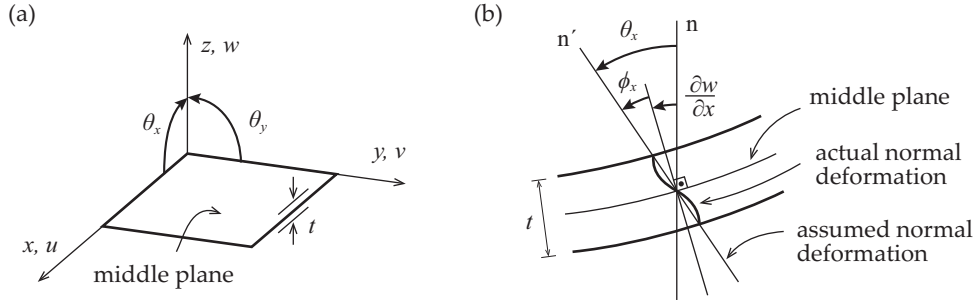
Figure 4.3 Reissner-Mindlin flat shell theory: (a) sign convention and (b) transverse displacement and rotations.

figure 4.3. In reality the plate normals are distorted during deformations, the rotations thus represent an average deformation of the normal.

$$\theta_x = \frac{\partial w}{\partial x} + \phi_x \qquad \theta_y = \frac{\partial w}{\partial y} + \phi_y \tag{4.2}$$

The expressions for the strain fields are obtained from the displacement fields. Note that $\varepsilon_z = 0$, besides it does not contribute to the internal work due to the plane stress assumptions of Reissner-Mindlin theory.

$$
\begin{aligned}
\varepsilon_x &= \frac{\partial u_z}{\partial x} & &= \frac{\partial u}{\partial x} - z\frac{\partial \theta_x}{\partial x} \\
\varepsilon_y &= \frac{\partial v_z}{\partial y} & &= \frac{\partial v}{\partial y} - z\frac{\partial \theta_y}{\partial y} \\
\gamma_{xy} &= \frac{\partial u_z}{\partial y} + \frac{\partial v_z}{\partial x} & &= \frac{\partial u}{\partial y} + \frac{\partial v}{\partial x} - z\left(\frac{\partial \theta_x}{\partial y} + \frac{\partial \theta_y}{\partial x}\right) \\
\gamma_{xz} &= \frac{\partial u_z}{\partial z} + \frac{\partial w_z}{\partial x} & &= -\theta_x + \frac{\partial w}{\partial x} = -\phi_x \\
\gamma_{yz} &= \frac{\partial v_z}{\partial z} + \frac{\partial w_z}{\partial y} & &= -\theta_y + \frac{\partial w}{\partial y} = -\phi_y
\end{aligned}
\tag{4.3}
$$

The strain vector $\boldsymbol{\varepsilon}$ is composed of in-plane strains $\boldsymbol{\varepsilon}_p$ due to membrane-bending effects and transverse shear strains $\boldsymbol{\varepsilon}_s$. Both are expressed in terms of generalized strain vectors for membrane deformations at the middle plane $\hat{\boldsymbol{\varepsilon}}_m$ (elongation), for bending effects $\hat{\boldsymbol{\varepsilon}}_b$ (curvature) and shear effects $\hat{\boldsymbol{\varepsilon}}_s$ (average shear deformations).

$$
\boldsymbol{\varepsilon} = \left\{ \begin{array}{c} \varepsilon_x \\ \varepsilon_y \\ \gamma_{xy} \\ \cdots \\ \gamma_{xz} \\ \gamma_{yz} \end{array} \right\} = \left\{ \begin{array}{c} \boldsymbol{\varepsilon}_p \\ \cdots \\ \boldsymbol{\varepsilon}_s \end{array} \right\} = \left\{ \begin{array}{c} \hat{\boldsymbol{\varepsilon}}_m - z\hat{\boldsymbol{\varepsilon}}_b \\ \cdots \\ \hat{\boldsymbol{\varepsilon}}_s \end{array} \right\}
\tag{4.4}
$$

The generalized strain vectors for membrane $\hat{\boldsymbol{\varepsilon}}_m$, bending $\hat{\boldsymbol{\varepsilon}}_b$ and shear $\hat{\boldsymbol{\varepsilon}}_s$ effects are :

$$\hat{\boldsymbol{\varepsilon}}_m = \left[\frac{\partial u}{\partial x}, \frac{\partial v}{\partial y}, \frac{\partial u}{\partial y} + \frac{\partial v}{\partial x}\right]^T = \left[\varepsilon_{x0}, \ \varepsilon_{y0}, \ \gamma_{xy0}\right]^T \tag{4.5}$$

$$\hat{\boldsymbol{\varepsilon}}_b = \left[\frac{\partial \theta_x}{\partial x}, \frac{\partial \theta_y}{\partial y}, \frac{\partial \theta_x}{\partial y} + \frac{\partial \theta_y}{\partial x}\right]^T = \left[\chi_x, \ \chi_y, \ 2\chi_{xy}\right]^T \tag{4.6}$$

$$\hat{\boldsymbol{\varepsilon}}_s = \left[\frac{\partial w}{\partial x} - \theta_x, \frac{\partial w}{\partial y} - \theta_y\right]^T = \left[\gamma_{xz}, \ \gamma_{yz}\right]^T \tag{4.7}$$

where $\varepsilon_{(.0)}$ are the membrane strains in the reference plane ($z = 0$), $\chi_{(.)}$ the curvatures and $\gamma_{(.)}$ the average transverse shear deformation.

4.2.2 In-plane concrete finite element

Discretized displacement fields

The ML-IP element is a Mindlin-type flat shell element with three nodes and five degrees of freedom per node (fig. 4.4a). The following section presents the interpolations functions used for the five displacement fields $(u, v, w, \theta_x, \theta_y)$. All displacements fields satisfy the C^0 continuity condition at the element borders that are required for the formulation of a Mindlin-type element.

The element will be divided into a finite number of layers, each of them governed by a plane EPSF. Each layer thus requires constant in-plane strains $\boldsymbol{\varepsilon}_p$ over the layer area. In order to fulfil this, linear interpolations functions for the in-plane displacements (u, v) and the rotations (θ_x, θ_y) are used.

$$u = \sum_{i=1}^{3} N_i u_i \qquad v = \sum_{i=1}^{3} N_i v_i \tag{4.8}$$

$$\theta_x = \sum_{i=1}^{3} N_i \theta_{xi} \qquad \theta_y = \sum_{i=1}^{3} N_i \theta_{yi} \tag{4.9}$$

where u_i and v_i are the in-plane displacements and θ_{xi} and θ_{yi} the rotations at node i. The linear shape functions N_i are given by area coordinates of a triangle $(\xi_1, \xi_2, \xi_3$ with $\xi_i = A_i/A^{(e)}$, see fig. 4.4b), in Cartesian coordinates they are expressed as follows:

$$N_i = \xi_i = \frac{1}{2A^{(e)}}(a_i + b_i x + c_i y) \tag{4.10}$$

with $a_i = x_j y_k - x_k y_j$, $b_i = y_j - y_k$, $c_i = x_k - x_j$ ($i = 1,2,3$; $j = 2,3,1$; $k = 3,1,2$) and the element area $A^{(e)}$.

A mandatory condition for the interpolation function of the deflections w is that the transverse shear strains γ_{sz} along the element sides are constant and defined by the rotations and transverse displacements at the end side nodes only. This condition is important for the OP shear elements (section 4.2.3) that deform identically to the borders of the ML-IP element and that allow computing the out-of-plane shear forces.
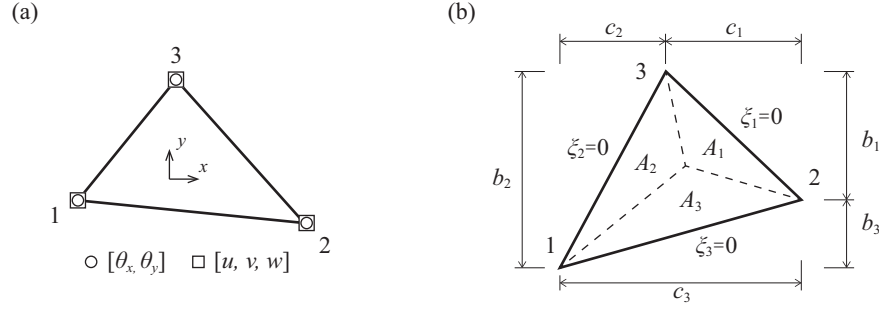
Figure 4.4 The three node Mindlin-type finite element: (a) nodal degrees of freedom and (b) area coordinates of the triangular element.

The following interpolation satisfies this requirement. It is based on the "linked interpolations" technique [Ona13, Tes85] that enriches the deflection field with higher order polynomial terms involving the nodal rotations. The quadratic interpolation function of the deflection w is of one order higher than for the rotations which reduces shear locking problems of the Mindlin-type element.

$$w = \sum_{i=1}^{3} N_i w_i + \frac{1}{8} \sum_{k=1}^{3} \bar{N}_i l_{ij} (\theta_{si} - \theta_{sj}) \tag{4.11}$$

N_i are the linear shape functions according to equation 4.10, l_{ij} is the length of the side ij, θ_{si} and θ_{sj} are the rotations along the tangential direction of the k-th side with nodes i and j ($\theta_{si} = \theta_{xi} \cos \phi_{ij} + \theta_{yi} \sin \phi_{ij}$ where ϕ_{ij} is the angle between side ij and the x axis) and $\bar{N}_i$ are quadratic shape functions vanishing at the corners.

$$[\bar{N}_1 \quad \bar{N}_2 \quad \bar{N}_3] = 4[\xi_1 \xi_2 \quad \xi_2 \xi_3 \quad \xi_3 \xi_1] \tag{4.12}$$

The deflection field can be rearranged in terms of the Cartesian nodal rotations θ_{xi} and θ_{yi}:

$$w = \sum_{i=1}^{3} N_i w_i + \sum_{i=1}^{3} L_i \theta_{xi} + \sum_{i=1}^{3} M_i \theta_{yi} \tag{4.13}$$

where $L_i = 1/8(\bar{N}_i c_k - \bar{N}_k c_j)$ and $M_i = 1/8(\bar{N}_k b_j - \bar{N}_i b_k)$, ($i = 1,2,3$; $j = 2,3,1$; $k = 3,1,2$).

The expression in equation 4.11 (resp. 4.13) ensures C^0 continuity of the deflections between elements because the deflection along the common element border is entirely defined by the degrees of freedom of the two edge nodes, for instance $w_{1-2} = w(\xi_3 = 0) = \xi_1 w_1 + \xi_2 w_2 + 0.5 \xi_1 \xi_2 l_{12}(\theta_{s1} - \theta_{s2})$.

As well, it can be verified that the transverse shear deformation along an element edge is constant and defined by the degrees of freedom of the two edge nodes (see following section).

For faster computation and programming convenience, the interpolated displacement fields $\mathbf{u} = \left[u(x,y), v(x,y), w(x,y), \theta_x(x,y), \theta_y(x,y)\right]^T$ are expressed in matrix format:

$$\mathbf{u} = \sum_{i=1}^{3} \mathbf{N}_i \mathbf{a}_i^{(e)} = [\mathbf{N_1}, \ \mathbf{N_2}, \ \mathbf{N_3}] \begin{Bmatrix} \mathbf{a}_1^{(e)} \\ \mathbf{a}_2^{(e)} \\ \mathbf{a}_3^{(e)} \end{Bmatrix} = \mathbf{N}\mathbf{a}^{(e)} \tag{4.14}$$

$$\mathbf{N}_i = \begin{bmatrix} N_i & 0 & 0 & 0 & 0 \\ 0 & N_i & 0 & 0 & 0 \\ 0 & 0 & N_i & L_i & M_i \\ 0 & 0 & 0 & N_i & 0 \\ 0 & 0 & 0 & 0 & N_i \end{bmatrix} \ ; \quad \mathbf{a}_i^{(e)} = \left[u_i, v_i, w_i, \theta_{xi}, \theta_{yi}\right]^T \tag{4.15}$$

where $\mathbf{a}_i^{(e)}$ is the displacement vector and $\mathbf{N}_i$ the shape function matrix at node i.

Discretized generalized strains

Substituting the previous displacement fields (eq. 4.8, 4.9, 4.13) into the equations 4.5-4.7 yields the generalized strains for membrane $\hat{\boldsymbol{\varepsilon}}_m$, bending $\hat{\boldsymbol{\varepsilon}}_b$ and shear $\hat{\boldsymbol{\varepsilon}}_s$ deformations. In the following expressions, the indices ($_{,x}$; $_{,y}$) indicate the first order derivatives according to x and y.

$$\hat{\boldsymbol{\varepsilon}} = \begin{Bmatrix} \hat{\boldsymbol{\varepsilon}}_m \\ \cdots \\ \hat{\boldsymbol{\varepsilon}}_b \\ \cdots \\ \hat{\boldsymbol{\varepsilon}}_s \end{Bmatrix} = \begin{Bmatrix} \varepsilon_{x0} \\ \varepsilon_{y0} \\ \gamma_{xy0} \\ \cdots \\ \chi_x \\ \chi_y \\ 2\chi_{xy} \\ \cdots \\ \gamma_{xz} \\ \gamma_{yz} \end{Bmatrix} = \begin{Bmatrix} u_{,x} \\ v_{,y} \\ u_{,y} + v_{,x} \\ \cdots \cdots \cdots \\ \theta_{x,x} \\ \theta_{y,y} \\ \theta_{x,y} + \theta_{y,x} \\ \cdots \cdots \cdots \\ w_{,x} - \theta_x \\ w_{,y} - \theta_y \end{Bmatrix} = \sum_{i=1}^{3} \begin{Bmatrix} N_{i,x} u_i \\ N_{i,y} v_i \\ N_{i,y} u_i + N_{i,x} v_i \\ \cdots \cdots \cdots \\ N_{i,x} \theta_{xi} \\ N_{i,y} \theta_{yi} \\ N_{i,y} \theta_{xi} + N_{i,x} \theta_{yi} \\ \cdots \cdots \cdots \\ N_{i,x} w_i + \left(L_{i,x} - N_i\right)\theta_{xi} + M_{i,x}\theta_{yi} \\ N_{i,y} w_i + L_{i,y}\theta_{xi} + \left(M_{i,y} - N_i\right)\theta_{yi} \end{Bmatrix} \tag{4.16}$$

$$= \sum_{i=1}^{3} \mathbf{B}_i \mathbf{a}_i^{(e)} = [\mathbf{B_1}, \ \mathbf{B_2}, \ \mathbf{B_3}] \begin{Bmatrix} \mathbf{a}_1^{(e)} \\ \mathbf{a}_2^{(e)} \\ \mathbf{a}_3^{(e)} \end{Bmatrix} = \mathbf{B}\mathbf{a}^{(e)}$$

where $\mathbf{B}$ and $\mathbf{B}_i$ are the element and nodal generalized strain matrices. The later can be expressed in terms of membrane, bending and shear contributions

$$\mathbf{B}_i = \begin{Bmatrix} \mathbf{B}_{mi} \\ \mathbf{B}_{bi} \\ \mathbf{B}_{si} \end{Bmatrix} \tag{4.17}$$

$$\mathbf{B}_{mi} = \begin{bmatrix} N_{i,x} & 0 & 0 & 0 & 0 \\ 0 & N_{i,y} & 0 & 0 & 0 \\ N_{i,y} & N_{i,x} & 0 & 0 & 0 \end{bmatrix} \quad ; \quad \mathbf{B}_{bi} = \begin{bmatrix} 0 & 0 & 0 & N_{i,x} & 0 \\ 0 & 0 & 0 & 0 & N_{i,y} \\ 0 & 0 & 0 & N_{i,y} & N_{i,x} \end{bmatrix}$$

$$\mathbf{B}_{si} = \begin{bmatrix} 0 & 0 & N_{i,x} & L_{i,x} - N_i & M_{i,x} \\ 0 & 0 & N_{i,y} & L_{i,y} & M_{i,y} - N_i \end{bmatrix} \tag{4.18}$$

The explicit expressions for the generalized strain matrices can be found in Appendix B.

The resulting generalized membrane and bending strains (eq. 4.19 to 4.20) are constant, which is consistent with the condition of a constant in-plane state of strain for the layered EPSF approach.

$$\hat{\boldsymbol{\varepsilon}}_m = \begin{Bmatrix} \varepsilon_{x0} \\ \varepsilon_{y0} \\ \gamma_{xy0} \end{Bmatrix} = \sum_{i=1}^{3} \begin{Bmatrix} b_i u_i \\ c_i v_i \\ c_i u_i + b_i v_i \end{Bmatrix} \tag{4.19}$$

$$\hat{\boldsymbol{\varepsilon}}_b = \begin{Bmatrix} \chi_x \\ \chi_y \\ 2\chi_{xy} \end{Bmatrix} = \sum_{i=1}^{3} \begin{Bmatrix} b_i \theta_{xi} \\ c_i \theta_{yi} \\ c_i \theta_{xi} + b_i \theta_{yi} \end{Bmatrix} \tag{4.20}$$

$$\hat{\boldsymbol{\varepsilon}}_s = \begin{Bmatrix} \gamma_{xz} \\ \gamma_{yz} \end{Bmatrix} = \sum_{i=1}^{3} \begin{Bmatrix} N_{i,x} w_i + (L_{i,x} - N_i)\theta_{xi} + M_{i,x}\theta_{yi} \\ N_{i,y} w_i + L_{i,y}\theta_{xi} + (M_{i,y} - N_i)\theta_{yi} \end{Bmatrix} \tag{4.21}$$

The shear deformations γ_{xz} and γ_{yz} are linear functions on y and x respectively, see Appendix B for the explicit expressions. For the OP element (section 4.2.3), the shear deformation must be expressed along the element border, which leads to the following expression:

$$\gamma_{sz_{ij}} = \left(\frac{\partial w}{\partial s} - \theta_s \right) \Bigg|_{\xi_k = 0} = \frac{w_j - w_i}{l_{ij}} - \frac{\theta_{si} + \theta_{sj}}{2} \tag{4.22}$$

where s is the tangential direction of the k-th element side with nodes i and j, θ_{si} and θ_{sj} are the tangential rotations and w_i and w_j the transverse displacements at the edge nodes. The entire derivation of the expression for $\gamma_{sz_{ij}}$ can be found in Appendix B.

The shear deformation along the element border γ_{sz} is constant and entirely defined by the degrees of freedom of the two edge nodes. The chosen interpolation function for the transverse displacement field thus respects the condition of constant shear deformation at the element borders and continuous shear deformation between elements.

Layer strains

The ML-EP finite element is divided into n_c concrete layers of constant thickness. Each layer l is defined by the planes $z = z_l$ and $z = z_{l+1}$ with $z_l \leq z \leq z_{l+1}$. The state-of-strain in the layer is evaluated at the layer centre $\bar{z}_l = (z_l + z_{l+1})/2$.

The in-plane state-of-strain in each layer l is then computed from the generalized membrane strains and the element curvatures:

$$\boldsymbol{\varepsilon_{p_l}} = \begin{Bmatrix} \varepsilon_x \\ \varepsilon_y \\ \gamma_{xy} \end{Bmatrix}_l = \begin{Bmatrix} \varepsilon_{x0} \\ \varepsilon_{y0} \\ \gamma_{xy0} \end{Bmatrix} - \bar{z}_l \begin{Bmatrix} \chi_x \\ \chi_y \\ 2\chi_{xy} \end{Bmatrix} = \hat{\boldsymbol{\varepsilon}}_m - \bar{z}_l \hat{\boldsymbol{\varepsilon}}_b \tag{4.23}$$

Due to the generalized bending strains (curvatures), the in-plane strains vary throughout the element thickness and with it the principal strain directions. Consequently, the principal strains and directions are computed individually for each layer:

$$\tan \alpha_l = \frac{\varepsilon_{y_l} - \varepsilon_{x_l} + \sqrt{\left(\varepsilon_{x_l} - \varepsilon_{y_l}\right)^2 + \gamma_{xy_l}^2}}{\gamma_{xy_l}} \tag{4.24}$$

$$\boldsymbol{\varepsilon_{1_l}} = \begin{Bmatrix} \varepsilon_1 \\ \varepsilon_2 \end{Bmatrix}_l = \begin{bmatrix} c^2 & s^2 & sc \\ s^2 & c^2 & -sc \end{bmatrix}_l \begin{Bmatrix} \varepsilon_x \\ \varepsilon_y \\ \gamma_{xy} \end{Bmatrix}_l = \mathbf{T_{1_l}} \boldsymbol{\varepsilon_{p_l}} \tag{4.25}$$

where α_l is the direction of the first principal strain ε_{1_l} relative to the x-axis and ε_{2_l} is the second principal strains with $\varepsilon_{1_l} \geq \varepsilon_{2_l}$. The principal strain vector $\boldsymbol{\varepsilon_{1_l}}$ is obtained from the in-plane strains by means of the transformation matrix $\mathbf{T_{1_l}}$ of the concerned layer, where $c = \cos(\alpha_l)$ and $s = \sin(\alpha_l)$.

Constitutive relationship and layer stresses

The constant state of strain in each layer allows determining the corresponding plane state-of-stress according to EPSF method by [Fer07] in which it is assumed that the principal strain directions coincide with the principal stress directions.

The principal stresses in the layers are thus computed directly from the principal strains using the elastic-plastic material law for concrete as defined in section 2.4.1. The concrete compressive stresses are limited to the effective concrete compressive strength $f_{cp,eff} = \eta_\varepsilon(\varepsilon_j) f_{cp}$ of the layer and the tensile strength is neglected. The concrete strength reduction factor η_ε is evaluated separately for each layer and each principal direction. The formulation by Vecchio and Collin [Vec86] presented in equation 2.25 is used.

$$\boldsymbol{\sigma_{1_l}} = \begin{Bmatrix} \sigma_1 \\ \sigma_2 \end{Bmatrix}_l = E_c \begin{Bmatrix} \varepsilon_1 \\ \varepsilon_2 \end{Bmatrix}_l = E_c \boldsymbol{\varepsilon_{1_l}} \qquad \text{with,} \qquad \begin{matrix} -\eta_\varepsilon(\varepsilon_{2_l}) f_{cp} \leq \sigma_{1_l} \leq 0 \\ -\eta_\varepsilon(\varepsilon_{1_l}) f_{cp} \leq \sigma_{2_l} \leq 0 \end{matrix} \tag{4.26}$$

The in-plane concrete stresses $\boldsymbol{\sigma_{p_l}}$ in the global x-y axes are obtained by using the previously defined transformation matrix $\mathbf{T_{1_l}}$ (eq. 4.25).

$$\boldsymbol{\sigma_{p_l}} = \begin{Bmatrix} \sigma_x \\ \sigma_y \\ \tau_{xy} \end{Bmatrix}_l = \begin{bmatrix} c^2 & s^2 \\ s^2 & c^2 \\ sc & -sc \end{bmatrix}_l \begin{Bmatrix} \sigma_1 \\ \sigma_2 \end{Bmatrix}_l = \mathbf{T_{1_l}^T} \boldsymbol{\sigma_{1_l}} \tag{4.27}$$
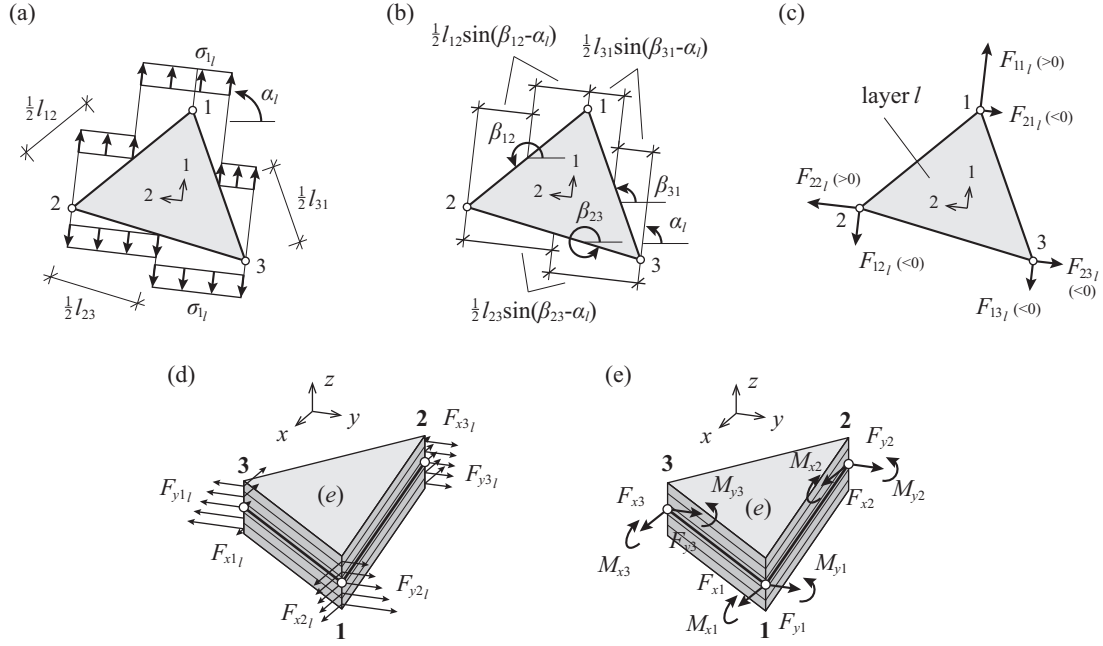
Figure 4.5 Computation of nodal forces in the ML-IP element: (a) first principal stress in a layer l, (b) projection of the element side lengths in the principal stress direction; (c) nodal force contributions of layer l, (d) layer forces in global coordinates and (e) resulting element nodal forces and moments.

Element nodal forces

The nodal forces that result from the stress fields in the concrete layers are determined in a similar way as in the plane EPSF method by Fernández Ruiz and Muttoni [Fer07]. The contribution of each layer to the nodal forces is evaluated in the principal stress directions and then transformed to the global x-y axes (fig. 4.5a-c). In a second step, this layer forces are integrated (by summation) over the element thickness in order to compute the element nodal forces (in-plane) and moments (fig. 4.5d-e).

The forces in a layer l at a node i are computed in the principal stress direction of the layer (α_l) and are designated by F_{1i_l} and F_{2i_l}. Since it has been assumed that the stresses are constant over the layer height, the forces are directly obtained from the stresses as follows:

$$\mathbf{F}_{1i_l} = \begin{Bmatrix} F_{1i_l} \\ F_{2i_l} \end{Bmatrix} = \left\{ \begin{array}{c} 0.5\,\sigma_{1_l}\,t_l\,\left[l_{ij}\sin(\beta_{ij} - \alpha_l) + l_{ki}\sin(\beta_{ki} - \alpha_l) \right] \\ -0.5\,\sigma_{2_l}\,t_l\,\left[l_{ij}\cos(\beta_{ij} - \alpha_l) + l_{ki}\cos(\beta_{ki} - \alpha_l) \right] \end{array} \right\} \tag{4.28}$$

with $i = 1,2,3, j = 2,3,1$ and $k = 3,1,2$

where $t_l = z_{l+1} - z_l$ is the thickness of layer l, l_{ij} and l_{ki} are the lengths of the element sides adjacent to node i and the angles β_{ij} and β_{ki} are the orientation of the element sides ij and ki relative to the x-axis., see figure 4.5a-c.

The layer forces at each node are then expressed in the global coordinates (fig. 4.5d):

$$\mathbf{F}_{pi_l} = \left\{ \begin{matrix} F_{xi} \\ F_{yi} \end{matrix} \right\}_l = \begin{bmatrix} c & -s \\ s & c \end{bmatrix}_l \left\{ \begin{matrix} F_{1i} \\ F_{2i} \end{matrix} \right\}_l = \mathbf{T}_{2_l}^T \, \mathbf{F}_{1i_l} \qquad \text{with, } i = 1, 2, 3 \tag{4.29}$$

where $\mathbf{T}_{2_l}$ is the second transformation matrix of the layer l with $c = \cos(\alpha_l)$ and $s = \sin(\alpha_l)$.

The in-plane nodal forces F_{xi} and F_{yi} and the out-of-plane nodal moments M_{xi} and M_{yi} are obtained by summating the in-plane layer forces $\mathbf{F}_{pi_l}$ over the element thickness (fig. 4.5d-e). Note that due to plane stress state in the layers, the ML-EPSF element does not allow computing out-of-plane nodal forces with this procedure, $F_{zi} = 0$.

$$\mathbf{F}_i^{(e)} = \left\{ \begin{matrix} F_x \\ F_y \\ \cdots \\ F_z \\ \cdots \\ M_x \\ M_y \end{matrix} \right\}_i = \sum_{l=1}^{n_c} \left\{ \begin{matrix} F_{xi_l} \\ F_{yi_l} \\ \cdots \\ 0 \\ \cdots \\ -\bar{z}_l F_{xi_l} \\ -\bar{z}_l F_{yi_l} \end{matrix} \right\} \qquad \text{with, } i = 1, 2, 3. \tag{4.30}$$

$$\mathbf{F}^{(e)} = \left\{ \begin{matrix} \mathbf{F}_1^{(e)} \\ \mathbf{F}_2^{(e)} \\ \mathbf{F}_3^{(e)} \end{matrix} \right\} \tag{4.31}$$

The element nodal forces $\mathbf{F}^{(e)}$ that result from the element nodal displacements $\mathbf{a}^{(e)}$ are assembled in the global force vector $\mathbf{F}$.

Element stress resultants

The stress resultants of the concrete ML-EPSF finite element can be computed directly from the plane state-of-stress in the layers $\boldsymbol{\sigma}_{p_l}$. The membrane forces $\hat{\boldsymbol{\sigma}}_m^{(e)}$ and bending forces $\hat{\boldsymbol{\sigma}}_b^{(e)}$ are defined by:

$$\hat{\boldsymbol{\sigma}}_m^{(e)} = \left\{ \begin{matrix} n_x \\ n_y \\ n_{xy} \end{matrix} \right\} = t_l \sum_{l=1}^{n_c} \left\{ \begin{matrix} \sigma_{x_l} \\ \sigma_{y_l} \\ \tau_{xy_l} \end{matrix} \right\} = t_l \sum_{l=1}^{n_c} \boldsymbol{\sigma}_{p_l} \tag{4.32}$$

$$\hat{\boldsymbol{\sigma}}_b^{(e)} = \left\{ \begin{matrix} m_x \\ m_y \\ m_{xy} \end{matrix} \right\} = t_l \sum_{l=1}^{n_c} \left\{ \begin{matrix} -\bar{z}_l \, \sigma_{x_l} \\ -\bar{z}_l \, \sigma_{y_l} \\ -\bar{z}_l \, \tau_{xy_l} \end{matrix} \right\} = t_l \sum_{l=1}^{n_c} -\bar{z}_l \, \boldsymbol{\sigma}_{p_l} \tag{4.33}$$

4.2.3 Out-of-plane concrete element

The out-of-plan (OP) concrete element (fig. 4.1) is thought to be a complement to the ML-IP element. The ML-IP element, due to the plane stress condition, transfers only in-plane forces and constant moments. However, in order to be able to model structural elements sub-

jected to out-of-plane shear forces and varying bending moments, the ML-IP element needs an "extension" which is the OP element. The role of the out-of-plane element is thus to complete the set of internal forces of the ML-IP element by out-of-plane shear forces.

Principle

The OP element is designed to be used together with the ML-IP element in order to model a typical membrane and bending behaviour with moderate out-of-plane shear load (non-governing for the failure mode). Figure 4.1c schematically illustrated the principle.

The basic idea is that the bending moment is computed using the ML-IP element and that the out-of-plane shear force is obtained from the OP elements. The transverse bending moment computed from the ML-IP element can be considered as the average moment of a linear moment diagram. The OP element provides the transverse shear force resulting from the shear deformation. In order to equilibrate the element and to obtain consistent internal force diagrams for bending and shear, the OP element additionally carries a linearly vary-ing bending moment whose gradient counterbalances the out-of-plane shear force and whose average is equal to zero.

The OP elements are beam-like elements that are placed along each border of the triangular ML-IP element, figure 4.1b. They deform identically to the ML-IP element border they are connected to, which means that they develop a constant curvature and a constant trans-verse shear deformation. The element constitutive relationships eventually lead to longitu-dinal bending moments (in the element axis) and vertical shear forces (transverse to the ML-IP element plane) at each element node, figure 4.1a.

Displacement field and discretization

The out-of-plane shear element is a beam element with two nodes and two degrees of free-dom per node: out-of-plane displacement w and rotation θ_s, see figure 4.2c. The element formulation is based on the Timoshenko theory, which is the equivalent of the Reissner-Mindlin plate theory (section 5.2.1) for beam elements.

In the present development, the shear deformations provided by the Timoshenko beam theory is considered as an auxiliary degree of freedom for the interpolations of the dis-placement fields. It decouples the slope of the element axis from the rotation of the axis normal (figure 4.3b), which then allows to impose a constant curvature to the transverse displacement field (condition of the ML-IP element) for any combination of nodal dis-placements $(w_1, \theta_{s1}, w_2, \theta_{s2})$ as represented in figure 4.2c.

The formulation of the out-of-plane element bases on the following assumptions:
- The shear deformation is constant along the element axis.
- The curvature is constant along the element axis.

- The element deformation is identical to the deformation of the ML-IP element border it is connected to.

The condition of constant curvature χ_s leads to a linear variation of the rotation of the normal along the element axis. It can be expressed as a function of the nodal rotations θ_{si} and the element length l.

$$\theta_s(s) = \int_s \chi_s ds = \chi_s s + \theta_{s1} = \frac{\theta_{s2} - \theta_{s1}}{l}s + \theta_{s1} \tag{4.34}$$

The definition of the element slope $(dw/ds = \theta_s + \gamma_{sz})$ and the condition of constant shear deformation γ_{sz} along the element axis thus allows expressing the transverse displacement field as follows:

$$w(s) = \int_s [\theta_s(s) + \gamma_{sz}]ds = w_1 + (\theta_{s1} + \gamma_{sz})s + \frac{1}{2}\chi_s s^2$$
$$= w_1 + \left(\frac{w_2 - w_1}{l} - \frac{\theta_{s2} - \theta_{s1}}{2}\right)s + \frac{\theta_{s2} - \theta_{s1}}{2\,l}s^2 \tag{4.35}$$

The displacement fields according to the previous equations ensure the continuity between the OP element and ML-IP element because they are identical to the displacement of the ML-IP element borders. Indeed, the interpolations functions of the ML-IP had been chosen to fulfil the same conditions (constant curvature and constant shear deformation along the element border that are entirely defined by the degrees of freedom of the two edge nodes).

The OP element displacement fields can thus be expressed in a similar format as for the ML-IP element (eq. 5.8 to 5.15) by replacing the shape function of the triangular element in area coordinates by the linear shape function of a beam element in natural coordinates ξ, figure 4.6a.

$$N_1(\xi) = \frac{1}{2}(1 - \xi) \quad ; \quad N_2(\xi) = \frac{1}{2}(1 + \xi) \qquad \text{with,} \qquad \begin{matrix} -1 \le \xi \le 1 \\ \xi = 2\,s/l - 1 \end{matrix} \tag{4.36}$$

In the local element axes the discretized displacement fields are given by:

$$\theta_s = \sum_{i=1}^{2} N_i \theta_{si} \quad ; \quad w = \sum_{i=1}^{2} N_i w_i + \frac{1}{2}N_1 N_2 l(\theta_{s1} - \theta_{s2}) \tag{4.37}$$

Similarly to the equations 5.13, the interpolations function can be expressed as a function of the nodal rotations θ_{xi} and θ_{yi} in the global coordinate system by substituting $\theta_{si} = \theta_{xi}\cos\phi + \theta_{yi}\sin\phi$, where ϕ is the angle between the OP element axis s and the x axis, figure 4.6b.
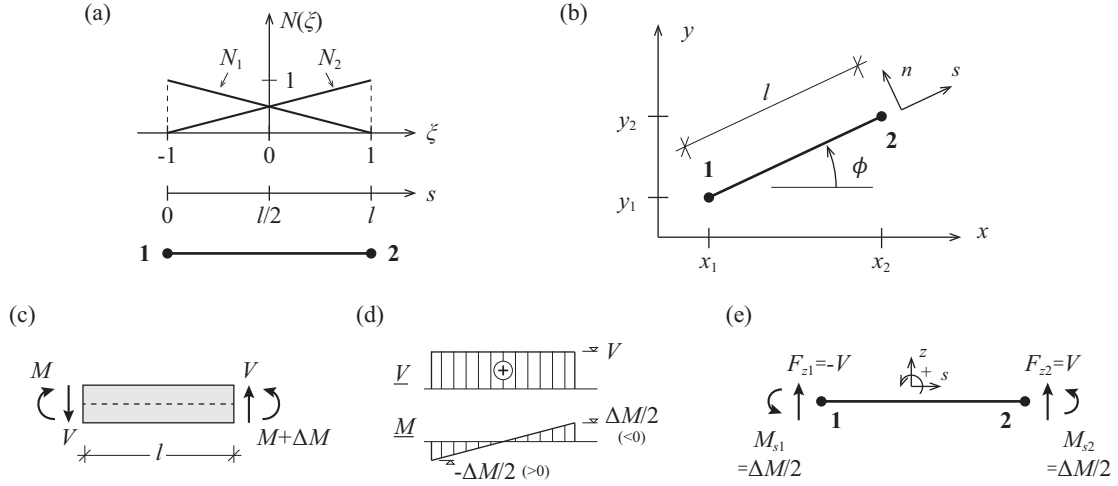
Figure 4.6 Two node out-of-plane element: (a) linear shape functions; (b) local and global coordinate system (c) equilibrium of internal forces; (d) assumed internal force diagrams and (e) nodal forces of the finite element.

$$\mathbf{u}' = \begin{Bmatrix} w(s) \\ \theta_s(s) \end{Bmatrix} = \sum_{i=1}^{2} \mathbf{N}_i \mathbf{a}_i^{(e)} = [\mathbf{N_1}, \ \mathbf{N_2}] \begin{Bmatrix} \mathbf{a}_1^{(e)} \\ \mathbf{a}_2^{(e)} \end{Bmatrix} = \mathbf{N} \mathbf{a}^{(e)} \tag{4.38}$$

$$\mathbf{N}_i = \begin{bmatrix} 0 & 0 & N_i & L_i & M_i \\ 0 & 0 & 0 & c_1 N_i/l & -b_1 N_i/l \end{bmatrix} \quad ; \quad \mathbf{a}_i^{(e)} = \begin{bmatrix} u_i, v_i, w_i, \theta_{xi}, \theta_{yi} \end{bmatrix}^T \tag{4.39}$$

with $c_i = x_j - x_i$; $b_i = y_i - y_j$; $L_i = c_i N_i N_j/2$; $M_i = -b_i N_i N_j/2$ for $i = 1, 2; j = 2, 1$.

Generalized strains

The shear deformation and the curvature of the OP element are computed according to the Timoshenko beam theory ($\gamma_{sz} = dw/ds - \theta_s$ and $\chi_s = d\theta_s/ds$). In the local coordinate system, the values can be read directly from the displacement functions in equations 4.34 and 4.35.

$$\chi_s = \frac{\theta_{s2} - \theta_{s1}}{l_{12}} \quad ; \quad \gamma_{sz} = \frac{w_2 - w_1}{l_{12}} - \frac{\theta_{s1} + \theta_{s2}}{2} \tag{4.40}$$

The shear deformations and the curvature are identical to ML-IP element deformations along the borders, see for instance $\gamma_{sz_{ij}}$ in equation 4.22.

For convenience reasons, the finite element method computes the curvature and shear deformation directly from the nodal displacement vector expressed in the global coordinate system $\mathbf{a}_i^{(e)} = [u_i, v_i, w_i, \theta_{xi}, \theta_{yi}]^T$. From equations 4.38 and 4.39, the following generalized strain vector for the OP element is obtained, where $\mathbf{B}_i$ is the generalized strain matrix at node i:

$$\hat{\boldsymbol{\varepsilon}} = \begin{Bmatrix} \hat{\boldsymbol{\varepsilon}}_b \\ \cdots \\ \hat{\boldsymbol{\varepsilon}}_s \end{Bmatrix} = \begin{Bmatrix} \chi_s \\ \cdots \\ \gamma_{sz} \end{Bmatrix} = \begin{Bmatrix} \theta_{s,s} \\ \cdots\cdots\cdots \\ w_{,s} - \theta_s \end{Bmatrix} = \sum_{i=1}^{2} \mathbf{B}_i \mathbf{a}_i^{(e)} = [\mathbf{B}_1, \ \mathbf{B}_2] \begin{Bmatrix} \mathbf{a}_1^{(e)} \\ \mathbf{a}_2^{(e)} \end{Bmatrix} = \mathbf{B}\mathbf{a}^{(e)} \tag{4.41}$$

$$\mathbf{B}_i = \begin{Bmatrix} \mathbf{B}_{bi} \\ \mathbf{B}_{si} \end{Bmatrix} = \frac{1}{2l^2} \begin{bmatrix} 0 & 0 & 0 & -2c_i & 2b_i \\ 0 & 0 & (-1)^i 2l & -c_1 l & b_1 l \end{bmatrix} \qquad \text{with, } i = 1, 2. \tag{4.42}$$

Constitutive relationship for transverse shear

The shear force is computed according to the Timoshenko beam theory using the shear deformation from equation 4.40 respectively 4.41.

$$V = GB \ \gamma_{sz} \tag{4.43}$$

In the present work, it is assumed that the OP finite element behaves elastically. This hypothesis is a strong simplification of the actual behaviour of concrete elements, but it is acceptable in the context of the proposed finite element method that focuses on the membrane transverse bending interaction (ML-IP element). The OP element is used to represent variations of the transverse bending moment along a structural element but not to model out-of-plane shear failures. Nonetheless, the constitutive relationship of the OP element might be enhanced in a future research project to account for such failure modes.

The shear modulus G and the reduced area B of the OP element are thus determined according to the theory of elasticity:

$$G = \frac{E_c}{2(1 - v)} = \frac{E_c}{2} \qquad \text{with, } v = 0 \tag{4.44}$$

$$B = \frac{5}{6} bh \tag{4.45}$$

The height h of the OP element is equal to the average thickness of the neighbouring ML-IP elements. The width b represents the contribution of the connected ML-IP elements to the transverse shear stiffness in the direction of the OP element axis. It is estimated as follows:
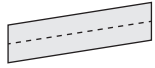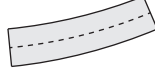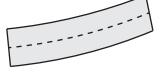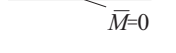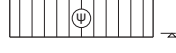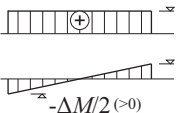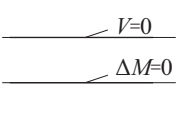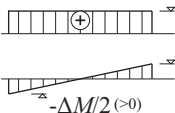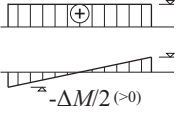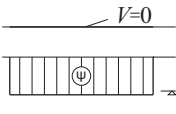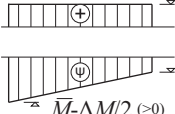
$$b = \sum_{i=1}^{n} \frac{A_i^{(e)}}{\Gamma_i^{(e)}} \qquad \text{with, } n \in \{1, 2\} \tag{4.46}$$

where $A_i^{(e)}$ is the area and $\Gamma_i^{(e)}$ the perimeter of the i-th connected triangular ML-IP element. The OP element is either connected to one ($n = 1$) or two ($n = 2$) ML-IP elements depending if it is located on the border (free edge of a structure) or in the FE model.

Equilibrium condition

In order to satisfy the equilibrium of internal forces, the OP element must carry a linearly varying bending moment. The total moment variation ΔM over the element length l is computed on the basis of the moment equilibrium condition (fig. 4.6.c):

	$\chi_s=0$ $\gamma_{sz}\neq 0$ $\{w_1,w_2\},\ \{\theta_{s1},\theta_{s2}\}=0$	$\chi_s\neq 0$ $\gamma_{sz}=0$ $\{w_1,\theta_{s1},w_2,\theta_{s2}\}\,|\,w_2=w_1+(\theta_{s1}+\theta_{s2})\cdot l/2$	$\chi_s\neq 0$ $\gamma_{sz}\neq 0$ $\{w_1,\theta_{s1},w_2,\theta_{s2}\}$
ML-IP elem.	$\overline{M}=0$	$\overline{M}\ (>0)$	$\overline{M}\ (>0)$
OP element	V; $\Delta M/2$ (<0); $-\Delta M/2\ (>0)$	$V=0$; $\Delta M=0$	V; $\Delta M/2$ (<0); $-\Delta M/2\ (>0)$
+	V; $\Delta M/2$ (<0); $-\Delta M/2\ (>0)$	$V=0$; $\overline{M}\ (>0)$	V; $\overline{M}+\Delta M/2$ (>0); $\overline{M}-\Delta M/2\ (>0)$

Figure 4.7 Schematically illustration of the behaviour of the OP element and the resulting internal forces in case of pure shear deformation (left), pure bending deformation (centre) and a general case of bending and shear deformation (right).

$$\Delta M = -Vl = -\gamma_{sz}GBl \tag{4.47}$$

It is assumed that the average moment of the element is zero which leads to a moment of $\mp\Delta M/2$ on both ends of the OP element (fig. 4.6d). This choice is justified by the fact that the OP element is not supposed to contribute to the average bending moment of the composed elements (ML-IP + OP), but only to equilibrate the internal forces. The average bending moment of the composed elements is computed by the non-linear ML-IP elements.

Figure 4.7 illustrates the behaviour of the OP element and the resulting internal forces diagrams for three cases of nodal displacements: a general case leading to a combination of shear and bending deformations ($\gamma_{sz}\neq 0$, $\chi_s\neq 0$) and the two extreme situations of pure shear ($\gamma_{sz}\neq 0$, $\chi_s=0$) and pure bending deformation ($\gamma_{sz}=0$, $\chi_s\neq 0$).

In case of pure shear deformation, the curvature is zero which leads to no internal forces in ML-IP element. The overall internal forces diagrams are thus entirely defined by the OP element. In case of pure bending deformation, the OP element does not contribute because the shear deformation is zero. The shear forces and the moment variation is equal to zero, the constant moment is thus directly obtained from the ML-IP. If both, shear and bending deformations exist, the resulting internal forces are a combination of the two elements: the average bending moment is provided by the non-linear ML-IP element, the out-of-plane shear forces and the moment variation by the OP element.

The combination of these two finite elements is thus able to account for situations with constant out-of-plane shear and linearly varying bending moments as well as pure bending behaviours.

Stiffness matrix and nodal force vector

The previous developments allow expressing the local force vector $\mathbf{F}'^{(e)}$ of the OP element (fig. 4.6e):

$$\mathbf{F}'^{(e)} = \begin{Bmatrix} F_{z1} \\ M_{s1} \\ \cdots \\ F_{z2} \\ M_{s2} \end{Bmatrix} = \begin{Bmatrix} -V \\ \Delta M/2 \\ \cdots\cdots \\ V \\ \Delta M/2 \end{Bmatrix} = \begin{Bmatrix} -1 \\ -l/2 \\ \cdots\cdots \\ 1 \\ -l/2 \end{Bmatrix} GB\gamma_{sz} \tag{4.48}$$

In order to assemble the global force vector of the finite element model, the element forces have to be expressed in the global coordinate system. Instead of first computing local element forces and then transforming them, they can be obtained directly from nodal displacement $\mathbf{a}_i^{(e)} = \left[u_i, v_i, w_i, \theta_{xi}, \theta_{yi}\right]^T$ using the stiffness matrix in $\mathbf{K}$ which is obtained as follows:

$$\mathbf{K} = \int_{vol} \mathbf{B}_s^T D \mathbf{B}_s dV = BGl\mathbf{B}_s^T \mathbf{B}_s \qquad \text{with, } \mathbf{B}_s = [\mathbf{B}_{s1}, \ \mathbf{B}_{s2}] \tag{4.49}$$

where $\mathbf{B}_s$ (eq. 4.42) is the generalized strain matrix for the shear deformation. The latter is already expressed in the global coordinate system.

The element nodal force vector $\mathbf{F}^{(e)}$ of the OP element is then given by:

$$\mathbf{F}^{(e)} = \begin{Bmatrix} \mathbf{F}_1^{(e)} \\ \mathbf{F}_2^{(e)} \end{Bmatrix} = \mathbf{K}\mathbf{a}^{(e)} \tag{4.50}$$

$$\mathbf{F}_i^{(e)} = \left[F_x, \ F_y, \ F_z, M_{\ x}, \ M_y\right]_i^T = \left[0, 0, \ F_z, \ M_x, \ M_y\right]_i^T \qquad \text{with, } i = 1,2.$$

During the solution procedure, the element nodal forces in $\mathbf{F}^{(e)}$ are assembled into the global force vector.

4.2.4 Rebar element

The reinforcing bars of the reinforced concrete are modelled with separate finite elements than for concrete. The reinforcement is modelled using bar elements with two nodes and two degrees of freedom per node (see figure 4.1a and 4.8a). The two element nodes lie in the same plane as the nodes of the ML-IP element (middle plane). In order to represent the rebars with their actual position inside the reinforced concrete section and to account for their contribution to the bending resistance, the finite bar element includes an additional parameter for the eccentricity of the rebar relative to the middle plane. Consequently, the bar element carries axial forces and bending moments. As in [Fer07] the dowel action that can develop in reinforcing bars is neglected, thus the finite element carries no transverse shear forces.

(a)

(b)
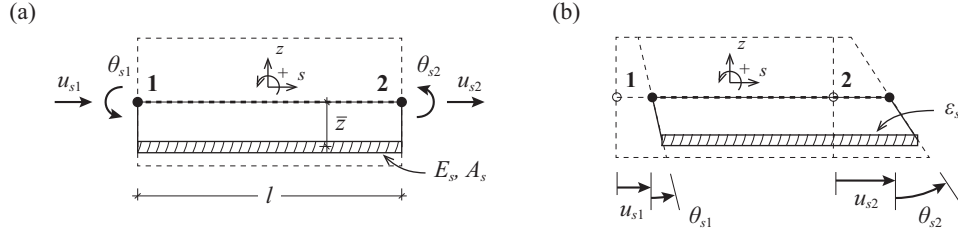
Figure 4.8 Finite bar element for reinforcing bars in concrete: (a) two-node element with four degrees of freedom (in local coordinate system) and (b) element deformation with constant axial strain.

The behaviour of the bar element is governed by an elastic-plastic material law for steel.

Displacement field and discretization

In the local element axes the discretized displacement fields are given by:

$$u_s = \sum_{i=1}^{2} N_i u_{si} \quad ; \quad \theta_s = \sum_{i=1}^{2} N_i \theta_{si} \tag{4.51}$$

where N_i are linear shape function for beam elements (eq. 4.36), u_{si} the nodal displacement and θ_{si} the nodal rotations in the element axis direction (s). The interpolation functions can be expressed in terms of the nodal displacements (u_i, v_i) and rotations (θ_{xi}, θ_{yi}) in the global coordinate system.

$$\mathbf{u}' = \begin{Bmatrix} u_s(s) \\ \theta_s(s) \end{Bmatrix} = \sum_{i=1}^{2} \mathbf{N}_i \mathbf{a}_i^{(e)} = [\mathbf{N_1}, \ \mathbf{N_2}] \begin{Bmatrix} \mathbf{a}_1^{(e)} \\ \mathbf{a}_2^{(e)} \end{Bmatrix} = \mathbf{N} \mathbf{a}^{(e)} \tag{4.52}$$

$$\mathbf{N}_i = \begin{bmatrix} c_1 N_i/l & -b_1 N_i/l & 0 & 0 & 0 \\ 0 & 0 & 0 & c_1 N_i/l & -b_1 N_i/l \end{bmatrix} \quad ; \quad \mathbf{a}_i^{(e)} = \begin{bmatrix} u_i, v_i, w_i, \theta_{xi}, \theta_{yi} \end{bmatrix}^T \tag{4.53}$$

with $c_1 = l \cos \phi = x_2 - x_1$ and $b_1 = -l \sin \phi = y_1 - y_2$, where l is the element length and ϕ the angle between the element axis s and the global x axis (same definition as for the OP element fig.4.6b).

Axial deformation and generalized strains

The axial deformation of the rebar element ε_s is directly obtained from the nodal displacements in the local reference systems, figure 4.8:

$$\varepsilon_s = \frac{u_{s2} - u_{s1}}{l} - \bar{z} \frac{\theta_{s2} - \theta_{s1}}{l} = \varepsilon_{s0} - \bar{z} \chi_s \tag{4.54}$$

where l is the element length and $\bar{z}$ is the eccentricity of the bar relative to the element axis defined by the two element nodes. The eccentricity allows to position the bar element so that it represents a reinforcing bar with its actual position in the thickness of the reinforced concrete element.

The element deformation can as well be expressed in terms of the element longitudinal deformation at the reference plane ε_{s0} and the bending deformation χ_s. These generalized strains can be obtained directly as a function of the nodal displacement in global coordinates $\mathbf{a}^{(e)}$ by derivation of the displacement fields u_s and θ_s in equation 4.52.

$$\hat{\varepsilon} = \begin{Bmatrix} \hat{\varepsilon}_m \\ \cdots \\ \hat{\varepsilon}_b \end{Bmatrix} = \begin{Bmatrix} \varepsilon_{s0} \\ \cdots \\ \chi_s \end{Bmatrix} = \begin{Bmatrix} u_{s,s} \\ \cdots\cdots\cdots \\ \theta_{s,s} \end{Bmatrix} = \sum_{i=1}^{2} \mathbf{B}_i \mathbf{a}_i^{(e)} = [\mathbf{B}_1, \mathbf{B}_2] \begin{Bmatrix} \mathbf{a}_1^{(e)} \\ \mathbf{a}_2^{(e)} \end{Bmatrix} = \mathbf{B}\mathbf{a}^{(e)} \tag{4.55}$$

$$\mathbf{B}_i = \begin{Bmatrix} \mathbf{B}_{mi} \\ \mathbf{B}_{bi} \end{Bmatrix} = \frac{1}{l^2} \begin{bmatrix} -c_i & b_i & 0 & 0 & 0 \\ 0 & 0 & 0 & -c_i & b_i \end{bmatrix} \qquad \text{with, } i = 1, 2. \tag{4.56}$$

with $c_i = x_j - x_i$ and $b_i = y_i - y_j$ for $i = 1, 2; j = 2, 1$.

The transformation between the axial deformation ε_s and the generalized strain matrix $\hat{\varepsilon}$ is performed using the transformation matrix $\mathbf{S}$ such that:

$$\varepsilon_s = [1, -\bar{z}] \begin{Bmatrix} \varepsilon_{s0} \\ \cdots \\ \chi_s \end{Bmatrix} = \mathbf{S}\hat{\varepsilon} \tag{4.57}$$

Constitutive relationship

The rebar element is governed by an elastic-plastic material law as in [Fer07] and has already been presented in section 2.1.4. The element stress σ_s is thus obtained from the element axial deformation as follows:

$$\sigma_s = \begin{cases} E_s \varepsilon_s, & |\varepsilon_s| \leq \varepsilon_y = f_s/E_s \\ E_h(\varepsilon_s - \varepsilon_y) + f_s, & \varepsilon_s > \varepsilon_y \\ E_h(\varepsilon_s + \varepsilon_y) - f_s, & \varepsilon_s < -\varepsilon_y \end{cases} \tag{4.58}$$

where f_s is the yield strength, E_s and E_h the modulus of elasticity and the hardening modulus for steel. If no hardening modulus is specified by the user, it is set to the default value $E_h = E_s * 10^{-4}$ in order to improve the convergence of the non-linear computation.

Nodal forces

The element nodal forces are composed of the axial forces F_{s1} and F_{s2} and the bending moments M_{s1} and M_{s2}, figure 4.1a. It is assumed that the stress is constant over the bar area A_s and the element length such that the element force vector in local coordinates is given by:

$$\mathbf{F}'^{(e)} = \begin{Bmatrix} F_{s1} \\ M_{s1} \\ \cdots \\ F_{s2} \\ M_{s2} \end{Bmatrix} = \sigma_s A_s \begin{Bmatrix} -1 \\ \bar{z} \\ \cdots\cdots \\ 1 \\ -\bar{z} \end{Bmatrix} \tag{4.59}$$

The element force vector in the global x-y coordinate system $\mathbf{F}^{(e)}$ is obtained directly from the element stress using the following expression:

$$\mathbf{F}^{(e)} = \begin{Bmatrix} \mathbf{F}_1^{(e)} \\ \mathbf{F}_2^{(e)} \end{Bmatrix} = \int_{vol} \mathbf{B}^T \mathbf{S}^T \sigma_s dV = \mathbf{B}^T \mathbf{S}^T \sigma_s A_s l$$

$$\mathbf{F}_i^{(e)} = \begin{bmatrix} F_x, & F_y, & F_z, M_x, & M_y \end{bmatrix}_i^T = \begin{bmatrix} F_x, & F_y, 0, & M_x, & M_y \end{bmatrix}_i^T \qquad \text{with } i = 1,2.$$

(4.60)

where $\mathbf{B}$ is the generalized strain matrix from equation 4.55 and $\mathbf{S}$ the transformation matrix defined in equation 4.57.

4.3 Modelling

Model geometry and materials

The proposed finite element method allows investigation plane reinforced concrete elements using flat shell elements for the concrete (ML-IP + OP element) and separate bar elements for the reinforcement. In order to build the finite element model, the middle plane of the structural element is first discretized using of a triangle mesh. The geometry of the mesh has to account for the in-plane position of the reinforcement and varying material and/or geometrical (thickness) properties of the structural element. Additionally, in order to reduce the effect discretization on the final results, the mesh should be as regular and homogeneous as possible (element size and shape) and avoid preferential directions for the triangle orientations. This is especially important for cases where out-of-plane loads are applied. Section 4.5.2 presents further details on the mesh sensitivity of the proposed FE method.

The mesh is then used to determine the nodes and the elements of the finite element model. Each mesh triangle is converted into a three-node concrete ML-IP finite element for which the thickness (t), the number of layers (n_c) and the material properties (E_c, f_{cp}) have to be defined. The out-of-plane (OP) concrete elements are added automatically along the ML-IP element borders. Their geometric and material properties are computed from the neighbouring ML-IP elements as presented earlier. The reinforcement is introduced in a separate step using two-node rebar elements that are added into the existing FE model of concrete elements (no additional nodes are created). For each rebar element the reinforcement area (A_s) and the material properties have to be defined (f_s, E_s and possibly E_h).

Before the computation, the nodes and elements of the finite element model are numbered and stored in matrices. Each node is defined with a unique node number and its global x-y coordinates (all nodes lie in the plane $z = 0$) that are stored in the nodal matrix. For each type of finite elements (ML-IP, OP, Rebar), a separate element matrix is created that contains the element number, the number of the nodes defining the element as well as the geometrical and material properties.

The number of nodes in the FE model (n_n) defines the total number of global degrees of freedom (n_{gdof}) of the model. Each node having five degrees of freedom (u, v, w, θ_x, θ_y), the total number of global degrees of freedom is given by $n_{gdof} = 5 \cdot n_n$, which defines the size of the FE problem to solve. Each nodal degree of freedom has an individual $gdof$ number that is required to assemble the global force vector $\mathbf{F}$, the global displacement vector $\mathbf{a}$ and the stiffness matrix of the equilibrium condition $\mathbf{F} = \mathbf{Ka}$.

External loads and boundary conditions

The external loads acting on the structural element are introduced into the FE model by means of nodal forces. In-plane forces Q_x and Q_y, out-of-plane forces Q_z and bending moments M_x and M_y can be applied to every node i. Theses external loads are stored in the load vector $\mathbf{F}_{ext}$ as follows:

$$\mathbf{F}_{ext} = \begin{Bmatrix} \mathbf{F}_{ext}^{(1)} \\ \mathbf{F}_{ext}^{(2)} \\ \vdots \\ \mathbf{F}_{ext}^{(n)} \end{Bmatrix} \quad \text{with} \quad \mathbf{F}_{ext}^{(i)} = \left[Q_x, Q_y, Q_z, M_x, M_y \right]_i^T \quad \text{for } i = 1 \text{ to } n_n \tag{4.61}$$

The kinematic boundary conditions, as for example supports and symmetry axes, are applied by imposing zero translation and/or rotations at the concerned nodes.

4.4 Method of solution

Owing to the nonlinear nature of the problem, the unknown nodal displacement values $\mathbf{a}$ are required for the determination of the material stiffness matrixes. Consequently, a direct solution of the finite element problem in form of $\mathbf{a} = \mathbf{K}^{-1}\mathbf{F}$ is not possible. As such, an iterative secant stiffness procedure is adopted. The full load is applied to the model and the iterative procedure is repeated until the solution has converged within a predefined tolerance or a maximum number of iterations has been performed. Convergence is evaluated using the difference between the applied and the computed nodal forces (residual forces) of the current iteration step.

4.4.1 Solution algorithm

The solution of the non-linear FE problem is based on a secant stiffness approach with updated stiffness matrix at every iteration. The different steps of the algorithm are illustrated in the flowchart of figure 4.9.

For a given displacement $\mathbf{a}_k$ at iteration step k, the global nodal force vector $\mathbf{F}_k$ is computed. The nodal force vector is established by evaluating the nodal forces of each finite element using the formulations presented earlier (section 5.2). The element deformations are determined from the element nodal displacement vector $\mathbf{a}^{(e)}$ and then introduced into the non-linear constitutive models for concrete or steel. The resulting internal stresses are inte-
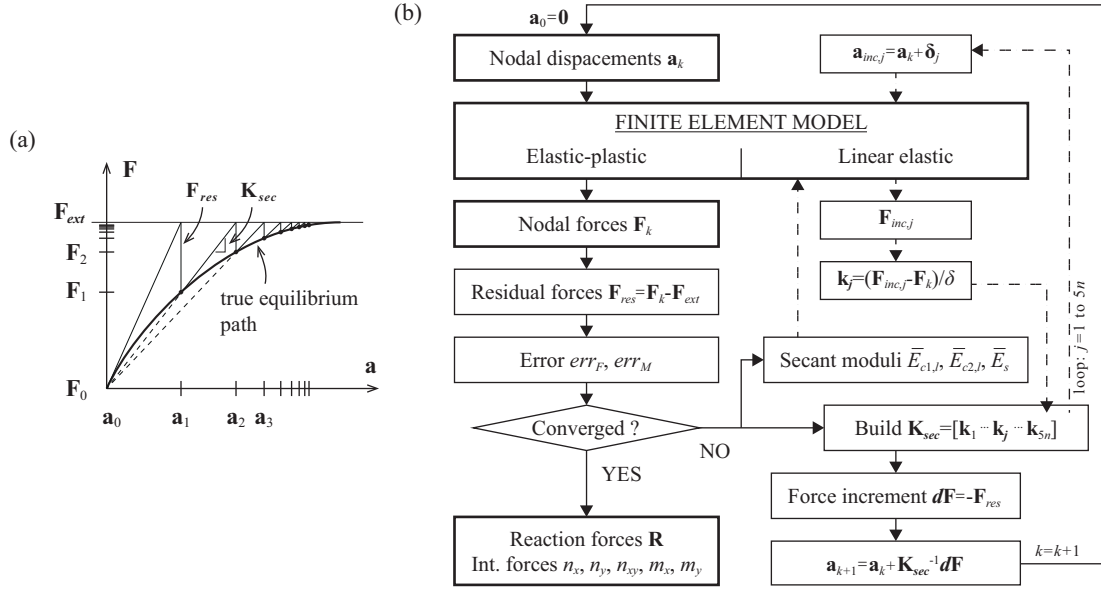
Figure 4.9 Adopted iterative solution procedure for the non-linear finite element problem: (a) schematic representation of the secant stiffness approach and (b) flowchart of the numerical steps.

grated to obtain the element nodal forces $\mathbf{F}^{(e)}$, which are then assemble into the global for vector $\mathbf{F}_k$ of the current iteration.

In order to determine if an acceptable solution of the problem has been found, the computed nodal forces $\mathbf{F}_k$ are compared to the applied external forces $\mathbf{F}_{ext}$. The residual forces $\mathbf{F}_{res} = \mathbf{F}_k - \mathbf{F}_{ext}$ are used to estimate the error of the current solution, which is then checked against the convergence criterion (see section 4.4.3 for the definition of the error and the convergence criterion). If the convergence criterion is fulfilled, the iterative procedure has converged and no further iterations are required. In this case, the reaction forces and the stress resultants of each element are evaluated based on the current (last) displacement field. However, if the convergence is not yet reached, the current displacement vector $\mathbf{a}_k$ has to be adjusted in order to improve the solution and the model has to be re-evaluated.

The displacement vector for the next iteration is given by $\mathbf{a}_{k+1} = \mathbf{a}_k + d\mathbf{a}$. The displacement increments for each degree of freedom are computed as follows:

$$d\mathbf{a} = \mathbf{K}_{sec}^{-1}d\mathbf{F} \qquad (4.62)$$

where $d\mathbf{F} = -\mathbf{F}_{res}$ is the force increment that is required to approach the exact solution ($\mathbf{F} = \mathbf{F}_{ext}$) within the next iteration and $\mathbf{K}_{sec}$ is the global secant stiffness matrix of the model. Due to the non-linear constitutive models for concrete and steel, the coefficients of the secant stiffness matrix depend on the current state-of-strain (i.e. the displacement vector $\mathbf{a}_k$) in the elements and are thus updated at every iteration.

The non-linear FE model is then evaluated for the new displacement vector. The resulting nodal forces $\mathbf{F}$ are again compared to the applied forces $\mathbf{F}_{ext}$ and the convergence criterion is examined. This procedure is repeated until convergence is reached or the maximum number of iterations has been performed.

4.4.2 Global stiffness matrix

The global secant stiffness matrix is evaluated based on the current deformation of the model, which allows thus to consider the actual state (elastic or plastic) of the different concrete and steel elements.

Due to the non-linear nature of the problem, the secant stiffness matrix is determined column by column. For this, one degree of freedom (j) of the current displacement vector $\mathbf{a}_k$ is increased by a very small displacement δ and the FE model is re-evaluated for the new increment nodal displacements $\mathbf{a}_{inc}$.

$$\mathbf{a}_{inc,j} = \mathbf{a}_k + \boldsymbol{\delta}_j, \qquad \text{with } \boldsymbol{\delta}_j = [0 \; \cdots \; \delta_j \; \cdots \; 0]^T \tag{4.63}$$

The resulting nodal forces $\mathbf{F}_{inc}$ are then compared to the current nodal forces $\mathbf{F}_k$ (not incremented) to determine the coefficients of the secant stiffness matrix of the j-th degree of freedom (column j of $\mathbf{K}_{sec}$). This procedure is repeated for every degree of freedom in the model until the entire secant stiffness matrix is defined.

$$\mathbf{k}_j = \left(\mathbf{F}_{inc,j} - \mathbf{F}_k\right)/\delta \tag{4.64}$$

$$\mathbf{K}_{sec} = \left[\mathbf{k}_1 \cdots \; \mathbf{k}_j \cdots \; \mathbf{k}_{5 \cdot n_n}\right] \tag{4.65}$$

The incremented nodal forces $\mathbf{F}_{inc}$ are computed assuming elastic secant stiffness constitutive relationships for the materials. The secant moduli of elasticity of each concrete layer and every rebar element are determined from the current deformations and stresses (at iteration k):

$$\bar{E}_{c1_l} = \sigma_{1_l}/\varepsilon_{1_l} \quad ; \quad \bar{E}_{c2_l} = \sigma_{2_l}/\varepsilon_{2_l} \quad ; \quad \bar{E}_s = \sigma_s/\varepsilon_s \tag{4.66}$$

It was observed that this assumption leads to a little slower (more iterations required) but generally more stable convergence than in the plane EPSF method of [Fer07]. At the same time, it reduces the computation time of the secant stiffness matrix that requires evaluating the entire FE model $5 \cdot n_n$ times at every iteration.

4.4.3 Error measurement and convergence criteria

Error of the finite element model

The proposed iterative non-linear finite element method might lead to solutions that are not in equilibrium with applied nodal forces (insufficient iterations, load higher than the resistance of the reinforced concrete element etc.). In order to estimate the error of the solu-

tion the residual forces of the model are normalized by the external forces. This procedure is similar to the method used in the plane EPSF method [Fer07] which has shown satisfying results in the past.

To avoid normalizing values with different units (for instance MN/MNm), two distinct error measures for nodal forces err_F and nodal moments err_M are computed:

$$err_F = \frac{\max|\mathbf{F}_F - \mathbf{R}_F - \mathbf{F}_{ext,F}|}{\max|\mathbf{F}_{ext,F}|} \quad ; \quad err_M = \frac{\max|\mathbf{F}_M - \mathbf{R}_M - \mathbf{F}_{ext,M}|}{\max|\mathbf{F}_{ext,M}|} \tag{4.67}$$

where $\mathbf{F}$ are the nodal forces predicted with FE method, $\mathbf{R}$ the predicted reactions forces and $\mathbf{F}_{ext}$ the loads acting on the model. For each error measure, only the corresponding terms, moments M or forces F, of these vectors are used.

Convergence criteria

The previous error measurements are used to establish a convergence criterion for the iterative the Newton-Raphson solution procedure.

The implement convergence criterion has two separate conditions: the error of the current iteration k has to be smaller than a predefined tolerance (for instance $tol = 10^{-3}$) and it has to be decreasing (or be stable) during the last iterations. These conditions have to be fulfilled by the two error measurements err_F and err_M.

$$\begin{cases} \{err_F\}_k < tol = 10^{-3} \\ trend\,(\{err_F\}_{k-30} \to \{err_F\}_k) \leq 0 \end{cases} \text{and} \begin{cases} \{err_M\}_k < tol = 10^{-3} \\ trend\,(\{err_M\}_{k-30} \to \{err_M\}_k) \leq 0 \end{cases} \tag{4.68}$$

The reason for the first criterion is obvious. The second criterion however is not strictly necessary if the first one is already satisfied; nonetheless it is implemented to increase the confidence in the obtained solution (stable solution). Indeed, with plane EPSF method it had been observed that the error does not always decrease monotonically and is highly varying from one iteration to another (oscillating), such that it is not obvious to decide if it decreasing or increasing (see [Mut16]). In most cases, the second criterion will not be determinant, since the convergence of the proposed method is significantly more stable than for the plane EPSF method (see example in figure 4.10b).

Additionally, a divergence criterion is implemented that interrupts the computation if the error is such that no solution fulfilling the global equilibrium condition can be found. It is assumed that if the error exceeds the value of 2.0 during the last 20 iterations, the computation has diverged.

Depending on the number of iterations chosen to evaluate the stability of the convergence (for instance the 30 last iterations) a high number of computations might by necessary before the convergence criterion. In order to avoid an infinite loop, a maximum number of iterations is predefined by the user, typically $k_{max} \geq 250$.

The proposed number of iteration for convergence (30 last iterations) and divergence (20 last iterations) have led to stable and satisfying results for the investigated cases but might need to be adjusted depending on the complexity of the model or the computational speed. Nonetheless, the value of the final error, its evolution during the iterations and the global equilibrium of the model (reactions versus loads), should always be examined at the end of a computation.

Apart of the previous convergence criteria that is based on the residual forces, many other methods can be found in the literature. A common method is to examine the change in deformation (nodal displacements and rotations) from one iterations to the other, as for instance used by M.-A. Polak in [Pol93]. It has been tested with the proposed finite element method but it did not lead to substantial improvements in the results or in the convergence of the finite element problem.

4.5   Benchmark and validation

The verification of the proposed finite element method is performed in several steps: in-plane behaviour, out-of-plane behaviour in case of constant moment and in case of out-of-plane force and eventually a comparison to experimental results of reinforced concrete elements subjected to in-plane and out-of-plane loads.

Since the proposed multi-layered finite element method resides on the plane EPSF method, the in-plane behaviour of the two methods is identical. Thus to verify the implementation of the finite element code and to examine the solution algorithm, the numerical results of several reinforced concrete elements subjected to in-plane loads are compared to the plane EPSF predictions. No additional benchmark tests are performed to validate the in-plane behaviour because it has already been extensively investigated in the past ([Fer07, Mut16]).

The out-of-plane behaviour, under constant transverse bending and under out-of-plane shear load, is first verified by comparing the numerical results to simple benchmark problems for which analytical solutions are known. This study shows that the proposed method can be a little sensitive to modelling parameters such as the number of concrete layers, the element size and the meshing pattern. Some general recommendations for appropriate modelling are provided.

Eventually the behaviour of the proposed FEM is compared to experimental tests on the panel elements subjected to a combination of in-plane and out-of-plane loads.

4.5.1   Convergence and code verification

The code implementation and the solution procedure of the non-linear finite element method are validated by comparing the behaviour under in-plane load to the predictions provided by the plane EPSF method.

The validation is performed on reinforced concrete elements from the literature: six panel elements subjected to uniform in-plane load (pure shear, shear and compression, shear and tension) by Vecchio and Collins [Vec82] and two beams tested in three-point bending (beam A1 by Vecchio and Shim [Vec04] and beam N1-N by Yoon et al. [Yoo96]). These elements have been chosen to test the behaviour of FEM in case of uniform (panels) and non-uniform (beam) stress fields, as well as under different failure modes: ductile failures with yielding of reinforcement and non-ductile failure governed by crushing of concrete.

The main characteristics of the models are shown in figure 4.10a and table 4.1. In order to compare the results, the finite element models of the beams and panels are exactly identical (mesh, material, geometry) for both methods. In the multi-layer FEM, the ML-IP elements are modelled with 20 layers and the reinforcement is represented with its actual position in the element thickness. These are the only differences to FE models of the plane EPSF method.

The summary of the results in the table 4.1 shows that the predicted failure loads for the panel and beam elements are quasi identical and that the failure modes are consistent with the test observations. Only minor differences between the two methods are observed when comparing stresses and strains. They mainly result from the residual error in the model. Indeed, the proposed solution method generally leads to smaller residual errors (see following paragraph). But on the overall, the predicted stress fields are identical, thus the implemented FE code is working properly.

Since identical solutions are obtained with both methods, it can as well be concluded that the implemented solution algorithm for the non-linear FE problem is working correctly. The evolution of the error during the solution procedure confirms this. Indeed, in the case of uniform stress fields (panel elements) or for small loads (significantly smaller than the failure load) the FEM converges rapidly to a solution (error $< 10^{-4}$ within less than 50 iterations). When the load approaches the failure load, crushing of concrete or yielding of reinforcement yields larger deformations in the model and a higher number of iterations is required. It was as well observed that the method converges in a more stable manner as the plane EPSF method (see fig. 4.10b). This generally leads to smaller residual errors and greatly helps to predict whether a computation is diverging or converging, since the trend is clearly visible. The difference between the two methods mainly results from the way the stiffness matrix is computed and in particular from the assumption to use a secant stiffness approach for the force increments.

From the previous observation it can thus be concluded that the finite element code is implemented correctly and that the solutions procedure is efficient.

(a)

(b)
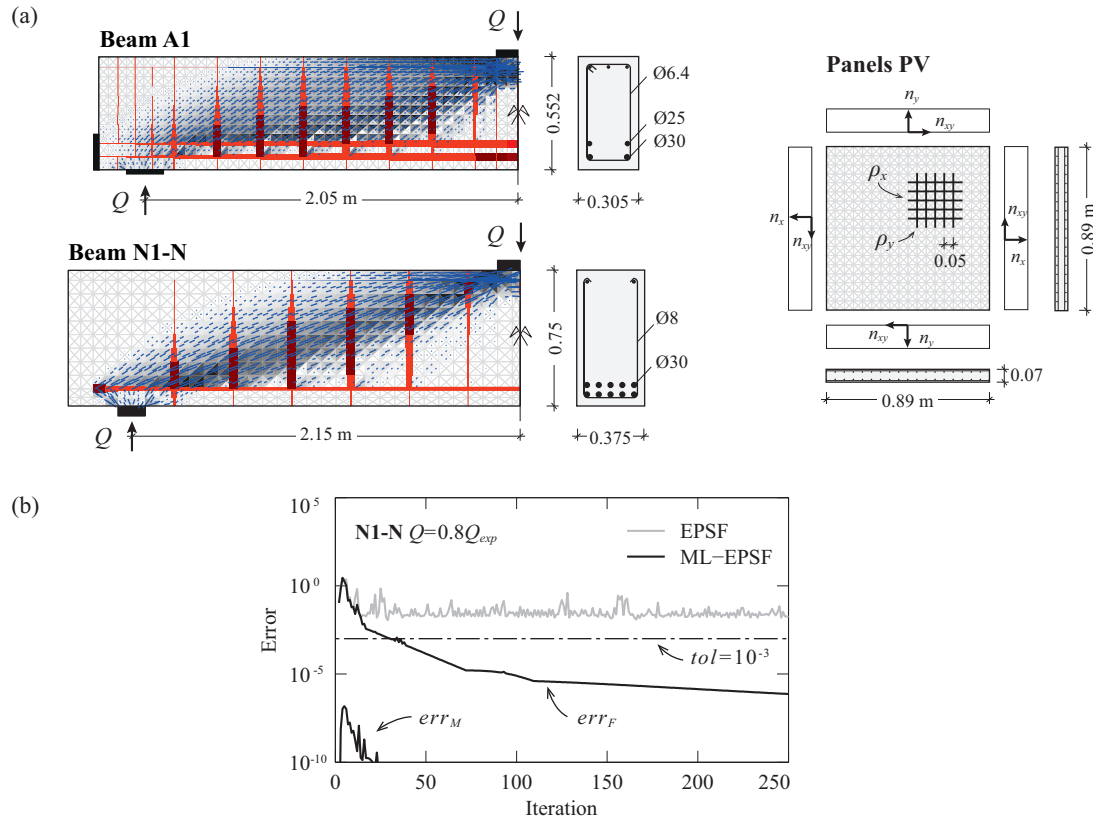
Figure 4.10 Validation of the ML-EPSF method for plane stress fields: (a) FE model and stress field for beam A1 [Vec04] at $Q_{exp}/Q = 0.95$, beam N1-N [Yoo96] at $Q_{exp}/Q = 1.07$ and panel elements PV [Vec82]; (b) convergence of the computation according to the plane EPSF and ML-EPSF method for beam N1-N for $Q = 0.8 \cdot Q_{exp}$.

Table 4.1 Resume of the failure load predictions according to the plane EPSF method Q_{EPSF} and the proposed multi-layer EPSF $Q_{ML-EPSF}$ for panels and beam subjected to in-plane loads and three-point bending.

Ref.	Specimen	Loading	Reinforcement		$\dfrac{Q_{exp}}{Q_{EPSF}}$	$\dfrac{Q_{exp}}{Q_{ML-EPSF}}$	failure mode
	Panel	$(n_{xy}; n_x; n_y)$	ρ_x [%]	ρ_y [%]			
	PV4	(1:0:0)	1.06		1.11	1.11	Y
	PV10	(1:0:0)	1.79	1.00	1.07	1.07	Y (y-dir.) + CS
[Vec82]	PV12	(1:0:0)	1.79	0.45	1.25	1.25	Y (y-dir.) + CS
	PV23	(1:-0.39:-0.39)	1.79		1.18	1.18	CS
	PV25	(1:-0.69:-0.69)	1.79		1.11	1.11	CS
	PV28	(1:0.32:0.32)	1.79		1.00	1.00	CS
	Beam		ρ_w [%]	ρ [%]			
[Vec04]	A1	3-pt. bending	0.1	1.94	0.94	0.95	SF
[Yoo96]	N1-N	3-pt. bending	0.08	2.8	1.06	1.07	DT

Y - yielding of reinforcement;   SF - shear flexural failure;
CS - concrete shear failure;   DT - diagonal tension.

4.5.2 Benchmark for out-of-plane behaviour

Since the proposed finite element method uses two types of finite elements to model the out-of-plane behaviour, the ML-IP element for bending and the OP element for shear, two distinct benchmark tests are performed to validate the behaviour of each of them. The ML-IP element is validated on an element with a constant moment and the OP element on an element with constant shear force and linearly varying moment.

Pure bending behaviour

The bending behaviour of the proposed finite element method is tested on a cantilever element with a concentrated moment at the end, figure 4.11. The sensitivity of the method to the element size, the number of layers in the concrete ML-IP elements and the element slenderness are examined by comparing the results to the analytical elastic solution.

The element size (mesh fineness M = 2 to M = 10) does not influence the results (fig. 4.11a-b), which is consistent with the expectations since the ML-IP element can exactly represent constant curvature deformations. Thus even a single row of elements (M = 1) would be sufficient in this case. Additionally, it is observed that the element thickness does not affect the results. Computations performed for a thick ($t/a = 0.3$) and a thin ($t/a = 0.03$) element lead to the exact same results, figure 4.11b.

Figure 4.11b shows the deflection at the cantilever end for different number of layers n_c. It can be seen that already for a small number ($n_c = 10$) the elastic prediction is very close to the analytical solution ($w_{max}/w_{a,max} = 1.01$). The numerical result converges rapidly to the exact solution when the number of layers is increased. In most situations the proposed finite element method will be used for reinforced concrete elements, in this case the influence of the number of concrete layers is even less important, see fig. 4.11b for $\rho_x = 0.5\%$.

The moment curvature diagram in figure 4.11c illustrates the non-linear behaviour of the cantilever. It can be overserved that the two regimes for uncracked behaviour and crack development, as typically observed for reinforced concrete elements, are not predicted by the finite element method. Instead, the initial bending stiffness is identical to the cracked stiffness. This behaviour results from the hypothesis that the concrete tensile strength is neglected, which leads to cracking of the cross section as soon as tensile strains appear. Another consequence of this hypothesis is that the tension stiffening effect can as well not be taken into account.

Close to the plastic bending strength, the moment-curvature diagram becomes non-linear as a consequence of the non-linear stress distribution in the concrete (upper layer start plastifying). With increasing curvature and eventual plastification of the reinforcement the expected plastic bending strength is reached.
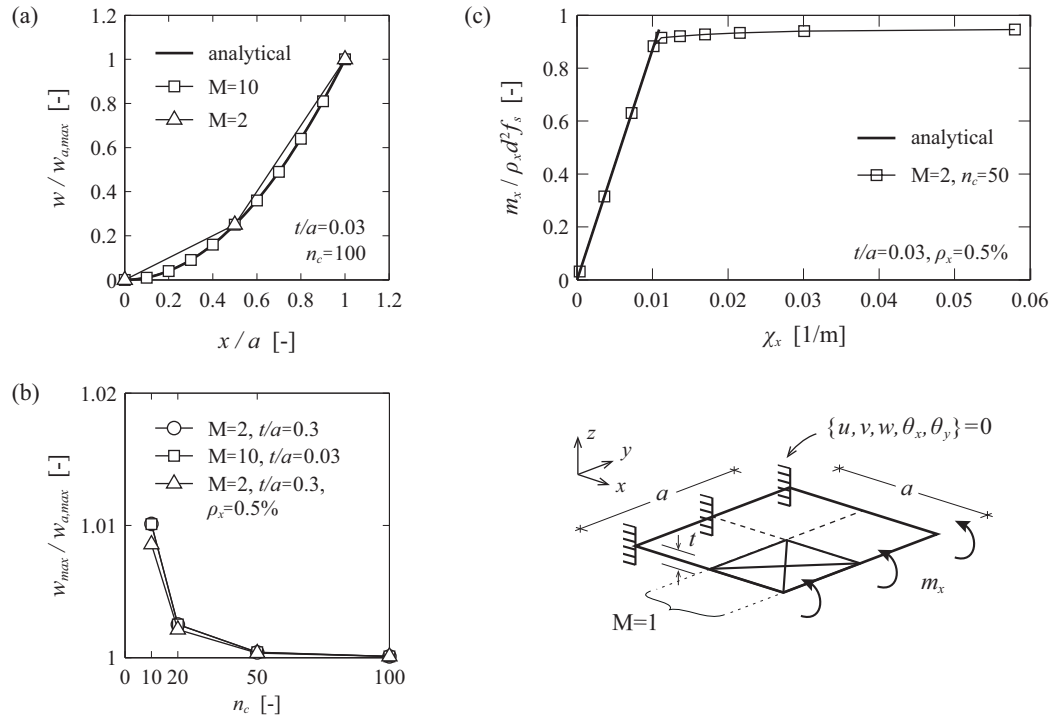
Figure 4.11 Behaviour of a reinforced concrete cantilever element subjected to a constant moment: (a) numerical and analytical solution for the elastic deflection; (b) convergence of maximum deflection as a function of the number of concrete layers and (c) moment-curvature diagram from non-linear FE analysis.

The finite element method is thus validated for cases of pure bending; the elastic and elastic-plastic behaviour of reinforced cantilever are correctly predicted. The element size does not affect the results and the number of concrete layers has only little influence. Nonetheless a minimum number of concrete layers should be used in order to obtain a representative stress distribution in concrete, especially for non-linear computations. In general, it was observed that for most cases 20 layers already lead to satisfying results.

Behaviour under out-of-plane loads and mesh sensitivity

The behaviour of the FEM under out-of-plane load is tested on a cantilever element with a uniform vertical load along the cantilever end as illustrated in figure 4.13. First, the global equilibrium and the reaction forces are investigated for different meshing patterns and element sizes. Then the element deformations are examined.

The global equilibrium of all the investigated cantilever elements is fulfilled, i.e. the computed nodal reaction forces and moments are in equilibrium with the applied vertical forces. Thus the combination of the multi-layer in-plane (ML-IP) element with the out-of-plane shear element (OP element) is behaving as expected and allows carrying out-of-plane loads by developing a bending-shear behaviour.
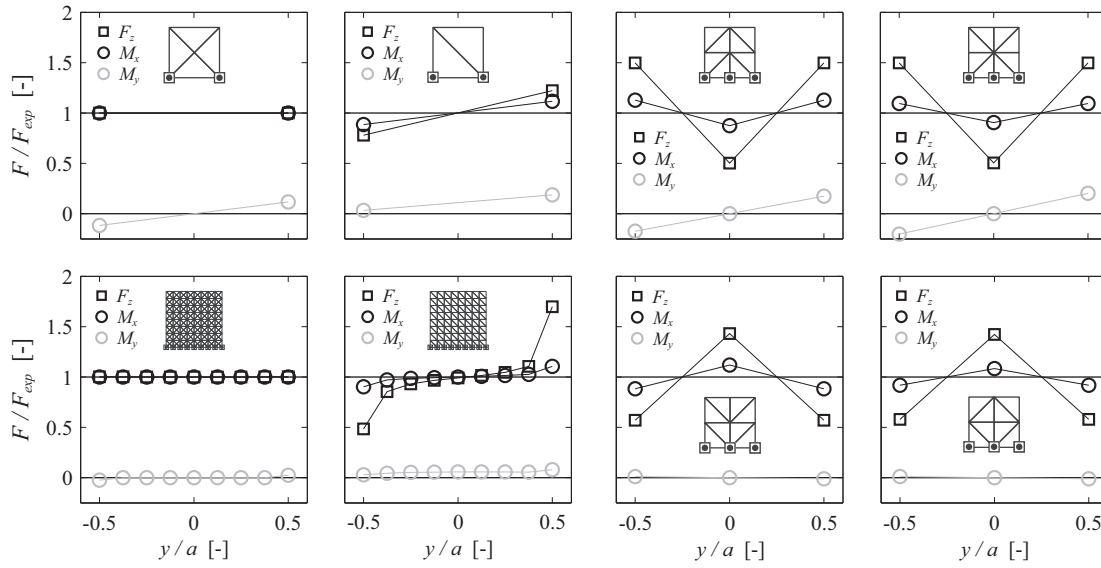
Figure 4.12 Distribution of the reaction forces along the support of cantilever element subjected to a uniform vertical load at the end. Influence of the meshing pattern, from left to right: cross shaped mesh, mesh with constant diagonals, mesh with converging and alternating diagonals.

The distribution of the reaction forces along the support of the cantilever is however dependent on the chosen meshing pattern, figure 4.12. Indeed, the meshing pattern directly influences the way the shear force is carried towards the support, because the OP shear elements that are placed along each segment of the triangular mesh can only carry the shear force in the direction of their axis. Thus, if the mesh has for instance diagonals with a preferential direction a certain amount of shear force will be deviated in this direction, which leads to a non-uniform distribution of the reactions forces (and stress resultants). This can for instance be seen in figure 4.12 (second column), where the reaction forces and moments increase in the direction indicated by the meshing pattern.

In case of meshes with converging or alternating diagonals, as for instance in figure 4.12 (third and fourth column), the distribution of the reaction force is significantly disturbed and not compliant with the expected results. These types of meshing patterns should be avoided in case of significant out-of-plane forces because the shear force is concentrated along certain axes, which could lead to unwanted and/or unpredictable behaviour, especially in case of non-linear computations.

The most reliable results are obtained for cross shaped meshes (square or rectangular mesh with two diagonals) as in figure 4.12 (first column). The mesh does not provide a preferential direction for the shear forces, thus the reaction forces F_z and reaction moments M_x are uniformly distributed along the support.

At the two corner nodes of the support, a transverse moment M_y appears. This moment is the projection of the axial moments M_s of the OP elements that are not perpendicular to the support. At the remaining nodes along the support $M_y = 0$ because two OP elements with opposition orientation are connected to each node such that the projections of their axial moments M_s compensate. Consequently, for non-symmetric meshes, the transvers moments M_y appears along the entire support line.
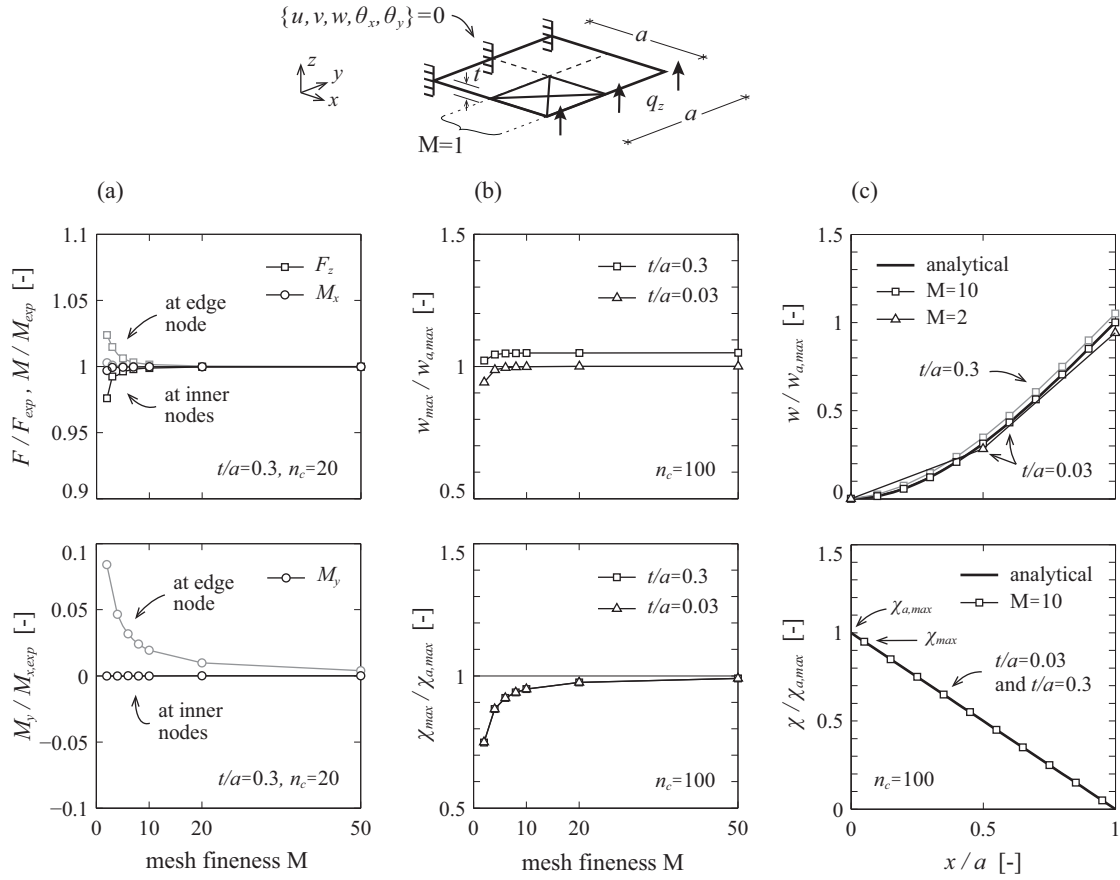
Figure 4.13a shows the influence of the mesh fineness (i.e. the element size) on the nodal reaction forces. The predicted nodal forces are normalized by the expected nodal forces assuming a uniform distribution. First, it can be seen that the reaction moments M_x are predicted very accurately, independently of the mesh fineness ($M/M_{exp} < 0.998$). The prediction for the vertical reaction forces F_z is a little less precise, but on the overall the error is small (very coarse mesh M=2: $F/F_{exp} \cong 0.975$) and the results rapidly tend to the expected values when the number of elements increases.

All the cantilever models predict a slight concentration of the reaction forces at the two corner nodes (fig. 4.13a). The error is of similar magnitude then for the central nodes and rapidly decreases with the element size ($F/F_{exp} \cong 1.001$ for M=10) so that the overall behaviour is not affected by this phenomenon. A similar observation can be made for the transverse moment M_y that localizes at the corner node; M_y is small compared to the main bending moment M_x and decreases rapidly with the element size.

In many practical cases it is not possible to create a regular mesh with symmetrical elements in both directions (complex formwork, reinforcement etc.). If the mesh is for instance refined in one direction, such that the width to height ratio of all the triangular finite elements in the model increases or decreased by a similar amount, the results are generally not affected by the distorted shape of the triangles. The precision can even increase since a mesh refinement usually leads to smaller elements size and higher number of elements and thus more exact estimates of the out-of-plane reactions forces. Nonetheless, as for the plane EPSF method, aspect ratios higher than 1:3 should possibly be avoided in order to ensure good behaviour of the FE model in non-linear computations [Mut16]. Furthermore, abrupt changes of the element aspect ratio between different regions should be avoided because this disturbs the distribution of the transverse shear force and by this the overall behaviour of the element. Especially in case of non-linear computations with out-of-plane shear forces sudden changes in the meshing pattern should be avoided.

As for the reaction forces, the precision of the predicted deflections and the deformations (curvature) improve with a finer mesh, figure 4.13b. The overall shape of deformed cantilever is well predicted if sufficient elements are used, see figure 4.13c. However, depending on the plate thickness t/a, the absolute value of the deformation can differ more or less significantly from the analytical value. Indeed, in the present example, the numerical deflection of a thin plate ($t/a = 0.03$) coincides well with the analytical value ($w_{max}/w_{a,max} =$

Figure 4.13 Influence of the mesh fineness M (element size $\propto 1/M$) and the element thickness (t/a) in case of a cantilever element subjected to a vertical load at the end: (a) vertical reaction forces F_z, main reaction moment M_x and transverse moment M_y; (b) maximum deflection and maximum curvature; (c) deflection and curvature along the cantilever axis.

0.999), which shows that the proposed FEM has no shear-locking problems (artificial stiffening of C^0-type elements when $t/a \to 0$). However, for a thick plate ($t/a = 0.3$) the maximum deflection at the cantilever end is overestimated by 5% compared to the analytical estimation.

Indeed, it is observed that the total shear deformation of the cantilever is significantly higher than analytically expected. Independently of the plate thickness, the shear deformation converges to $\gamma/\gamma_a = 2$ (sufficient mesh fineness), which leads to the conclusion that the approximated shear stiffness of the OP elements (GB in eqs. 4.44-4.45) is too small, thereby predicting higher deflections in thick elements (shear stiffness does not increase in the same proportion as bending stiffness when thickness increases). A more researched estimation of the shear stiffness could probably improve the predictions of the out-of-plane displacement. In the context of the present research it is however neglected since it has only

(a)   (b)   (c)
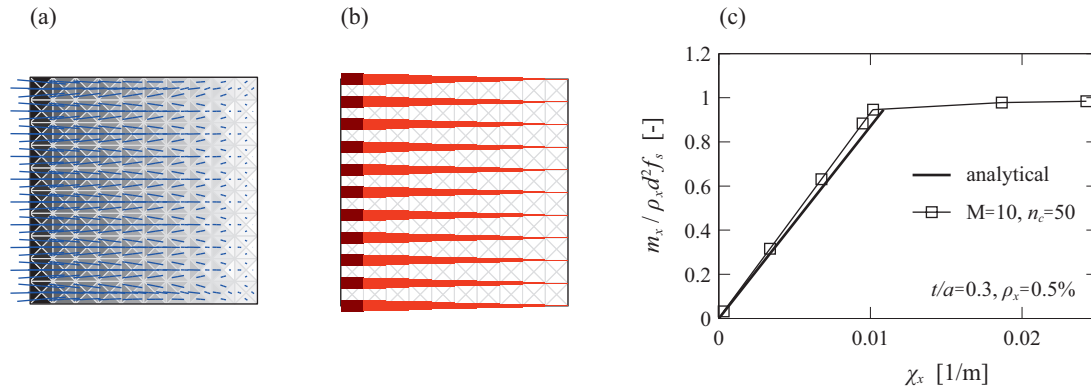
Figure 4.14 Reinforced cantilever element subjected to vertical load at the end: (a) EPSF with concrete crushing in the top layer and (b) yielding of the bottom reinforcement at ultimate failure load $q_{z,u} = 0.155$ MN/m; (c) moment-curvature diagram at the support.

little influence on the investigated behaviour that is governed by in-plane and bending deformations mainly.

The overestimated deflection for thick elements does not compromise the convergence of the curvature. As it can be seen in figure 4.13b, the element thickness has no influence of the predicted curvature that converges to the analytical value when the mesh fineness increases. For coarse meshes (M small) the maximum curvature is underestimated, which is normal because the ML-IP elements are constant curvature elements and can thus only represent the average deformation over the element length. In the present example the maximum analytical curvature, measured at the support ($x = 0$), is compared to the numerical curvature measured in the ML-IP element closest to the support, but which represents the average deformation of a segment of size ($\cong 1/M$). Consequently, the curvature obtained with FEM is smaller. But if the curvature is compared to the analytical value in the centre of the finite element ($x \cong 1/2M$) both curvatures coincides, as it can be observed in figure 4.13c showing the numerical and analytical curvature along the element axis. This shows that the FEM precisely predicts the average analytical curvature and that the precision of the finite element result only depends on the number of discretization points used to represent the actual behaviour. The fact that a good precision of the predicted curvature is obtained with the proposed FEM is essential to ensure adequate behaviour for non-linear computations (bending stiffness depends on the curvature).

The non-linear behaviour under out-of-plane forces is tested on the same cantilever element with a reinforcement ratio of $\rho_x = 0.5\%$. Failure occurred by yielding of the bending reinforcement (fig. 4.14b, dark red) and crushing of concrete (fig. 4.14a, black) close to the support. The failure load corresponding to the plastic bending strength of the cross section at the support is very well predicted: $q_{z,y}/q_{z,exp} = 1.00$ at the onset of yielding and $q_{z,u}/q_{exp} = 1.04$ at ultimate state (with steel hardening), the corresponding moment curva-

ture diagram is shown in figure 4.14c. It seems as if the FEM predicts a slightly stiffer behaviour, but this is rather a matter of representation. In fact, the curvature that is used is measured at the element centre, whereas the moment is measured at the support. If the curvature is linearly extrapolated from the element centre to the support ($\chi_x/(1 - 1/2M)$), the predicted bending stiffness is quasi identical to the analytical cracked bending stiffness ($EI/EI_a = 1.01$).
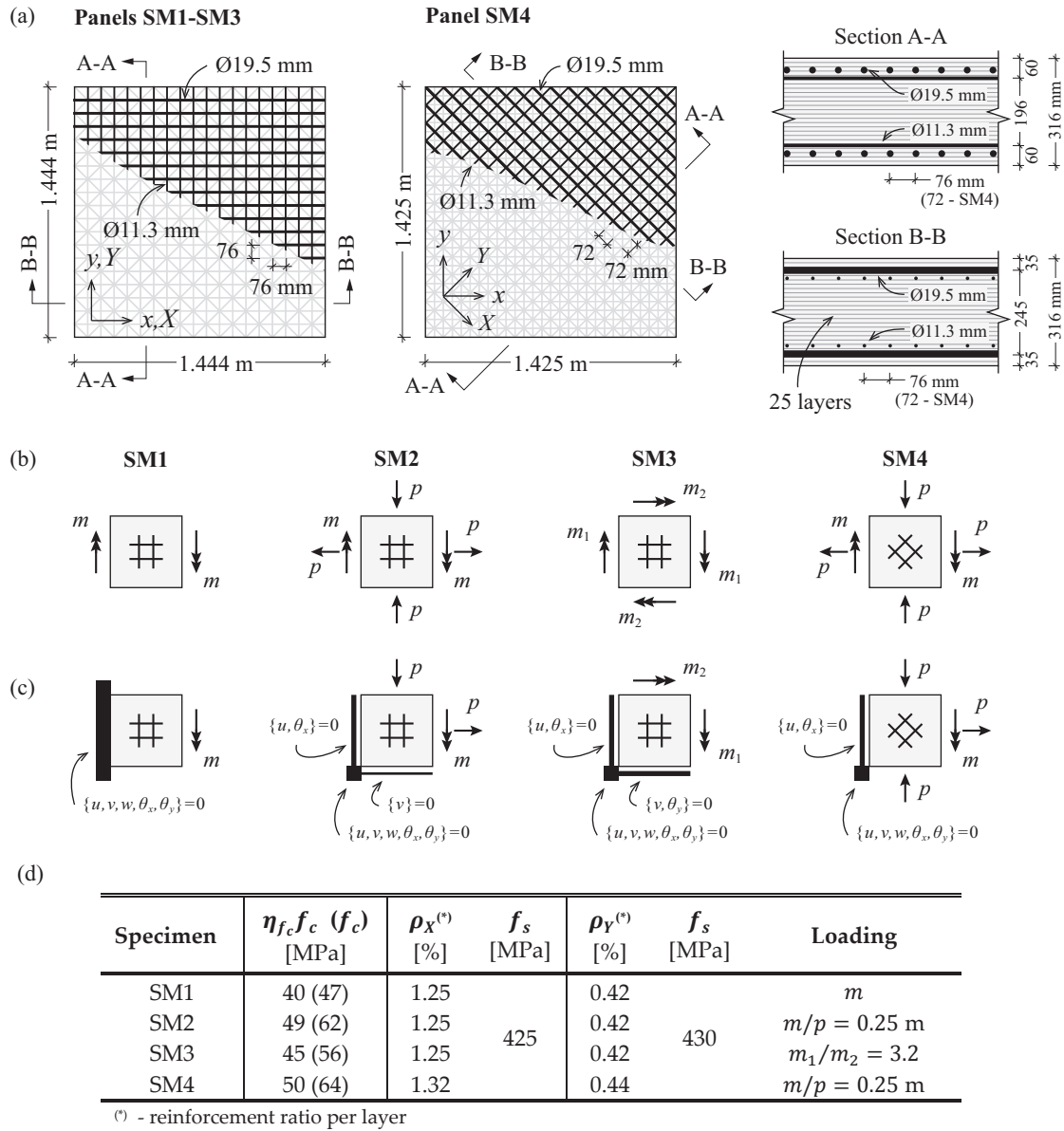
To sum up, it can be said that the proposed finite element method is as well validated for elements subjected to out-of-plane loads. On the overall, the elastic and elastic-plastic behaviour is well predicted. However, in case out-of-plane forces, the method is sensitive to the mesh pattern and element size, but gives goods results if a regular cross shape mesh and a sufficient number of finite elements is used. The element thickness (slenderness) affects the predictions for the out-of-plane deflections, but not the bending deformation (curvature) such that bending failure modes can be correctly assessed.

4.5.3 Validation with experimental tests

Previous benchmark tests showed that for simple elements the proposed FEM predicts the plastic bending strength as it is typically used in the plastic design approach. However, to further corroborate the FEM, its ability to represent the non-linear behaviour of real reinforcement concrete elements is investigated by comparison to experimental data from the literature.

To this purpose reinforced concrete shell elements subjected to combinations of biaxial bending and in-plane normal forces are investigated. At this state of the validation processes only elements without out-of-plane shear force are investigated. This load case, that is typical for shell structures, has however only be scarcely investigated in the past so that the number of available experimental data is very limited.

A test series of four large-scale panel elements performed by Polak and Vecchio [Pol94] to study the effect of the reinforcement orientation and the presence of in-plane forces on the out-of-plane flexural behaviour is chosen to test the ML-EPSF method. A schematic representation of the orthogonally reinforced concrete elements is given in figure 4.15a. In panels SM1 to SM3, the reinforcement was placed parallel to the panel edges, whereas in panel SM4 it was placed with an angle of 45° to the edges. The loading cases were such that forces were uniform throughout the panels and the in-plane and bending loads where applied in a constant ratio, see figure 4.15b,d. Specimen SM1 was tested in pure uniaxial bending, specimens SM2 and SM4 in uniaxial bending coupled with biaxial in-plane forces and specimen SM3 in pure biaxial bending. The bending and tension forces are applied in-line with strong reinforcement direction (x-direction), except for panel SM4. For specimens SM1, SM2 and SM4 at the ultimate moment, the loading was terminated due to excessively large deformations but without any apparent signs of concrete crushing. In case of specimen SM3 a bending failure with yielding and concrete crushing in the direction of the higher

(a)

(b)

(c)

(d)

Specimen	$\eta_{fc}f_c$ (f_c) [MPa]	$\rho_X^{(*)}$ [%]	f_s [MPa]	$\rho_Y^{(*)}$ [%]	f_s [MPa]	Loading
SM1	40 (47)	1.25		0.42		m
SM2	49 (62)	1.25	425	0.42	430	$m/p = 0.25$ m
SM3	45 (56)	1.25		0.42		$m_1/m_2 = 3.2$
SM4	50 (64)	1.32		0.44		$m/p = 0.25$ m

$^{(*)}$ - reinforcement ratio per layer

Figure 4.15 Modelling of Polak's [Pol94] four shell elements under combined biaxial in-plane loads and bending: (a) ML-EPSF finite element model; (b) loading patterns; (c) modelled boundary conditions and (d) material and loading parameters.

moment appeared. The skewed reinforcement layout of the specimen SM4 led to an appreciably more non-linear behaviour as for the specimens with in-line reinforcement. Additionally significant force redistributions and crack reorientations were observed throughout the loading.

The geometrical and material properties of the finite element models are summarized in figure 4.15a-d. The concrete is modelled with ML-IP elements of 25 layers and the elastic-plastic constitutive law for concrete in compression uses the effective compressive strength

$f_{cp} = \eta_{f_c} f_c$ (eq. 2.23, where f_c is the measured compressive cylinder strength) in order to ensure ductile behaviour of the high strength concrete. The reinforcement is modelled with its respective yielding strength and actual position in the depth of the element (four layers). The non-linear finite element analyses are performed for several loads levels until the ultimate load is reached.

Table 4.2 compares the predicted and observed moments at the onset of yielding of the reinforcement in x and y direction and the ultimate bending moments. Generally the yielding moments correlate very well, with a mean experimental-to-numerical value of 1.02 and a coefficient of variation of 0.01. The corresponding stress fields are shown in figure 4.17. The ultimate moment capacities are somewhat underestimated (average: 1.12), especially for the two specimens with in-plane forces (SM2 and SM4). Note that in most cases the maximum deformation of the concrete in compression (ε_{cu}) is governing the ultimate moment predictions. However, only for element SM3 (biaxial bending) concrete crushing was actually observed during testing.

The limitation of the deformation of concrete is a choice that has been made to identify failure modes due to crushing of concrete. Indeed, in the proposed FEM excessively high concrete deformations can appear without that the computation diverges. This situation appears especially in cases of uniaxial or biaxial compression where the transverse strains are zero or negative. In this cases the concrete strength reduction factor is always equal to one so that the effective concrete compressive strength does not decrease ($\varepsilon_1 \leq 0 \rightarrow \eta_\varepsilon = 1$), even for very high axial deformations (elastic-perfectly plastic constative law, no concrete softening). Thus, in order to exclude solutions that might be in equilibrium with the applied loads but that have unrealistically high deformations, a maximum allowable concrete compressive deformation was fixed. In the present case it is set to $\varepsilon_{cu} = 3‰$, which is proposed by code recommendations for concrete in bending (SIA262 [SIA13]) and is in agreement with the concrete compressive tests performed during the experimental campaign by

Table 4.2   Resume and comparison of predicted and experimental yielding and failure loads for panel tests performed by Polak and Vecchio [Pol94].

Specimen	Experimental [kNm/m]		Predicted [kNm/m]		Exp. / Pred. Ratio [-]	
	m_y	m_u	m_y	m_u	m_y	m_u
SM1	437	477	429	465[*]	1.02	1.03
SM2	302	421	284	337[*]	1.06	1.25
SM3-X	435	488	429	478[*]	1.01	1.02
SM3-Y	138	151	137	149	1.01	1.01
SM4-X	160	205	160	160	1.00	1.28
SM4-Y	116		115		1.01	
				mean	1.02	1.12
				COV	0.01	0.12

[*] - failure when outermost concrete layer reached ultimate deformation $\varepsilon_{cu} = 3‰$
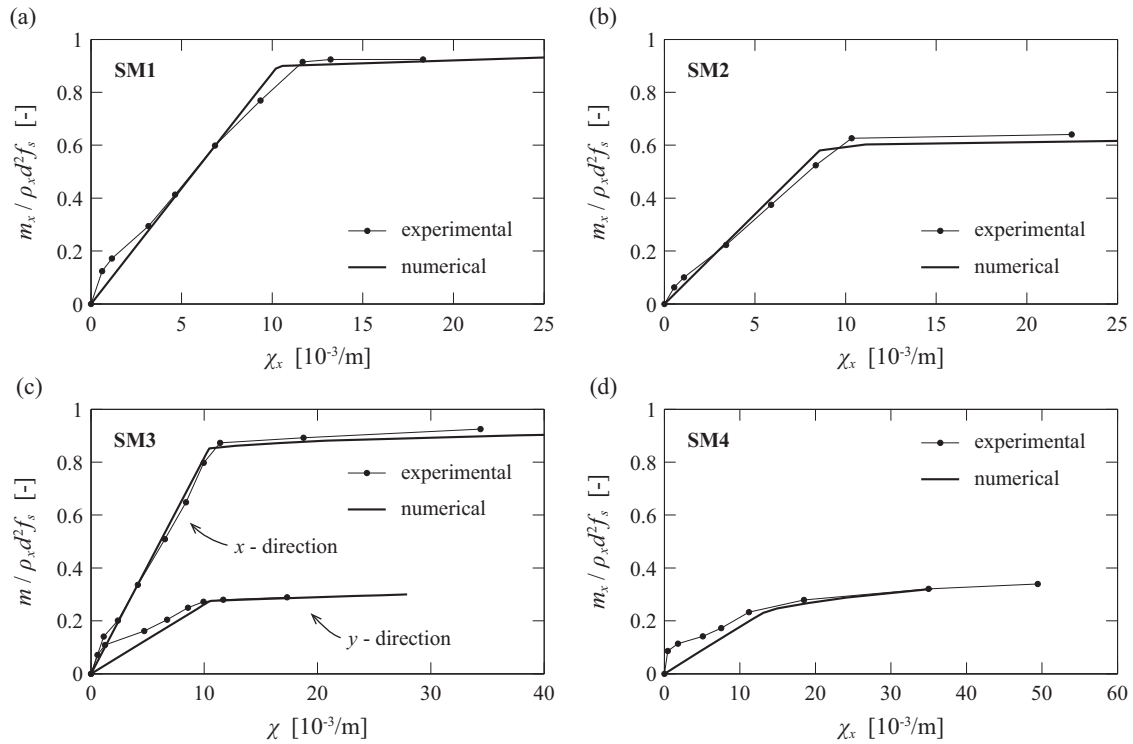
Figure 4.16 Comparison of experimental and numerical moment-curvature responses of four shell elements under combined biaxial in-plane loads and bending moments by Polak and Vecchio [Pol94]: (a) panel SM1, pure uniaxial bending; (b) panel SM2, uniaxial bending with biaxial in-plane forces; (c) panel SM3, pure biaxial bending and (d) panel SM4, uniaxial bending with biaxial in-plane forces and skew-directional reinforcement.

Polak and Vecchio [Pol94].

Consequently, loading was stopped when the ultimate deformation was reached in one of the concrete layers (generally the outermost layer on the bending compression side). In the case of panels SM1 to SM3 this condition was the determining factor. If higher concrete deformation were accepted, the finite element model can be loaded up to the experimental failure load. Compared to the experimental observations, where no concrete crushing was observed (SM1 and SM2), this assumption is maybe a little too unfavourable, but it leads to safe estimates of the ultimate bending moment for all of the investigated cases.

Other factors might be contributing to the difference observed at the ultimate load. Extremely large deformations levels were applied in the test (several times greater than the yield limit) such that affects from strain hardening and the testing facility on the experimental results cannot be excluded. Furthermore, it is difficult to simulate the same boundary condition in the finite element model as those of the shell element tester. In some cases (especially for SM4) this leads to perturbations of the stress field in the regions of the load introduction and the supports, see figure 4.17. These local perturbations of the stress field

might induce an anticipated failure when the panel element enters a highly non-linear regime caused by biaxial yielding of the reinforcement on the bending tension side. Especially in the case of the panel SM4, this seems to be the main reason why the element cannot be loaded beyond the point where yielding of the second reinforcement occurs.

A more representative comparison of the numerical and experimental responses is made in the moment-curvature diagrams in figure 4.16. On the overall a very good correlation can be seen in the post-cracking and post-yielding phases. The actual behaviour in the pre-cracking phase cannot be predicted with the proposed method since the tensile strength of concrete is neglected. Consequently, the bending stiffness in this phase already corresponds to the cracked bending stiffness.

For all the panel elements, the predicted cracked bending stiffness is very close to the experimental stiffness. Note that even for the panel SM4, where significant tension stiffening and load redistribution where measured, the overall behaviour is very well predicted by the FEM. Of course the tension stiffening effect cannot be accounted for in the model because the tensile strength of concrete is neglected. This leads to higher deformations in the crack formation phase, but once yielding of the reinforcement occurs, the actual behaviour is well predicted.

Due to the reinforcement that is rotated by 45° to the loading direction in panel SM4, significant crack rotations were observed during the loading procedure. Just prior to yielding of the weak reinforcement (y-direction), the cracks were rotated by 8° from the direction of the applied tensile force. After yielding, the crack rotations became much more prominent. A very similar observation is made with the ML-EPSF method, if we assume that the crack direction can be approximated by the direction of the first principal strain (tensile strength being neglected and assuming that principal strain directions coincide with the principal stress directions, the crack direction is normal to the direction of the first principal strain). On average the predicted principal strain direction was rotated by 9° prior to yield and then increased up to 17° at the onset of yielding of the stronger reinforcement (x-direction), which correlates very well with the experimental observations.

On the overall, it is found that the proposed non-linear finite element method models accurately the response of shell elements subjected to a combination of biaxial in-plane and bending loads. The yielding moments are predicted with good accuracy and safe estimates were obtained for the ultimate moments.

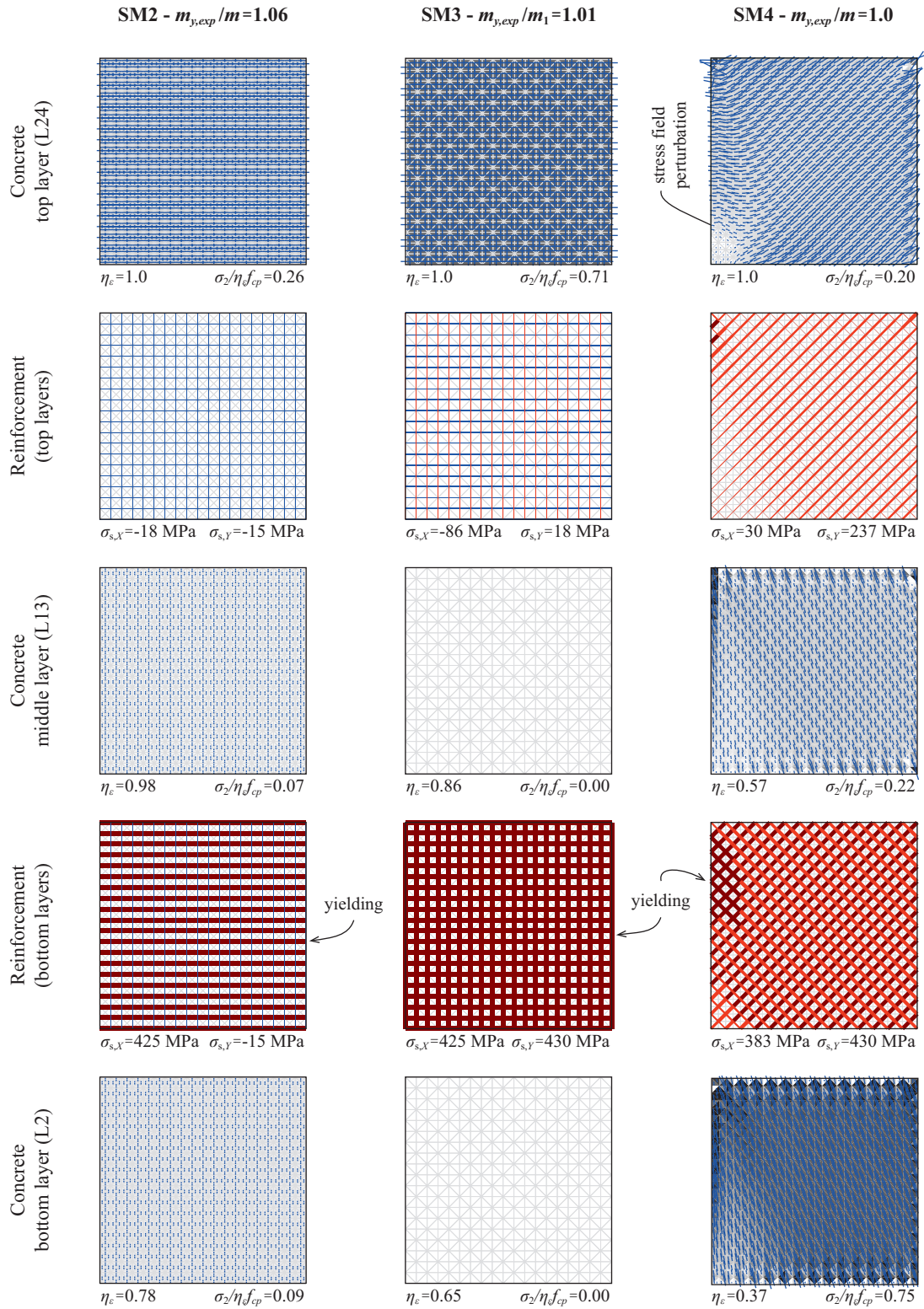**Figure 4.17** ML-EPSF predictions for Polak's panels [Pol94] at the onset of yielding of the strong reinforcement direction (ρ_X): Stress field in the concrete for top, middle and bottom layers as well as top and bottom reinforcement layers.

4.5.4 Synopsis

A summary of the main observations and findings made during the testing of the proposed multi-layered elastic-plastic stress field finite element method is presented hereafter:

- The finite element code and the solution procedure are correctly implemented and the convergence of the non-linear computations is stable.

- The non-linear behaviour of structural elements subjected to only in-plane loads is correctly assessed and sensitively identical to the plane EPSF predictions.

- The non-linear behaviour of shell elements under combined biaxial in-plane and bending loads is predicted with high accuracy, capturing load redistributions and crack rotations. Excellent estimates of the yielding moments and safe estimates of the ultimate moments are obtained.

- A simple benchmark test on a cantilever element with an out-of-plane load showed that the combination of the ML-IP elements with the OP elements successfully transfers the internal shear and bending forces to the support. On the overall, the elastic and elastic-plastic behaviour was consistent with the analytical solutions.

- For out-of-plane loads, the deflection is slightly influenced by the slenderness of the finite elements. However, no effect on the bending deformation (curvature) is observed, such that bending failure modes can be correctly assessed.

- In case of out-of-plane shear loads the method is sensitive to the mesh pattern and element size but provides good results if a regular cross shape mesh and a sufficient number of finite elements are used.

- Little influence of the number of concrete layers on the overall behaviour is observed. A minimum of 20 layers should though be used to obtain a representative stress profile in the concrete, especially in case of non-linear computations.

On the overall it can be said that the proposed non-linear finite element method gives good predictions for the behaviour of reinforced elements subjected to in-plane loads and combinations of in-plane and out-of-plane bending loads. Acceptable predictions are obtained in case of out-of-plane loads on simple elements, if an appropriate meshing pattern is chosen and the ultimate load is governed by a bending failure.

More extensive testing of the FEM is required to validate its correct behaviour in case of more complex structural elements and load configurations. In particular, the behaviour under non-uniform stress fields, as in beams with transverse bending in the web, and elements with out-of-plane shear loads (slabs) has to be analysed.

Nonetheless, the fact that precise and safe estimates of the yield and ultimate moments can be obtained while making conservative assumptions for the concrete compressive strength and the admissible deformations (according to code recommendations) shows that the proposed ML-EPSF finite element method is a promising tool for the design of reinforced concrete elements subjected to the combined action of in-plane forces and out-of-plane bending moments.

Chapter 5 Conclusion

In the present thesis several applications of the elastic-plastic stress field (EPSF) method to investigate plane reinforced concrete elements subjected to in-plane and out-of-plane actions are developed and special attention was payed to the interaction of in-plane shear and transverse bending in beam webs.

5.1 Summary and conclusions

To establish consistent stress fields for combined membrane and transverse bending actions, a multi-layered EPSF (ML-EPSF) approach is established. It allows overcoming certain limitations of former models by providing static and kinematic compatible solutions that respect the plastic condition of the material and that lead to a licit mechanism at failure. Simultaneously it provides a detailed insight into the stress field that develops under the influence of a transverse bending moment, such as the distribution of concrete stresses, their inclination and the effective concrete compressive strength over the element thickness. Additionally it accounts for the non-linear dependencies between concrete and reinforcement in the forces transfer action.

1) Based on the ML-EPSF approach a sectional analysis tool to investigate the in-plane shear transverse bending interaction in beam webs has been developed. The ML-EPSF panel element allowed for a detailed analysis of the phenomenological behaviour of the stress field, to identify parameters that play a major role in the overall interaction mechanism as well as to establish explicit interaction diagrams for the assessment of the ultimate resistance.

2) Observations on the interaction mechanism that develops in a web segment led to propose a simplified verification method for beam elements in practice. The proposed method uses the plane EPSF finite element method by Fernández Ruiz and Muttoni [Fer07] that predicts well the actual in-plane (longitudinal) behaviour of structural elements. The influence of transverse bending moment is considered in a simplified manner.

3) The need for a consistent representation of the in-plane and out-of-plane static and kinematic behaviour of entire structural elements (internal forces redistributions between web and flanges, along the longitudinal axis) led to develop a more general tool. The proposed non-linear finite element method (NL-FEM) for plane reinforcement concrete elements is based on the ML-EPSF approach and accounts for

117

in-plane (normal and shear) and out-of-plane (bending and shear) actions. The NL-FEM allows studying the in-plane shear transverse bending interaction mechanism on the structural element level and provides exact solutions according to the theory of plasticity for in-plane and out-of-plane bending failure modes.

The following paragraphs present a brief summary of the achieved results and main conclusions of the work.

In-plane shear transverse bending interaction in beam webs

By means of the ML-EPSF it could be shown that the actual effect of transverse bending moment on the in-plane shear resistance of beam webs is less pronounced than predicted by rigid-plastic (RP) models. Especially in the range of small transverse moments, which is probably the most important range in practical applications, it was observed that the shear resistance is significantly less affected. The model confirmed as well the general concept of the force transfer actions assumed in former models, which are that the compression field in the web shifts towards the bending compression side and that additional bending resistance is activated by rearranging stirrup forces from the bending compression side to tension side. Additionally, Menn's assumption [Men86] of a pure bending compression zone on the outermost face of the web in case of predominant transverse bending actions could be confirmed. However, the multi-layered analysis also points out that the assumption of a constant stress field is a strong simplification of the actual behaviour. Indeed, it could be shown that the stress field is highly non-linear in the transverse direction (stress distribution, inclination, concrete strength reduction factor) and that it strongly depends on the intensity of the applied transverse moment, which is not considered in the RP models. In particular, it could be observed that the bending compression, apart from causing additional compression in the concrete, has as well a positive effect on the stress field inclination (↗) and the effective concrete compressive strength (↗) which reduces the loss of shear resistance caused by the transverse moment.

In general, the ML-EPSF analysis allowed observing that the concrete strength reduction factor η_ε plays a major role for the combined in-plane shear transverse bending resistance and that the RP interaction models make very conservative assumptions regarding this parameter. Indeed, the predicted reduction factors are generally higher, for pure shear but as well for moderate transverse bending moments, which sensitively increases the predicted shear resistance in these cases. Furthermore, the variable nature of the reduction factor (a function of the transverse strain) and the kinematic compatibility conditions of the ML-EPSF model allow establishing a continuous transition between pure in-plane shear and pure transverse bending behaviour, an issue encountered in most former models.

Parameters that are found to have a decisive influence on the overall interaction mechanism are the amount of shear reinforcement and the longitudinal deformation. High shear reinforcement ratios, such that $V_{R,s} > V_{R,c}$, lead to a plateau in the interaction diagram indi-

cating that small transverse bending moments have almost no influence on the shear re-sistance. Indeed, it could be shown that in these situations, due to the reserve capacity of the shear reinforcement, small moments can be carried by changes in the stirrup forces only, while the stress field in the concrete is barely disturbed. Similar observations are made for asymmetric shear reinforcement layouts ($\rho_{w,t} \neq \rho_{w,c}$). The longitudinal defor-mation ε_x, which is an input parameter for the ML-EPSF analysis (not considered in RP models), has a non-negligible effect on the overall interaction. It is observed that a smaller axial deformation, like for instance in prestressed elements, reduces the sensitivity of the shear resistance to the transverse bending moment.

Simplified plane EPSF verification method for beam elements with transverse bending moments

The proposed simplified verification method provides safe estimates of the bearing capaci-ty of beams subjected to transverse bending moments in the web and is conceived for engi-neers in practice that are already familiar with EPSF finite element analysis. The advantage of this method, compared to the previous sectional analysis tool is that it directly accounts for the actual non-linear in-plane behaviour of the element, including redistribution of in-ternal forces, local yielding etc. Additionally, the method does not require making assump-tions on the stress field inclination and the concrete strength reduction factor, which are obtained automatically. The method combines kinematic and static consistent stress fields for in-plane actions with an equilibrium based approach to consider the effect of a trans-verse bending moment in the web. The obtained predictions can thus be considered as en-hanced lower bound solutions of the longitudinal bearing capacity.

The validation by means of a comparison to experimental tests performed by Kaufmann and Menn [Kau76] showed that the method leads to safe but not overly conservative esti-mates of the failure loads ($Q_{exp}/Q = 1.17$). Failure modes are as well consistently predicted. The simplified verification method tends to be more conservative when failure due to con-crete crushing is to be expected, as well as for higher transverse bending moments (light tendency). For the investigated beams ([Kau76]) the method predicts an average reduction of the bearing capacity of 7% in case of ductile failure modes (yielding of shear reinforce-ment) and 25% when the concrete is governing. This indicates that the method might re-quire some improvement, but more comparisons to experimental data are required to con-firm the these observations.

Influence of transverse bending moments in beam elements

Investigations of the failure load of experimental beam elements ([Kau76]) by means of the plane EPSF lead to suggest that the effect of the transverse moment on the longitudinal bearing capacity of beams is almost negligible. This seems to be especially true for elements with ductile failure modes and sufficient redistribution capacity in the transverse direction of web (shift of the compression field and rearrangement of the stirrup forces), where an

average ratio of $Q_{exp}/Q_{EPSF} = 1.04$ was observed. Elements for which concrete failure is to be expected showed a small influence of the transverse moment on the bearing capacity, $Q_{exp}/Q_{EPSF} = 0.98$. The analysis led to suggest that there are internal force redistributions that develop in the non-linear regime (between web and flanges, along the element axis) which significantly contribute to counterbalance the effect of the transverse bending moment on the stress field and thereby reduce the influence on the longitudinal bearing capacity.

It can thus be concluded that in beam elements the effect of the transverse bending moment is less pronounced than what would be expected according sectional analysis tools. It must however be noted that previous observations are based on a very small number of experiments and that more comparisons and test data are required in order to confirm if and under which conditions the influence of a transverse bending moment in beams could indeed be almost neglected.

Regarding the proposed analysis tools, it can thus be said that the ML-EPSF panel element provides valid and valuable information at a local level, this is however not always representative of the overall behaviour of the entire structural element. The simplified verification method in return is able to account for redistributions at the structural level (the entire beam is modelled), but the effect of the transverse bending moment is considered on a similar basis as in sectional analysis tools and thus the method provides rather conservative predictions.

Non-linear finite element method

The aim to extend the field of application of the elastic-plastic stress fields and the need for an appropriate tool to investigate the actual effect of transverse bending on the bearing capacity of beams led to develop a non-linear finite element method for in-plane and out-of-plane actions on reinforced concrete elements. This includes the development of three new finite elements, the finite element program with pre- and post-processing tools as well as a solution procedure for the non-linear problem. As in the plane EPSF FEM, concrete and steel are modelled by separate finite elements. The multi-layered in-plane (ML-IP) element for concrete is based on the ML-EPSF approach and is used in combination with out-of-plane (OP) shear elements in order to account for transverse shear forces. Reinforcing steel is modelled by special bar elements that account for the actual position of the rebar in the element width.

The validation of the proposed NL-FEM with respect to experimental test data showed that the non-linear behaviour of shell elements under in-plane loads and combinations of in-plane loads and out-of-plane bending moments is predicted with high accuracy, capturing load redistributions and crack rotations. Excellent estimates of yielding moments and ultimate loads are obtained. Regarding the behaviour in case of out-of-plane loads, elastic and

elastic-plastic analyses of a simple structural element provided good predictions, if an appropriate meshing pattern is chosen and the ultimate load is governed by a bending failure.

It can be concluded that the proposed non-linear ML-EPSF finite element method is a promising tool for the design as well as for the assessment of plane reinforced concrete elements that are primarily subjected to combinations of in-plane forces and out-of-plane bending moments. More extensive testing of the FEM is though required to validate the behaviour in case of more complex structural elements and load configurations.

5.2   Outlook for future research

To further develop the stress field methods in general and the proposed EPSF approaches in particular, as well as to improve the knowledge about the behaviour of beam-like elements subjected to out-of-plane actions the following topics could be of interest for future researches:

- The analysis of experimental tests on beams with transverse bending moments showed that panel elements (numerical or experimental) are not always suitable for modelling the actual behaviour of the structural element. However, test on entire structural elements or beam-like elements with combined in-plane and out-of-plane actions are extremely scarce in the literature. More experimental data on structural elements are needed to assess the level of safety of the presently used and the proposed assessment approaches as well as to get a clearer picture of the actual interaction. The influence of following parameters should be studied more in detail: amount of shear reinforcement ρ_w, asymmetric shear reinforcement $\rho_{w,c}/\rho_{w,t}$, transverse moment ratio m/m_{R0}, varying transverse moment over the web height, web slenderness, influence of flanges, influence of prestressing and ducts.

- Analyses performed on Kaufmann's beams ([Kau76]) showed that elements with brittle failure modes are probably more sensitive to the influence of the transverse bending moment. Such situations are frequently encountered in the verification of older existing structures, in particular box-girder bridges, that have high levels of longitudinal prestressing and low shear reinforcement ratios. The longitudinal bearing capacity of such elements can often only be verified by means of refined analysis tools such as the EPSF method that yields stress fields with very low inclinations, but which simultaneously leads to potential brittle failure modes. It thus might be useful to study if such elements still have sufficient deformation capacity to account for the influence of the transverse bending moment and to what extent their longitudinal bearing capacity is affected by the latter.

- The proposed simplified verification method for beams with transverse bending moments in the web leads to conservative estimates, especially in case of high concrete solicitations due to shear. The method could be improved by accounting for

the mostly beneficially effect of the transverse bending compression. It would increase the average stress field inclination and the effective concrete compressive strength, which would lead to a less severe web width reduction Δb_w and thereby increase the predicted bearing capacity of the elements. This could for instance be achieved by applying, in the finite element model, vertical compression forces that represent the bending compression on the top and the bottom of the web.

- Interaction of in-plane shear and transverse bending moments does not only occur in beam webs, but for instance as well in the deck slab of box-girder bridges. In the vicinity to the connection with the web, the slab is simultaneously subjected to a significant out-of-plane bending moment resulting from the external loads and to in-plane shear induced by bearing function of the web. Tests on panel elements by Polak [Pol94] showed that membrane actions can have significant influence on the bending resistances. Experiments on compression and tension flanges ([Bad77, Bac79, Eib88, Sch85]) showed as well non-negligible influence of the transverse bending moment on the in-plane shear resistance of these elements. It would thus be of interest to study the in-plane shear transverse bending interaction in these elements by means of the proposed refined analysis tool. The ML-EPSF finite element method provides large flexibility for the element geometries and model parameters and has shown to provide good results, especially in case of combined in-plane and out-of-plane bending actions.

- Further validations of the proposed ML-EPSF finite element method in case of out-of-plane actions (especially shear) are still required and might lead to enhance the assumptions on the out-of-plane concrete finite element. This could be particularly interesting for ongoing research on the behaviour of flat slabs on linear or punctual supports subjected out-of-plane loads, for which an accurate estimation of the cracked bending and shear stiffness is important to correctly assess internal force redistributions that influence on the bearing capacity.

- The proposed ML-EPSF finite element has been developed to investigate reinforced concrete elements by means of a two-dimensional representation of the geometry (in-plane). It could also be considered to extend the method to model the actual three-dimensional geometry of structural elements that are composed of several plane elements with different orientations in space.

References

[Arg14]   **Argirova G., Fernández Ruiz M., Muttoni A.** *How simple can nonlinear finite element modelling be for structural concrete?*, Informes de la Construcción, Vol. 66, 8 p., Spain, December, **2014**.

[Bac79]   **Bacchetta A., Bachmann H.** *Versuche über Längsschub, Querbiegung und Quervorspannung in Zugplatten von Betonträgern*, Institut für Baustatik und Konstruktion ETH Zürich, Birkhäuser Verlag Basel Boston Stuttgart, N° 6504-10, 127 p., Zürich, Switzerland, November, **1979**.

[Bac14]   **Backes M.-R., Fernández Ruiz M., Muttoni A.** *Interaction between in-plane shear forces and transverse bending moments in concrete bridge webs*, Proc. of the 10th *fib* International PhD Symposium in Civil Engineering, Quebec, pp. 403-408, Canada, **2014**.

[Bad77]   **Badawy M., Bachmann H.** *Versuche über Längsschub und Querbiegung in Druckplatten von Betonträgern*, Institut für Baustatik und Konstruktion ETH Zürich, Birkhäuser Verlag Basel und Stuttgart, N° 6504-8, 124 p., Zürich, Switzerland, June, **1977**.

[Bel95]   **Belarbi A., Hsu C.-T. T.** *Constitutive laws of softened concrete in biaxial tension-compression*, ACI Structural Journal, Vol. 92, No. 5, pp. 562-573, USA, September-October, **1995**.

[Cam13]   **Campana S.** *Éléments en béton armé soumis à une combinaison de flexion, effort tranchant et forces de déviation*, EPFL, IBETON, Thèse N. 5574, 162 p., Lausanne, Switzerland, janvier, **2013**.

[CEB76]   **Comité Euro-International du Béton (CEB)** *Code modèle pour les structures en béton*, Système international de réglementation technique unifiée des structures, Vol. II, Bulletin d'Information, No. 117, Paris, December, **1976**.

[CEN05]   **European Committee for Standardization (CEN)** *Eurocode 2: Design of concrete structures - Part 2: Concrete bridges*, 103 p., Brussels, Belgium, October, **2005**.

References

[Coo79]   **Cookson P. J.** *A general yield criterion for orthogonally reinforced concrete slab elements*, IABSE Colloquium - Plasticity in reinforced concrete, Vol. 29, pp. 43-50, Zürich, Switzerland, **1979**.

[Dru61]   **Drucker D. C.** *On structural concrete and the theorems of limit analysis*, IABSE International Association for Bridge and Structural Engineering, IABSE-Reports 21, Zürich, Switzerland, **1961**.

[Eib88]   **Eibl J.** *Die Flanschbemessung von Plattenbalken bei Schub und Querbiegung*, Beton - und Stahlbetonbau, Vol. 83, Heft 5, pp. 127-132, Berlin, Germany, **1988**.

[Ewa77]   **Ewald G.** *Überlagerung von Scheiben- und Plattentragwirkung am Beispiel stark profilierter Stahlbeton- und Spannbetonträger bei hoher Schub- und begrenzter Querbiegebeanspruchung*, Institut für Bauingenieurwesen III, Technische Universität München, 211 p., Munich, Germany, **1977**.

[Fan95]   **Fanti G., Mancini G.** *Ultimate limit state design of structural concrete shell elements*, CEB Bulletin d'Information, No. 223, pp. 167-207, Lausanne, Switzerland, June, **1995**.

[Fer07]   **Fernández Ruiz M., Muttoni A.** *On development of suitable stress fields for structural concrete*, ACI, Structural Journal, Vol. 104 n°4, pp. 495-502, Farmington Hills, USA, July-August, **2007**.

[Fer08]   **Fernández Ruiz M., Muttoni A.** *Shear strength of thin-webbed post-tensioned beams*, ACI Structural Journal, V. 105 No 3, pp. 308-317, USA, May-June, **2008**.

[FIB13]   **Fédération International du Béton (FIB)** *fib Model code for concrete structures 2010, 434 p., Ernst & Sohn, Germany, 2013*.

[Fre01]   **Frey F., Jirousek J.** *Méthode des éléments finis (TGC volume 6) - Analyse des structures et milieux continues*, Presses Polytechnique et Universitaires Romandes, 298 p., Lausanne, Suisse, **2001**.

[Gas03]   **Gaspar R.** *Dimensionamento das almas de pontes celulares*, Tese - Escola Politécnica, University of São Paulo, 250 p., Brazil, **2003**.

[Gas13]   **Gaspar R., Stucchi F. R.** *Web design of box girders concrete bridges*, Engineering structures, 57, pp. 267-275, **2013**.

[Gio99]   **Giordano L., Mancini G., Napoli P., Recupero A.** *Shear-transverse bending interaction in the webs of R.C./P.R.C. box bridges*, First International Conference on Advances in Structural Engineering and Mechanics, pp. 943-948, Seoul, Korea, August, **1999**.

[Kau76]   **Kaufmann J., Menn C.** *Versuche über Schub bei Querbiegung*, Institut für Baustatik und Konstruktion ETH Zürich, Birkhäuser Verlag Basel und Stuttgart, N° 7201-1, 92 p., Zürich, Switzerland, December, **1976**.

[Kau98]   **Kaufmann W.** *Strength and deformations of structural concrete subjected to in-plane shear and normal forces*, IBK report, 234, 147 p., Zürich, Switzerland, July, **1998**.

[Kir86]   **Kirschner U.** *Investigating the behaviour of reinforced concrete shell elements*, PhD Dissertation, 83 p., Toronto, Canada, June, **1986**.

[Kos09]   **Kostic N.** *Topologie des champs de contraintes pour le dimensionnement des structures en béton armé*, Thèse EPFL, N° 4414, 235 p., Lausanne, Switzerland, **2009**.

[Kup73]   **Kupfer H., Ewald G.** *Überlagerung von Scheibenschub und Plattenbiegung im Spannbetonbrückenbau, Versuchsergebnisse an dem Träger V I/68*, Technische Universität München, Institut für Bauingenieurwesen III, Lehrstuhl für Massivbau, ca. 250 Bl., Munich, Germany, **1973**.

[Lou95]   **Lourenço P. B., Figueiras J. A.** *Solution for the design of reinforced concrete plates and shells*, Journal of Structural Engineering, Vol. 121, Issue 5, pp. 815-823, May, **1995**.

[Mar80]   **Marti P.** *Zur plastischen Bemessung von Stahlbeton*, ETH, Dissertation Nr. 6602, 176 p., Zürich, Switzerland, November, **1980**.

[Mar90]   **Marti P.** *Design of concrete slabs for transverse shear*, ACI Structural Journal, Vol. 87 No 2, pp. 180-190, Detroit, USA, March - April, **1990**.

[MAT13]   **MATLAB Release 2013b**, The MathWorks, Inc., Natick, Massachusetts, United States.

[Men86]   **Menn C.** *Stahlbetonbrücken*, Springer-Verlag, Wien, New York, 533 p., **1986**.

[Min51]   **Mindlin R. D.** *Influence of rotatory inertia and shear on flexural vibration of isotropic, elastic plates*, Journal of Applied Mechanics, 18, pp. 31-38, **1951**.

References

[Mut90]   **Muttoni A.** *Die Anwendbarkeit der Plastizitätstheorie in der Bemessung von Stahlbeton*, Birkhäuser Verlag, Institut für Baustatik und Konstruktion ETH Zürich, 176 p., Basel, Switzerland, **1990**.

[Mut97]   **Muttoni A., Schwartz J., Thürlimann B.** *Bemessung von Betontragwerken mit Spannungsfeldern*, Birkhäuser Verlag, 145 p., Basel, Switzerland, **1997**.

[Mut15]   **Muttoni A., Fernández Ruiz M., Niketic F.** *Design versus assessment of concrete structures using stress fields and strut-and-tie models*, ACI Structural Journal, V. 112 No 5, pp. 605-616, Farmington Hills, USA, September-October, **2015**.

[Mut16]   **Muttoni A., Fernández Ruiz M., Nikétic F., Backes M.-R.** *Assessment of existing structures based on elastic-plastic stress fields – Modelling of critical details and investigation of the in-plane shear transverse bending interaction*, OFROU Report, 131 p., Bern, Switzerland, **2016**. (in press)

[Nie11]   **Nielsen M. P., Hoang L. C.** *Limit analysis and concrete plasticity. 3rd Edition.*, CRC Press, 788 p., Boca Raton, USA, **2011**.

[Ona09]   **Oñate E.** *Structural analysis with the finite element method. Linear statics - Vol.1 : Basis and solids*, Springer-CIMNE, 472 p., **2009**.

[Ona13]   **Oñate E.** *Structural analysis with the finite element method. Linear statics - Vol.2 : Beams, plates and shells*, Springer-CIMNE, 864 p., **2013**.

[Pol93]   **Polak M. A., Vecchio F. J.** *Non-linear analysis of reinforced-concrete shells*, ASCE Journal of Structural Engineering, Vol. 119, No. 12, pp. 3439-3462, December, **1993**.

[Pol94]   **Polak M. A., Vecchio F. J.** *Reinforced concrete shell elements subjected to bending and membrane loads*, ACI Structural Journal, Vol. 91, No. 3, pp. 261-268, May, **1994**.

[Pop73]   **Popovics S.** *A numerical approach to the complete stress-strain curve of concrete*, Cement and Concrete Research, 3, pp. 583-599, USA, **1973**.

[Rei45]   **Reissner E.** *The effect of transverse shear deformation on the bending of elastic plates*, ASME Journal of Applied Mechanics, 12, pp. A69-77, **1945**.

[Rup14]   **Rupf M.** *Querkraftwiderstand von Stahlbeton- und Spannbetonträgern mittels Spannungsfeldern*, EPFL, IBETON, Thèse N° 6004, 132 p., Lausanne, Switzerland, **2014**.

[Sch85] **Schieferstein M.** *Der Zugflansch von Stahlbetonplattenbalken unter Längsschub und Querbiegung bei kritischer Druckbeanspruchung des Betons*, 191 p., Karlsruhe, Germany, **1985**.

[See09] **Seelhofer H.** *Ebener Spannungszustand im Betonbau : Grundlagen und Anwendungen*, Diss. Eidgenössische Technische Hochschule (ETH) Zürich, Nr. 18486, 247 pp., Zürich, Switzerland, **2009**

[SIA76] **Swiss Society of Engineers and Architects** *SIA 162/34: Résistance à la rupture et dimensionnement des structures en béton armé et en béton précontraint*, SIA, 14 p., Zürich, Switzerland, **1976**.

[SIA89] **Swiss Society of Engineers and Architects** *SIA 162 – Betonbauten*, SIA, Zürich, Suisse, **1989**.

[SIA13] **Swiss Society of Engineers and Architects** *SIA 262 - Betonbau*, Schweizerischer Ingenieur- und Architektenverein, 102 p., Zurich, Switzerland, **2013**.

[Stu90] **Stucchi F. R., Borges L. A.** *Dimensionamento das almas de vigas celulares*, 2. Simpósio EPUSP de estruturas de concreto , pp. 359-401, São Paulo, Brasil, **1990**.

[Swa75] **Swann R. A.** *Distortional bending in the web of prestressed concrete beams*, Magazine of Concrete Research, Vol. 27, pp. 239-244, December, **1975**.

[Tes85] **Tessler A., Hughes T. J. R.** *A three-node Mindlin plate element with improved transverse shear*, Computer Methods in Applied Mechanics and Engineering, Vol. 50, pp. 71-101, **1985**.

[Thü77] **Thürlimann B.** *Schubbemessung bei Querbiegung*, Schweizerische Bauzeitung, Vol. 95, Heft 26, pp. 478-481, Switzerland, **1977**.

[Vec82] **Vecchio F. J., Collins M. P.** *Response of reinforced concrete to in-plane shear and normal stresses*, Department of civil engineering, University of Toronto, Publication No. 82-03, 332 p., March, **1982**.

[Vec86] **Vecchio F. J., Collins M. P.** *The modified compression-field theory for reinforced concrete elements subjected to shear*, ACI Journal, Vol. 83, No. 2, pp. 219-231, USA, March - April, **1986**.

[Vec94] **Vecchio F. J., Collins M. P., Aspiotis J.** *High-strength concrete elements subjected to shear*, ACI, Structural Journal, 91, pp. 423-433, Farmington Hills, USA, July, **1994**.

References

[Vec04]   **Vecchio F. J., Shim W.** *Experimental and analytical investigation of classic concrete beam tests*, Journal of Structural Engineering, 130, 9, USA, 03., **2004**.

[Wag29]   **Wagner H.** *Ebene Blechwandträger mit sehr dünnem Stegblech*, Zeitschrift für Flugtechnik und Motorluftschiffahrt, V. 20, pp. 200-207, 227-233, 256-262, 279-284, 306-314, **1929**.

[Yoo96]   **Yoon Y.-S., Cook W. D., Mitchell D.** *Minimum shear reinforcement in normal, medium and high-strength concrete beams*, ACI, 93, 9, USA, 10., **1996**.

Appendix A Rigid-plastic stress fields

This appendix presents the formulas used for the calculation of the shear strength of beams by means of rigid-plastic stress fields with and without transverse bending moments presented in Chapter 2.

A.1   Shear strength according to SIA262

In SIA262 [SIA13] the shear strength of reinforced concrete beams is determined based on the rigid-plastic stress field presented above. The shear strength of the concrete strut $V_{R,c}$ and the strength of the shear reinforcement $V_{R,s}$ are defined as follows:

$$V_{R,c} = k_c \cdot f_{cp} \cdot b_w \cdot z \cdot \sin\theta \cdot \cos\theta \tag{A.26}$$

$$V_{R,s} = f_s \cdot \rho_w \cdot b_w \cdot z \cdot \cot\theta \tag{A.27}$$

The inclination of the compression field θ is recommended to be chosen between $30°(25°) \leq \theta = 45°$. The concrete strength reduction factor k_c accounts for the effect of transverse strain (cracking) on the compressive strength of the concrete strut. Generally, $k_c = 0.55$ can be assumed, if no yielding of the longitudinal reinforcement is expected in the investigated section. In case of a refined analysis, k_c can as well be determined on the basis of the web deformation [SIA13].

A.2   Normalization factors

A.2.1 Shear resistance V_{R0}

The plastic strength of the compression strut and the yielding strength of the reinforcement are reached simultaneously for a compression field inclination of θ_0. $V_{R0} = V_{R,c} = V_{R,s}$ is the corresponding shear resistance.

$$V_{R0} = f_s \cdot \rho_w \cdot b_w \cdot z \cdot \sqrt{\frac{k_c \cdot f_{cp}}{f_s \cdot \rho_w} - 1} \tag{A.28}$$

$$\sin^2\theta_0 = \frac{f_s \cdot \rho_w}{k_c \cdot f_{cp}} \tag{A.29}$$

For conventional reinforcement ratios, V_{R0} is the maximum shear resistance of the beam.

A.2.2 Plastic transverse bending strength m_{R0}

The transverse bending strength m_{R0} of the web cross section is defined as follows:

$$m_{R0} = f_s \cdot \rho_{w,t} \cdot b_w \cdot \left(b_w - b' - \frac{f_s \cdot \rho_{w,t} \cdot b_w}{2 \cdot f_{cp}} \right) \tag{A.30}$$

Where $\rho_{w,t} = A_{sw,t}/(b_w \cdot s)$ is the shear reinforcement ratio on the bending tension side of the web and b' the position of the reinforcement in the width of the web.

A.3 Shear transverse bending interaction by Thürlimann, adapted according to SIA262:2013

This section shows how the author adapted the original interaction formula for in-plane shear and transverse bending by Thürlimann [Thü77] (presented in section 2.1.3) in order to conform the definition of the shear resistance according to SIA262 [SIA13].

The minimum web width b_e required to resist the shear force V can be expressed as follows:

$$\frac{b_e}{b_w} = \frac{V}{k_c \cdot f_{cp} \cdot b_w \cdot z \cdot \sin\theta \cdot \cos\theta} \tag{A.31}$$

The inclination of the compression field can be expressed as a function of the stirrup force per unit length that is defined by $R = (f_s \cdot \rho_{w,t} \cdot b_w)/\zeta$ in Thürlimann's model.

$$\tan\theta = \frac{z \cdot R}{V} = \frac{f_s \cdot \rho_{w,t} \cdot b_w \cdot z}{\zeta \cdot V} \tag{A.32}$$

Using the trigonometric relationship $\cos\theta \sin\theta = \tan\theta/(1 + \tan^2\theta)$, the equation A.32 can be substituted in equation A.31 such that:

$$\frac{b_e}{b_w} = \frac{1}{k_c \cdot f_{cp} \cdot \zeta \cdot \rho_{w,t} \cdot f_s} \cdot \frac{(\zeta \cdot V)^2 + \left(f_s \cdot \rho_{w,t} \cdot b_w \cdot z \right)^2}{(b_w \cdot z)^2} \tag{A.33}$$

The adapted $(m - V)$ interaction model is then obtained by replacing the expression for b_e/b_w in Thürlimann's orginial formulation.

$$m = m_s + m_c$$

$$= \left(F_{s,t} - F_{s,c} \right) \cdot \left(\frac{b_w}{2} - b' \right) + R \cdot \left(\frac{b_w}{2} - \frac{b_e}{2} \right) \tag{A.34}$$

$$= \frac{\rho_{w,t} \cdot b_w^2 \cdot f_s}{2\zeta}$$

$$\cdot \left\{ (2\zeta - 1) \cdot \left(1 - \frac{2b'}{b_w} \right) \right.$$

$$\left. + \left[1 - \frac{\rho_{w,t} \cdot f_s}{\zeta \cdot k_c \cdot f_{cp}} \cdot \left[\left(\frac{\zeta \cdot V}{\rho_{w,t} \cdot f_s \cdot z \cdot b_w} \right)^2 + 1 \right] \right] \right\}$$

Appendix B   Multi-layered in-plane finite element

The appendix presents some additional information and explicit expressions regarding the finite element formulation of the multi-layered in-plane concrete element presented in Chapter 4.

B.1   Discretized displacement field

This section presents the explicit expressions and matrix formulations of the generalised membrane, bending and shear strains.
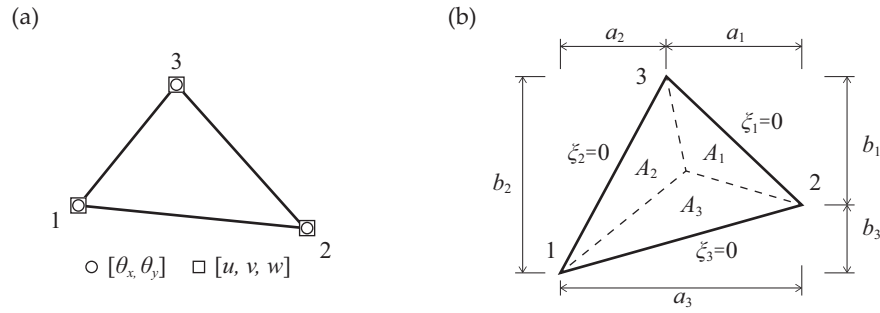
Figure B.**1**   The three node Mindlin-type finite element: (a) nodal degrees of freedom and (b) area coordinates of the triangular element.

The interpolated displacement fields $\mathbf{u} = \left[u(x,y), v(x,y), w(x,y), \theta_x(x,y), \theta_y(x,y)\right]^T$ defined in Chapter 4 are expressed in matrix format:

$$\mathbf{u} = \sum_{i=1}^{3} \mathbf{N}_i \mathbf{a}_i^{(e)} = [\mathbf{N_1}, \, \mathbf{N_2}, \, \mathbf{N_3}] \begin{Bmatrix} \mathbf{a}_1^{(e)} \\ \mathbf{a}_2^{(e)} \\ \mathbf{a}_3^{(e)} \end{Bmatrix} = \mathbf{N}\mathbf{a}^{(e)} \tag{B.1}$$

$$\mathbf{N}_i = \begin{bmatrix} N_i & 0 & 0 & 0 & 0 \\ 0 & N_i & 0 & 0 & 0 \\ 0 & 0 & N_i & L_i & M_i \\ 0 & 0 & 0 & N_i & 0 \\ 0 & 0 & 0 & 0 & N_i \end{bmatrix} \quad ; \quad \mathbf{a}_i^{(e)} = \left[u_i, v_i, w_i, \theta_{xi}, \theta_{yi}\right]^T \tag{B.2}$$

where $\mathbf{a}_i^{(e)}$ is the displacement vector and $\mathbf{N}_i$ the shape function matrix at node i.

N_i are linear shape functions defined by the area coordinates of a triangle (ξ_1, ξ_2, ξ_3 with $\xi_i = A_i/A^{(e)}$, see fig. B.1) and $\bar{N}_i$ are quadratic shape functions vanishing at the corners:

$$N_i = \xi_i = \frac{1}{2A^{(e)}}(a_i + b_i x + c_i y) \quad ; \quad \bar{N}_i = 4\xi_i\xi_j; \tag{B.3}$$

$$L_i = \frac{1}{8}(\bar{N}_i c_k - \bar{N}_k c_j) \quad ; \quad M_i = \frac{1}{8}(\bar{N}_k b_j - \bar{N}_i b_k) \tag{B.4}$$

with $a_i = x_j y_k - x_k y_j$, $b_i = y_j - y_k$, $c_i = x_k - x_j$ for $i = 1,2,3$; $j = 2,3,1$; $k = 3,1,2$ and the element area $A^{(e)} = [x_1(y_2 - y_3) + x_2(y_3 - y_1) + x_3(y_1 - y_2)]/2 = [x_1 b_1 - x_2 b_2 + x_3 b_3]/2$.

B.2   Explicit expression for the generalized strains

Substituting the previous displacement fields into the expression for the generalized strains yields

$$\hat{\varepsilon} = \begin{Bmatrix} \hat{\varepsilon}_m \\ \cdots \\ \hat{\varepsilon}_b \\ \cdots \\ \hat{\varepsilon}_s \end{Bmatrix} = \begin{Bmatrix} \varepsilon_{x0} \\ \varepsilon_{y0} \\ \gamma_{xy0} \\ \cdots \\ \chi_x \\ \chi_y \\ 2\chi_{xy} \\ \cdots \\ \gamma_{xz} \\ \gamma_{yz} \end{Bmatrix} = \begin{Bmatrix} u_{,x} \\ v_{,y} \\ u_{,y} + v_{,x} \\ \cdots\cdots\cdots \\ \theta_{x,x} \\ \theta_{y,y} \\ \theta_{x,y} + \theta_{y,x} \\ \cdots\cdots\cdots \\ w_{,x} - \theta_x \\ w_{,y} - \theta_y \end{Bmatrix} = \sum_{i=1}^{3} \begin{Bmatrix} N_{i,x}u_i \\ N_{i,y}v_i \\ N_{i,y}u_i + N_{i,x}v_i \\ \cdots\cdots\cdots \\ N_{i,x}\theta_{xi} \\ N_{i,y}\theta_{yi} \\ N_{i,y}\theta_{xi} + N_{i,x}\theta_{yi} \\ \cdots\cdots\cdots \\ N_{i,x}w_i + (L_{i,x} - N_i)\theta_{xi} + M_{i,x}\theta_{yi} \\ N_{i,y}w_i + L_{i,y}\theta_{xi} + (M_{i,y} - N_i)\theta_{yi} \end{Bmatrix} \tag{B.5}$$

$$= \sum_{i=1}^{3} \mathbf{B}_i \mathbf{a}^{(e)} = [\mathbf{B}_1, \mathbf{B}_2, \mathbf{B}_3] \begin{Bmatrix} \mathbf{a}_1^{(e)} \\ \mathbf{a}_2^{(e)} \\ \mathbf{a}_3^{(e)} \end{Bmatrix} = \mathbf{B}\mathbf{a}^{(e)}$$

Where $\mathbf{B}$ and $\mathbf{B}_i$ are the element and nodal generalized strain matrices. The later can be expressed in terms of membrane, bending and shear contributions:

$$\mathbf{B}_i = \begin{Bmatrix} \mathbf{B}_{mi} \\ \mathbf{B}_{bi} \\ \mathbf{B}_{si} \end{Bmatrix} \tag{B.6}$$

$$\mathbf{B}_{mi} = \begin{bmatrix} N_{i,x} & 0 & 0 & 0 & 0 \\ 0 & N_{i,y} & 0 & 0 & 0 \\ N_{i,y} & N_{i,x} & 0 & 0 & 0 \end{bmatrix} \quad ; \quad \mathbf{B}_{bi} = \begin{bmatrix} 0 & 0 & 0 & N_{i,x} & 0 \\ 0 & 0 & 0 & 0 & N_{i,y} \\ 0 & 0 & 0 & N_{i,y} & N_{i,x} \end{bmatrix}$$

$$\mathbf{B}_{si} = \begin{bmatrix} 0 & 0 & N_{i,x} & L_{i,x} - N_i & M_{i,x} \\ 0 & 0 & N_{i,y} & L_{i,y} & M_{i,y} - N_i \end{bmatrix} \tag{B.7}$$

Explicit expressions for the generalized strain matrices are obtained when substituting the shape functions according to equations B.3 and B.4:

$$\mathbf{B}_{mi} = \frac{1}{2A^{(e)}} \begin{bmatrix} b_i & 0 & 0 & 0 & 0 \\ 0 & c_i & 0 & 0 & 0 \\ c_i & b_i & 0 & 0 & 0 \end{bmatrix} \quad ; \quad \mathbf{B}_{bi} = \frac{1}{2A^{(e)}} \begin{bmatrix} 0 & 0 & 0 & b_i & 0 \\ 0 & 0 & 0 & 0 & c_i \\ 0 & 0 & 0 & c_i & b_i \end{bmatrix}$$

(B.8)

$$\mathbf{B}_{si} = \frac{1}{2A^{(e)}} \begin{bmatrix} 0 & 0 & b_i & \#1 & \#2 \\ 0 & 0 & c_i & \#3 & \#4 \end{bmatrix}$$

where

$$\#1 = 2A^{(e)}\left(L_{i,x} - N_i\right) = \left[\frac{1}{2A^{(e)}}\left(b_i b_j c_k - b_i b_k c_j\right) - b_i\right] x$$
$$+ \left[\frac{1}{4A^{(e)}}\left(b_j c_i c_k - b_k c_i c_j\right) - c_i\right] y$$
$$+ \frac{1}{4A^{(e)}}\left(a_i b_j c_k - a_i b_k c_j + a_j b_i c_k - a_k b_i c_j\right) - a_i$$

$$\#2 = 2A^{(e)}M_{i,x} = \frac{1}{4A^{(e)}} b_i\left(b_j c_k - b_k c_j\right) y - \frac{1}{4A^{(e)}} b_i\left(a_j c_k - a_k b_j\right)$$

$$\#3 = 2A^{(e)}L_{i,y} = \frac{1}{4A^{(e)}} c_i\left(b_j c_k - b_k c_j\right) x + \frac{1}{4A^{(e)}} c_i\left(a_j c_k - a_k b_j\right)$$

$$\#4 = 2A^{(e)}\left(M_{i,y} - N_i\right) = \left[\frac{1}{4A^{(e)}}\left(b_i b_j c_k - b_i b_k c_j\right) - b_i\right] x$$
$$+ \left[\frac{1}{2A^{(e)}}\left(b_j c_i c_k - b_k c_i c_j\right) - c_i\right] y$$
$$+ \frac{1}{4A^{(e)}}\left(a_i b_j c_k - a_i b_k c_j - a_j b_k c_i + a_k b_j c_i\right) - a_i$$

If $A^{(e)}, a_i, b_i$ and c_i are expressed in terms of the nodal coordinates x_i, y_i, expression #1 and #4 yield linear functions on y and x respectively. Thus the shear deformation $\gamma_{xz} = f(y)$ is constant in x direction and the transverse shear deformation $\gamma_{yz} = f(x)$ is constant in y direction.

B.3 Derivation of the tangential transverse shear deformation γ_{sz}

The transverse shear deformation γ_{sz} along the borders of the ML-EP element is required to compute the transverse shear force in the OP element. It is derived from the transverse displacement field w and the rotation fields θ_x and θ_y that are first evaluated along the k-th element side with the nodes i and j ($\xi_k = 0$) and then expressed as function of the tangential directions s of k-th element side.

From $w = \sum_{i=1}^{3} N_i w_i + \frac{1}{8}\sum_{k=1}^{3} \bar{N}_i l_{ij}\left(\theta_{si} - \theta_{sj}\right); \; \theta_x = \sum_{i=1}^{3} N_i \theta_{xi}; \; \theta_y = \sum_{i=1}^{3} N_i \theta_{yi}$ we get:

$$w_{ij} = w\left(\xi_i, \xi_j = 1 - \xi_i, \xi_k = 0\right) = \xi_i w_i + (1 - \xi_i)w_j + \frac{1}{2}\xi_i(1 - \xi_i)l_{ij}\left(\theta_{si} - \theta_{sj}\right)$$

$$\theta_{s_{ij}} = \theta_s\left(\xi_i, \xi_j = 1 - \xi_i, \xi_k = 0\right) = \left(\theta_x \cos\phi_{ij} + \theta_y \sin\phi_{ij}\right)\Big|_{\xi_i,\xi_j=1-\xi_i,\xi_k=0}$$

$$= \left(\xi_i\theta_{xi} + (1-\xi_i)\theta_{xj}\right)\cos\phi_{ij} + \left(\xi_i\theta_y + (1-\xi_i)\theta_{yj}\right)\sin\phi_{ij} = \xi_i\theta_{si} + (1-\xi_i)\theta_{sj}$$

where l_{ij} is the length of the k-th element side and s the tangential coordinate such that $s_{i\to j} = l_{ij}(1-\xi_i)$ and $d\xi_i/ds = -1/l_{ij}$.

The tangential shear deformation along the element border ij is then computed as follows

$$\gamma_{sz_{ij}} = \frac{dw_{ij}}{ds} - \theta_{s_{ij}} = \frac{dw_{ij}}{d\xi_i}\frac{d\xi_i}{ds} - \theta_{s_{ij}} = \frac{w_j - w_i}{l_{ij}} - \frac{\theta_{si} + \theta_{sj}}{2} \tag{B.9}$$

Curriculum Vitae

NAME	**Backes**
FIRST NAME	**Marie-Rose**
DATE OF BIRTH	20 March 1986
NATIONALITY	Luxemburgish
E-MAIL	backesmarierose@gmail.com

EDUCATION

- o Doctoral candidate in Civil Engineering,   **Sep. 2011 – Nov. 2016**
  École Polytechnique Fédérale de Lausanne (EPFL), Lausanne, Switzerland
  Thesis: "*Application of stress fields for the interaction between in-plane and out-of-plane forces in reinforced concrete shell elements*"

- o BSc and MSc in Civil Engineering, EPFL, Lausanne, Switzerland   **Sep. 2006 – Jul. 2011**
  Specialization in "Structural Engineering"
  Thesis on shape optimization and design of a reinforced concrete shell: "*Optimisation de la forme structural du Rolex Learning Center*".

EMPLOYMENT HISTORY

- o EPFL, Lausanne, Switzerland, doctoral assistant   **Aug. 2011 – Nov. 2016**
  - o Numerical research on the interaction of in-plane shear and transverse bending interaction in reinforced concrete beam webs.
  - o Development of a non-linear finite element program for establishing elastic-plastic stress fields in reinforced concrete subjected to in-plane and out-of-plane actions.
  - o Teaching assistant for courses "Structures", "Bridge Conception", "Advanced Concrete Structures", "Concrete Bridges" and "Stress field" projects as well as several theoretical and practical semester/master projects.

- o EPFL, Lausanne, Switzerland   **Mar. 2011 – Jun. 2011**
  - o teaching assistant for Civil Engineering course "Informatics I and II"

AWARDS

- *fib* PhD Symposium, Québec, Canada, 2014: award for outstanding paper and presentation.
- Holcim Junior Trophy Switzerland: Gold Medal for the most outstanding Master Thesis on reinforced concrete structures in 2011.

PUBLICATIONS

- Muttoni A., Fernández Ruiz M., Nikétic F., Backes M.-R. "*Assessment of existing structures based on elastic-plastic stress fields – Modelling of critical details and investigation of the in-plane shear transverse bending interaction*", OFROU Report, Switzerland, 2016. (in press)
- Backes M.-R., Fernández Ruiz M., Muttoni A., "*Interaction between in-plane shear forces and transverse bending moments in concrete bridge webs*", 10th *fib* International PhD Symposium in Civil Engineering, Quebec, Canada, 2014.
- Backes M.-R., "*Optimisation de la forme structural du Learning Center*", Le Béton – Matière en Devenir, Colloque Béton, EPF Lausanne, Switzerland, 2011.

LANGUAGES

- o **Luxemburgish**: mother tongue / **French**: fluent / **English**: fluent / **German**: fluent